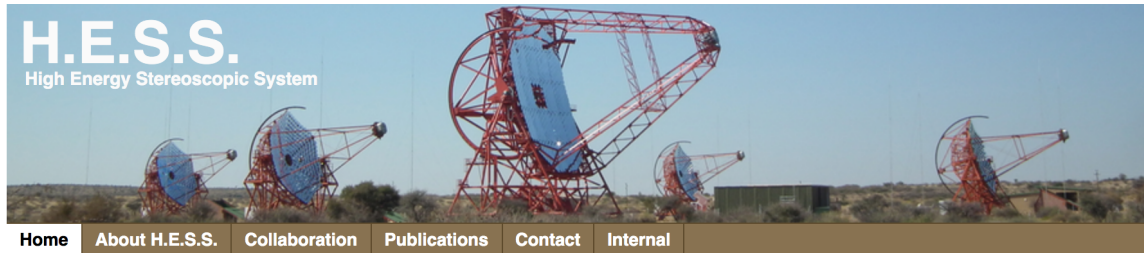


Astrofisica Nucleare e Subnucleare
TeV Astrophysics – III

Exercise #6

- Find the information about the 3 major currently operating IACT telescopes
- Visit the web site of CTA
- Find relevant info for HAWC and LHAASO

HESS



Welcome

Welcome to the webpages of H.E.S.S., one of the leading observatories studying *very high energy* (VHE) gamma-ray astrophysics. To learn more about H.E.S.S. and the high energy universe, or to view pictures from the telescopes and the site in Namibia visit the [About H.E.S.S.](#) section.

Follow H.E.S.S. on [Twitter](#), on [Facebook](#) and on [Instagramm](#) for news regarding the H.E.S.S. instrument and its science.

News

For older news see our [News Archive](#)

H.E.S.S. discovers the first VHE gamma-ray Nova. March 10, 2022

In 2021 the H.E.S.S. collaboration discovered the first Nova emitting very high energy (VHE) gamma-ray light. The recurrent Nova RS Ophiuchi exploded on August 8, 2021. The H.E.S.S. telescopes were turned to the constellation Ophiuchus in the night after the first sightings and promptly detected the explosion. Gamma-ray emission from Novae was completely unexpected until the Fermi-LAT experiment serendipitously detected low energy gamma radiation in 2010. While further Novae were observed with LAT, the soft spectra detected in this energy range suggested that such explosions would not generate radiation that was 1000 times more energetic and hence be detectable in the VHE gamma-ray band. The H.E.S.S. discovery is a

<https://www.mpi-hd.mpg.de/hfm/HESS/>

to the H.E.S.S. observations for more of the event. Further

Source of the Month



May 2022 - *The beginnings of H.E.S.S.*

[More Info](#) | [All Sources](#)

[Options for External Proposals for H.E.S.S. Observations](#)

[Requests for Follow-up Observations of TOOs](#)

[The HESS Source Catalog](#)

[The HESS First Public Test Data Release](#)

[The H.E.S.S. Prize Hall of Fame](#)

[H.E.S.S. Ph.D. Theses](#)

MAGIC



© Daniel Lopez, IAC

Welcome to MAGIC!

The pioneering instrument for covering the electromagnetic spectrum in the energy range above 30 GeV

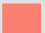
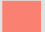




© Daniel Lopez, IAC

<https://magic.mpp.mpg.de/>

Statement of MAGIC scientists in solidarity with Ukraine

Recent MAGIC Highlights

-  MAGIC Telescope System detects energetic nuclear blast from vampire star
-  Cosmic Cataclysm allows precise test of General Relativity
-  **BREAKING THE LIMITS!** Discovery of the highest energy-photons from a gamma-ray burst
-  MAGIC telescopes trace origin of a rare cosmic neutrino

VERITAS

VERITAS

Very Energetic Radiation Imaging Telescope Array System



[Home](#) [Contact](#) [News \(most recent: 2022-Feb-24\)](#) [Whipple](#) [Internal](#)

Home

Welcome to VERITAS

 Published: 01 January 2004



Quick link to our [results](#) pages (one page per paper, with descriptive text and all figures).

[VERITAS \(Very Energetic Radiation Imaging Telescope Array System\)](#) is a ground-based gamma-ray instrument operating at the Fred Lawrence Whipple Observatory (FLWO) in southern Arizona, USA. It is an array of four 12m optical reflectors for gamma-ray astronomy in the GeV - TeV energy range. These imaging Cherenkov telescopes are deployed such that they have the highest sensitivity in the VHE energy band (50 GeV - 50 TeV), with maximum sensitivity from 100 GeV to 10 TeV. This VHE observatory effectively complements the NASA [Fermi](#) mission.



View of the FLWO basecamp and the VERITAS array. Click on the image for a hi-res version.

<https://veritas.sao.arizona.edu/>

CTA

[Home](#) [About](#) [Science](#) [Project](#) [News](#) [Outreach & Education](#)



Cherenkov Telescope Array Exploring the Universe at the Highest Energies

10 BILLION LIGHT YEARS

Gamma Ray Bursts

1 BILLION LIGHT YEARS

Featured Video



Latest News



**HENRIETTA SWAN LEAVITT:
SHORTENING
ASTRONOMICAL AND
SOCIETAL DISTANCES**
2022-APRIL-29

<https://www.cta-observatory.org/>

HAWC

HAWC

The High-Altitude Water Cherenkov Gamma-Ray Observatory

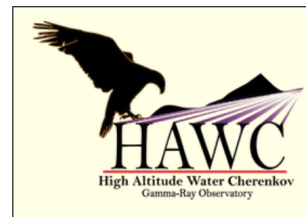
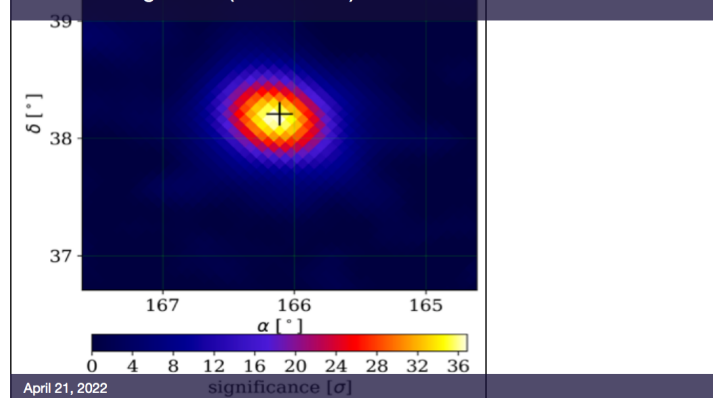
[Home](#) [News](#) [Science](#) [Observatory](#) [Details](#) [Publications](#) [Public data](#) [Collaboration](#) [Support](#) [Español](#)

Statement from the HAWC Leadership (March 24, 2021)

The HAWC Collaboration stands in solidarity with the Asian, Desi, and Pacific Islander community and against hate and racism. We are outraged by the recent horrific crime in Atlanta that we see as part of a larger pattern of discrimination and racism targeting Asian Americans. As in our message of June 8, 2020 (below), we reiterate our belief that scientific discoveries are made not by hardware, but by people and that we can only achieve the best scientific results when we include people of all ethnicities, races, gender identities, and backgrounds in the process. We also believe that it is our role to speak out against violence, discrimination and oppression wherever it occurs. We once again pledge to do more to bring change to our collaboration, our institutions, our countries and society as a whole.

Latest News

HAWC reports the detection of gamma rays coming from the central zone of two galaxies (read more...)



Quick Links:

Conacyt Thematic Networks

- [La Red HAWC](#)

News

- [New Papers from HAWC](#)
- [Conference Proceedings](#)
- [Latest News](#)



Like



Share

- [Follow @HAWC_Obs](#)

TeV Astronomy

- [Catalog of TeV Sources](#)
- [TeV Review Papers](#)

Milagro Links

- [Milagro \$\gamma\$ -Ray Observatory](#)
- [Milagro Publications](#)

For HAWC Collaborators

- [HAWC Star Chart](#)
- [HAWC Internal Pages](#)

<https://www.hawc-observatory.org/>

LHAASO

LHAASO
The Large High Altitude Air Shower Observatory

Chinese | IHEP | CAS

Search

Home News&Events Science Observatory Publications Public data Collaboration Gallery

bird view of LHAASO

Spotlight at LHAASO

LHAASO Discovers a Dozen PeVatrons and Photons Exceeding 1 PeV and Launches Ultra-High-Energy Gamma Astronomy Era

China's Large High Altitude Air Shower Observatory (LHAASO)—one of the country's key national science and technology infrastructure facilities—has found a dozen ultra-high-energy (UHE) cosmic acc...

Related Links

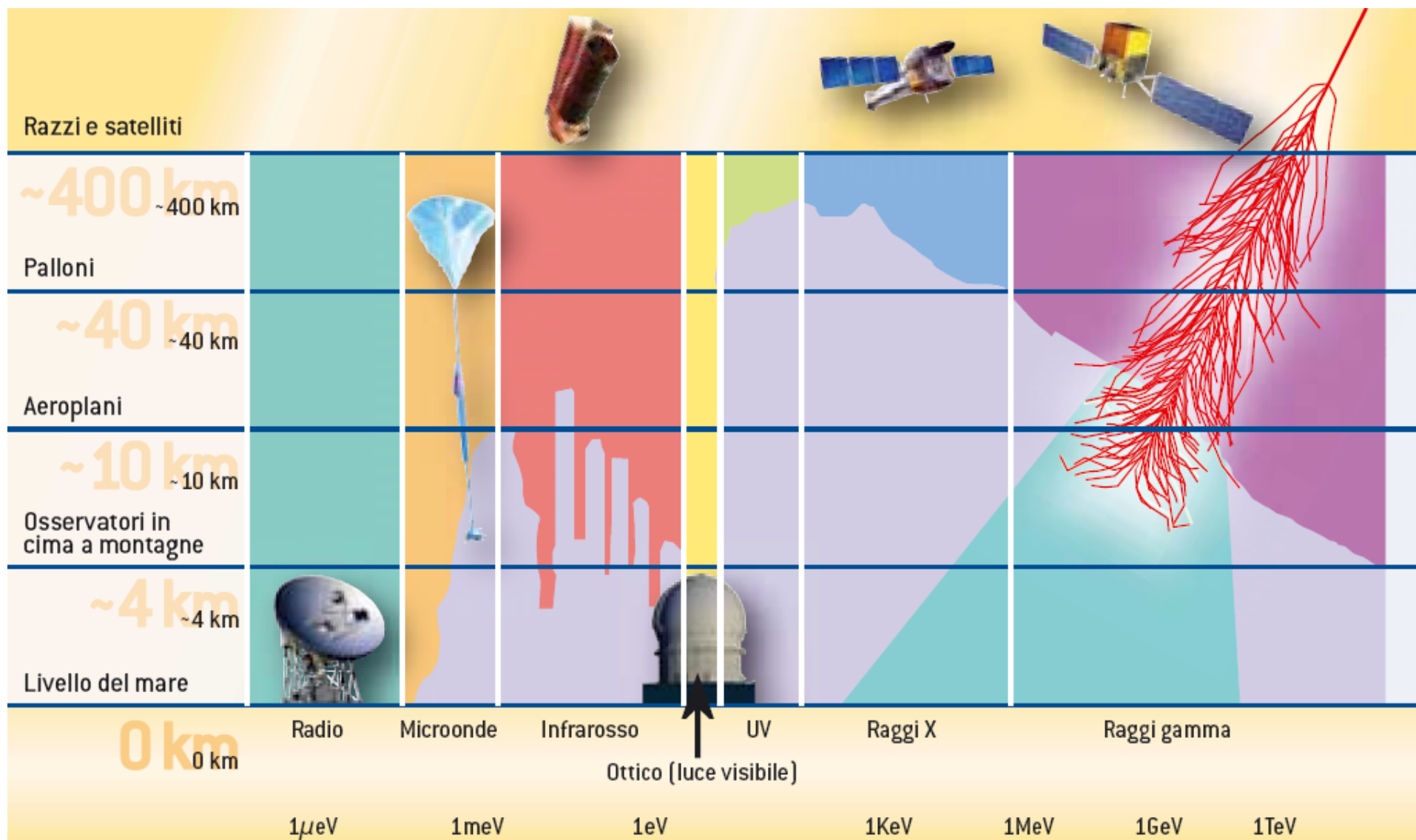
- > AUGER
- > ICECUBE
- > CTA

Contact Us

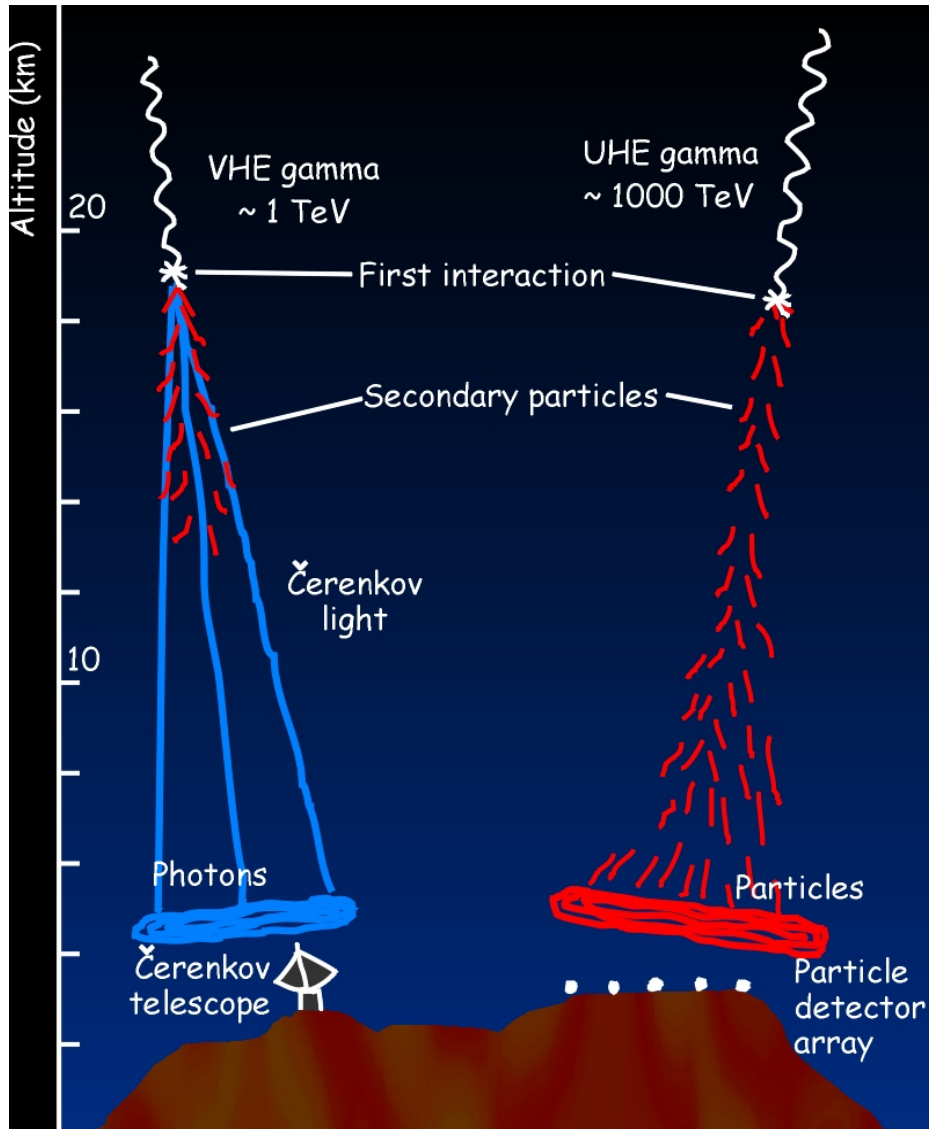
E-mail: zhoubin@ihep.ac.cn
TEL: 01088235181
Address: 19(B), Yuquan Road, Shijingshan District, Beijing (Postcode: 100049)

<http://english.ihep.cas.cn/lhaaso/>

The opacity of the atmosphere



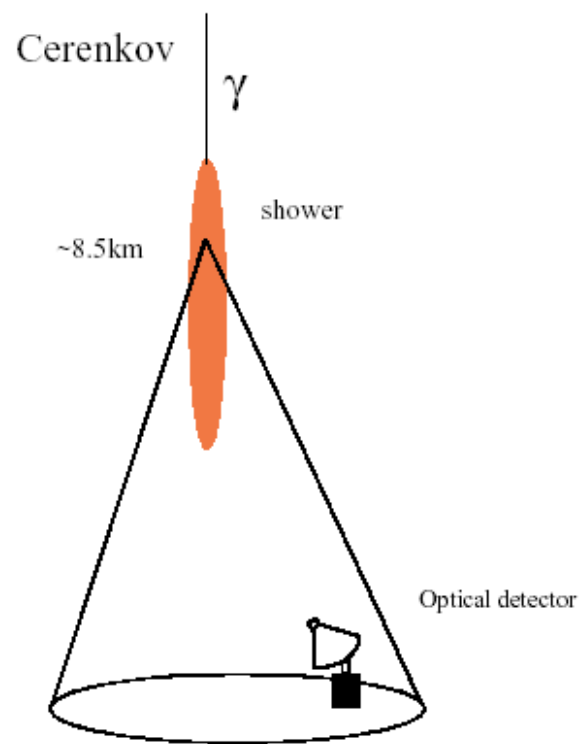
IACT & EAS experiments



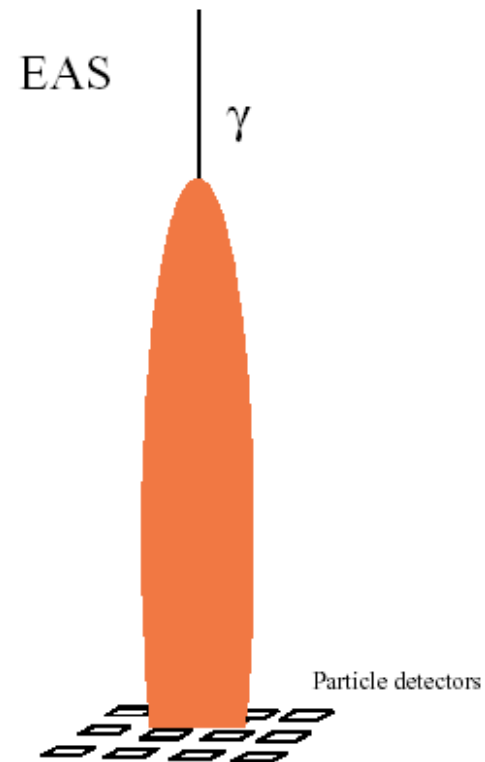
- Cherenkov experiments consist of almost-optical telescopes devoted to detect Cherenkov light.
- EAS (Extensive Air Shower) experiments are huge arrays or carpets of particle detectors.
- Cherenkov experiments have lower energy thresholds, but also a lower duty-cycle as well as a smaller field of view.

TeV detectors

Cerenkov and Extensive air shower (EAS) gamma ray telescope concepts



~ 40.000 m² , but no anticoincidence shield !

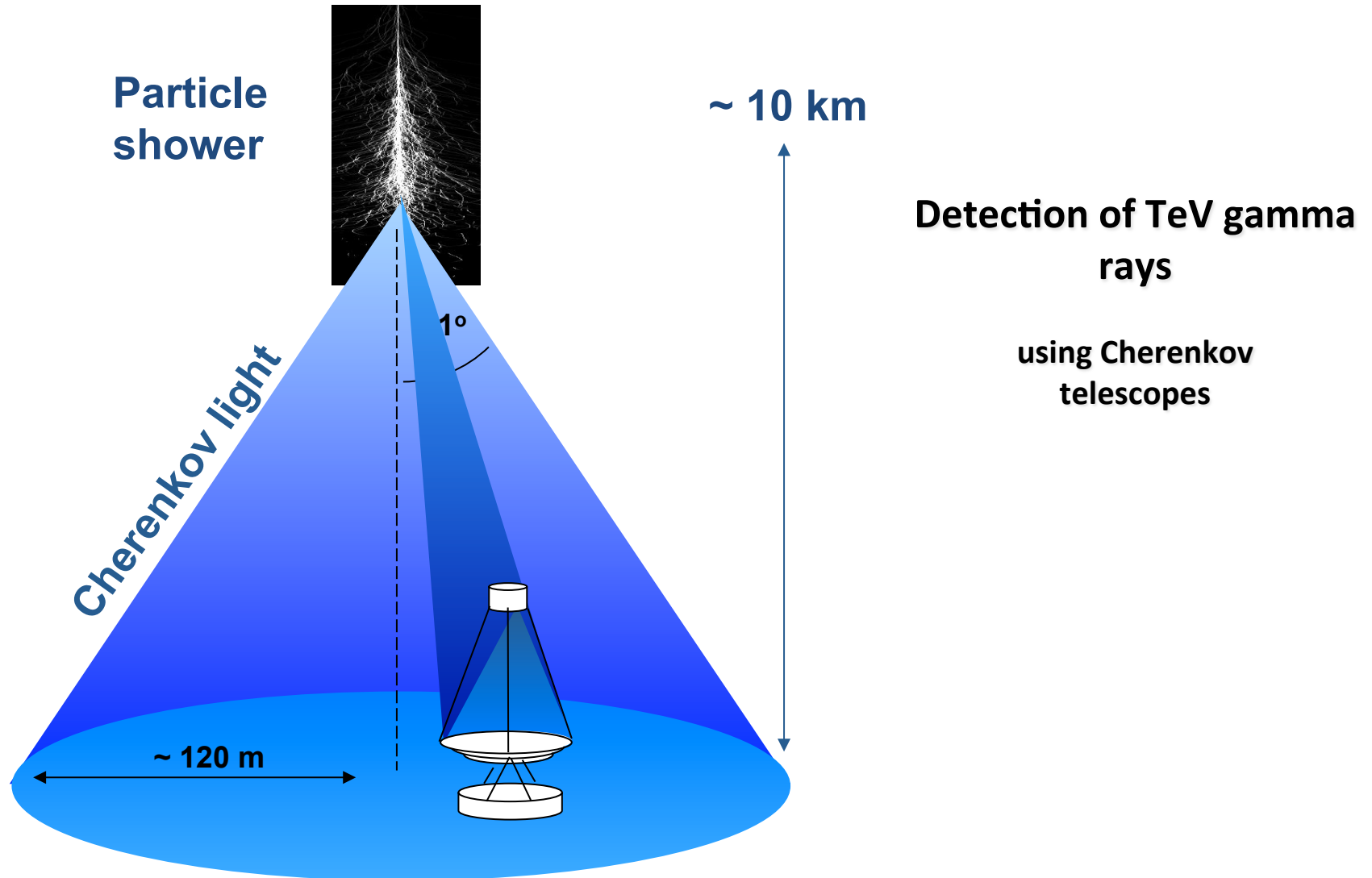


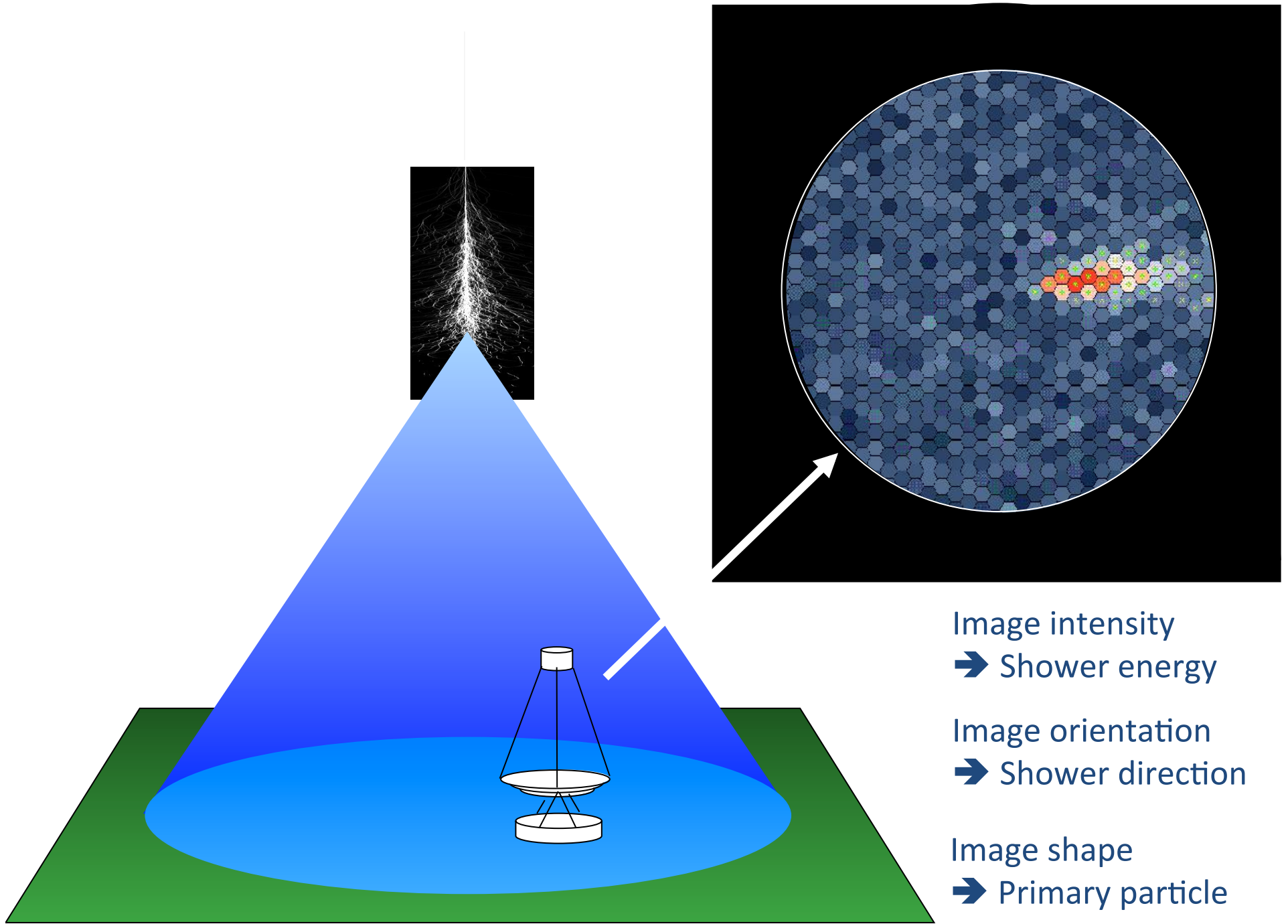
Complementary Capabilities

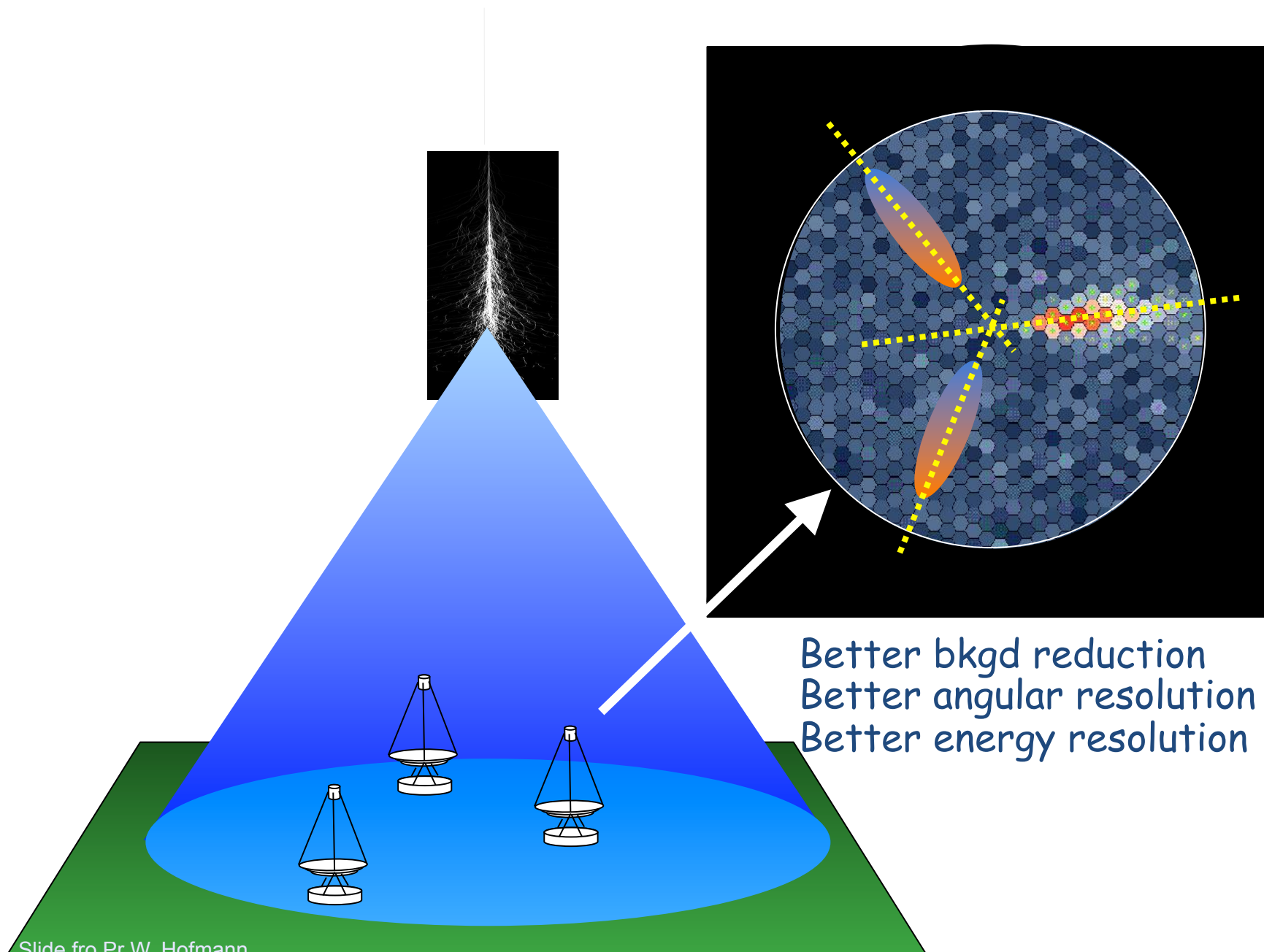
Parameter	Ground-based		Space-based
	ACT	EAS	Pair
angular resolution	good	fair	good
duty cycle	low	high	high
area	large	large	small
field of view	small	large	large & can repoint
energy resolution	good	fair	good w/ smaller systematic uncertainties

The next generation of ground-based and space-based facilities are well matched!

Observation technique







Better bkgd reduction
Better angular resolution
Better energy resolution

MAGIC telescopes



MAGIC – II

+ The telescope(s)

4



Design

- Solar power-plant design
- 17-m diameter
- $F/D=1$
- ~500kg camera
- Signal digitization off-telescope
- 64 tons total moving weight
- Fast-movement (GRBs): 20 sec ptp

Performance

- Energy threshold ~50 GeV (~ 25 GeV with a special trigger)
- FOV 3.5deg
- Energy Resolution ~16% ($E > 300$ GeV)
- Angular Resolution ~0.07deg ($E > 300$ GeV)
- Sensitivity (5σ in 50 hours) ~0.8% Crab Nebula flux (> 250 GeV)

Colin, ICRC 2008

Michele Doro - From MAGIC to MAGIC stereo - Ricap 2011

Several "firsts"

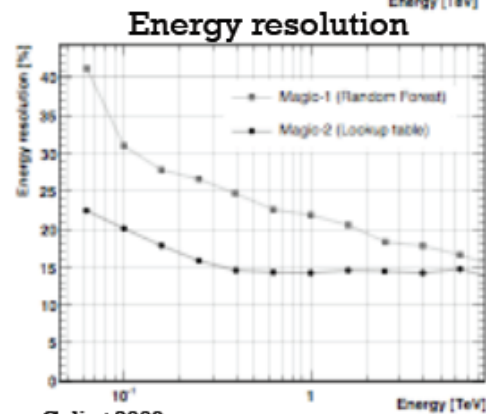
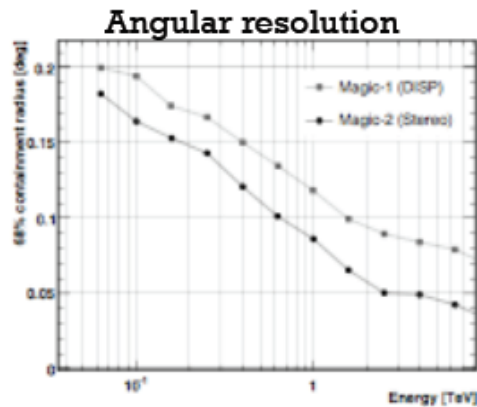
- Worldwide largest mirror dish.
- Lightweight CFRP tubes for structure
- Diamond milled light weight all-aluminum sandwich mirrors
- Active mirror control
- Low gain hemispherical PMTs with diffuse lacquer coating
- Transmission over 160 m by optical
- 2 GHz FADCs

MD, ICAPTT 2008

MAGIC – II

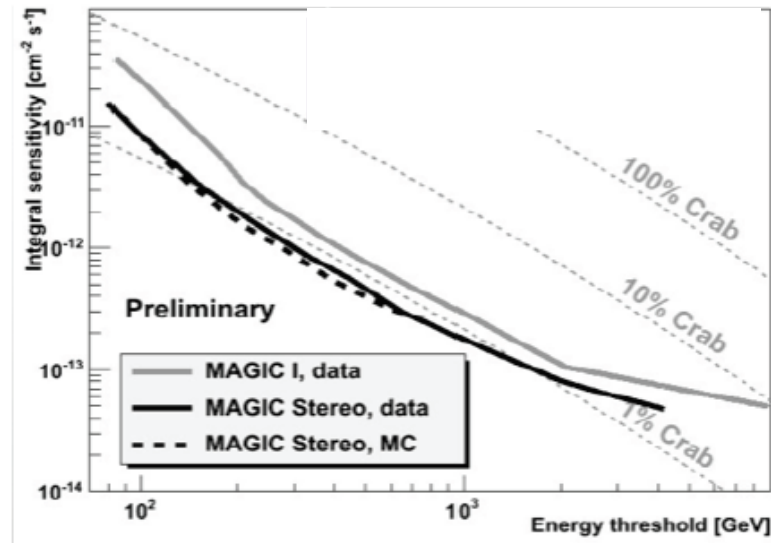
+ Improvements

7



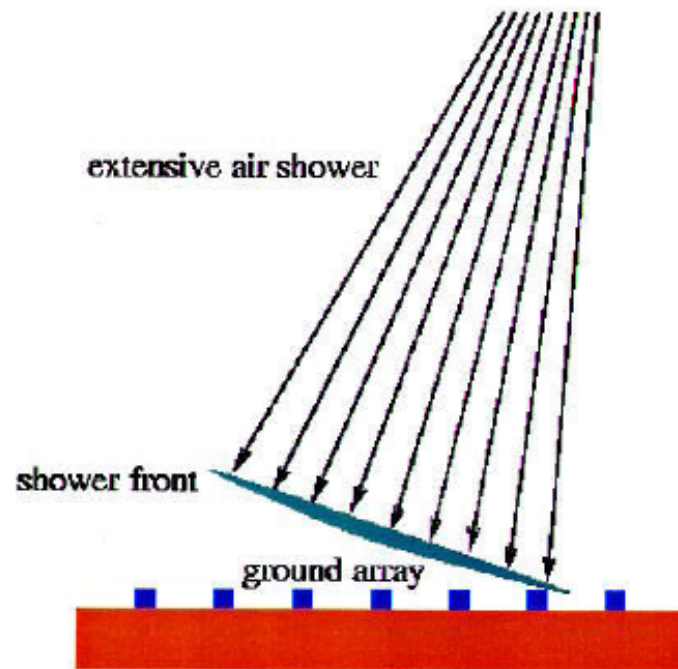
Colin+2009

- Extended sources and morphology now possible
- Sensitivity improved of 100% over most of the energy range
- Better performance specially at low energy (<100 GeV)



TeV detectors

Air Shower Arrays



Reconstruction of the γ direction
with the particles arrival times

Large field of view: $\sim \pi$ sr

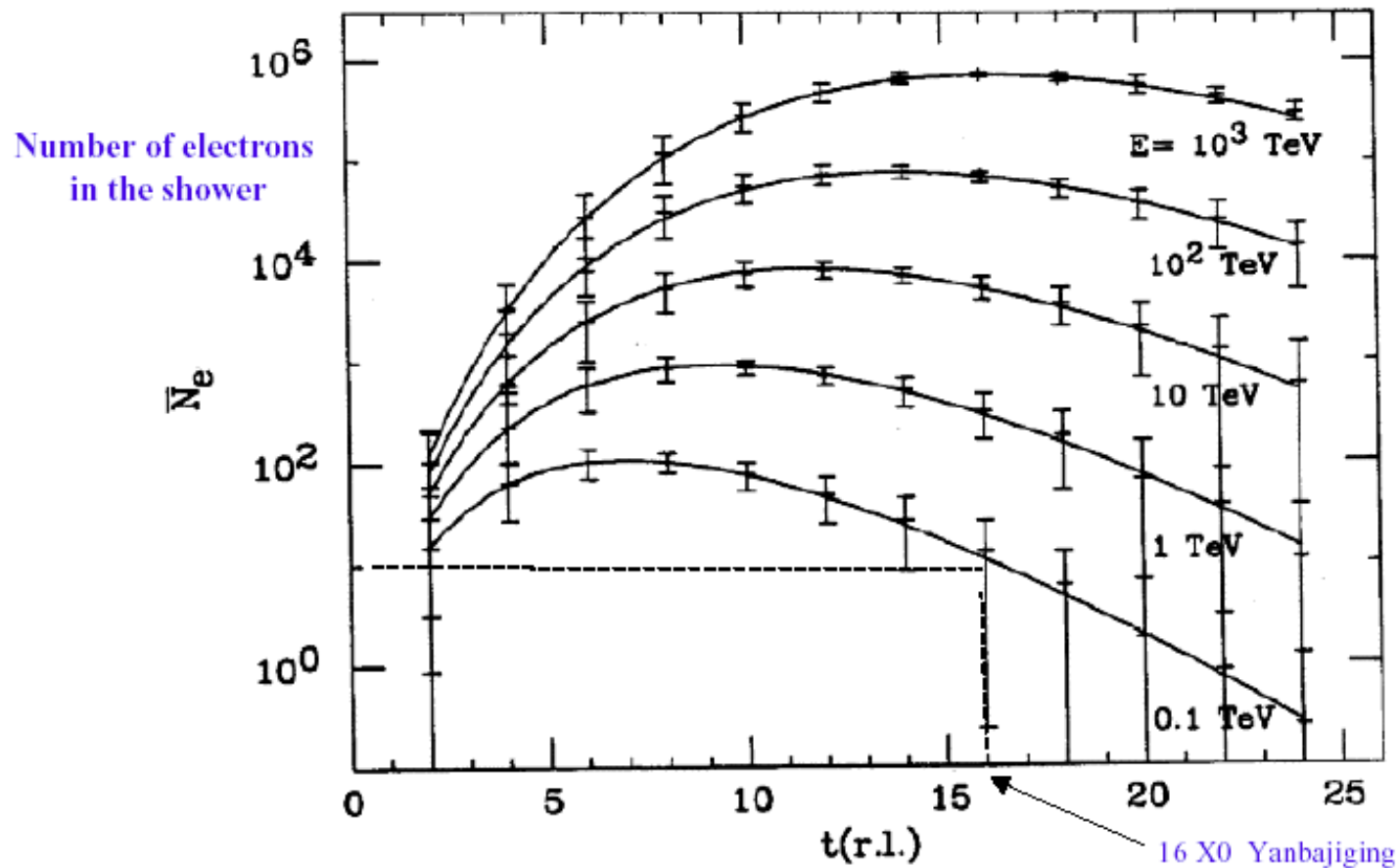
Duty cycle $\sim 100\%$

Gamma-hadrons discrimination:

μ -poor showers

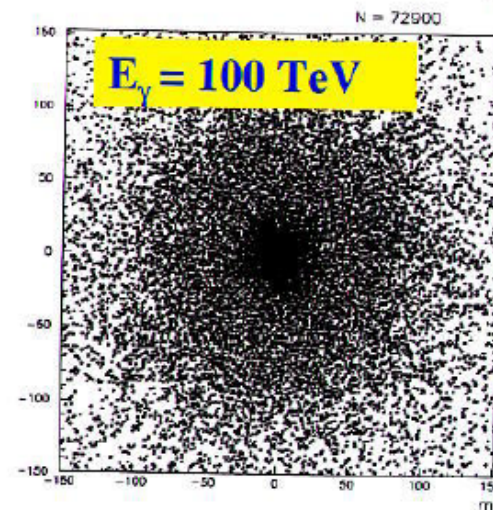
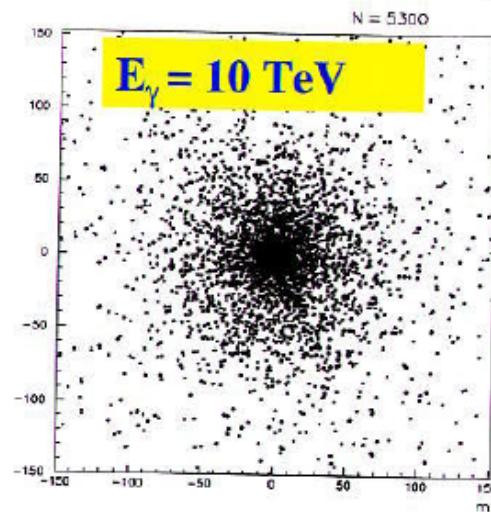
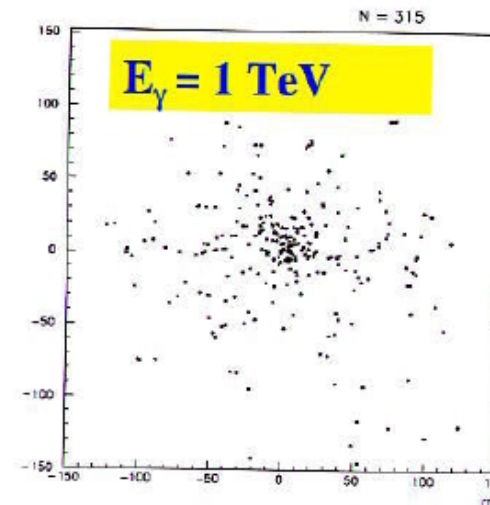
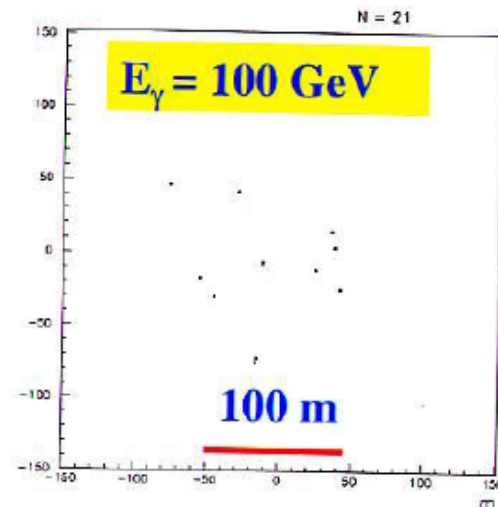
TeV detectors

Longitudinal development of the electron component of photon initiated shower
(with electron threshold energy of 5 MeV and fluctuations superimposed)

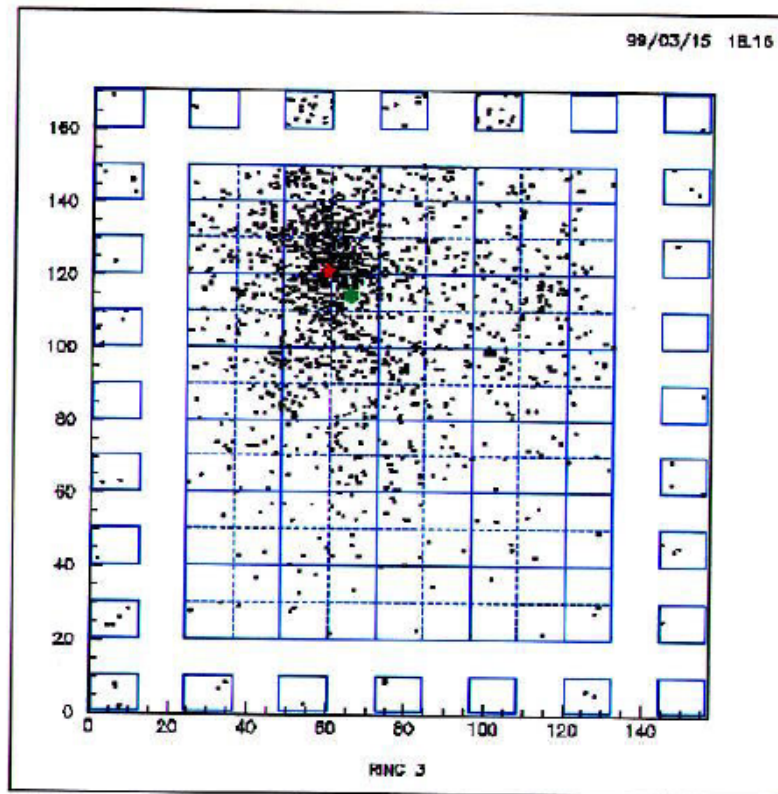


TeV detectors

EAS
at
4300 m



TeV detectors



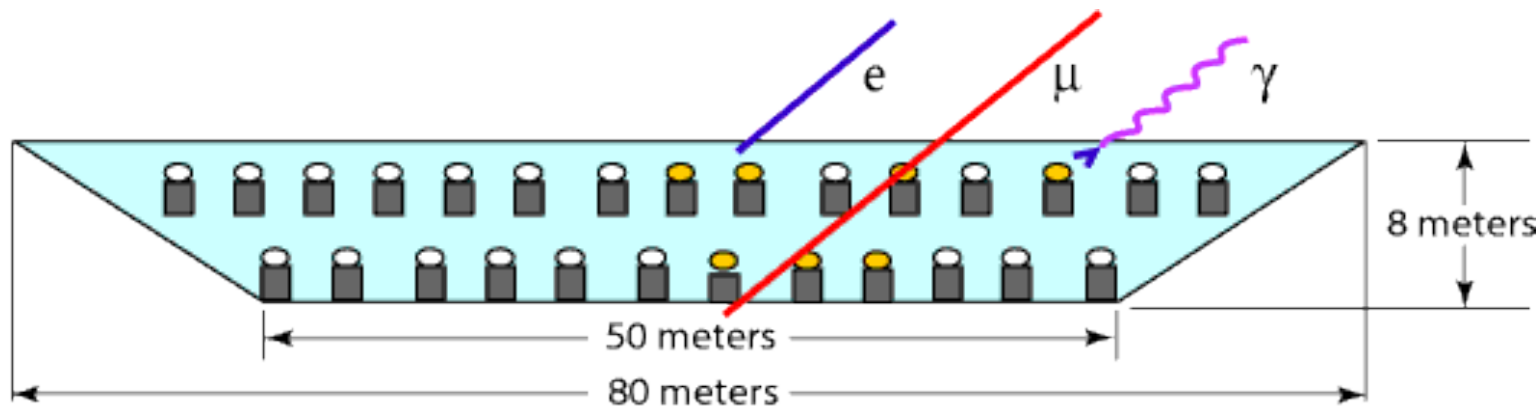
Montecarlo
simulation
of a 10 TeV
air shower

EAS technique

Charged particles produce Cherenkov photons in water
~1400 times more Cherenkov photons than in air per
unit length track of charged particle
Cherenkov cone in water $\sim 41^\circ$ (in air: less than 1°)

Uniform sky view with an array of PMTs

Direction reconstruction through PMTs signal times



Wide Angle Telescopes

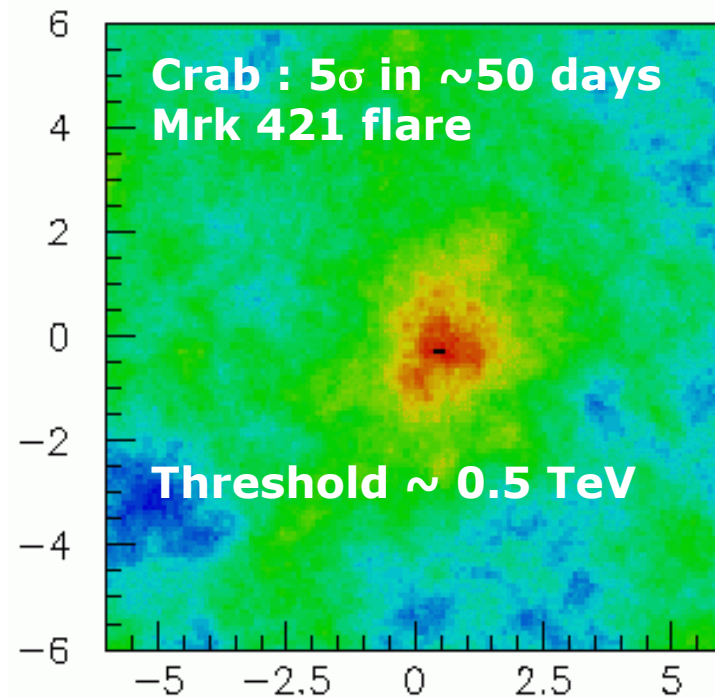
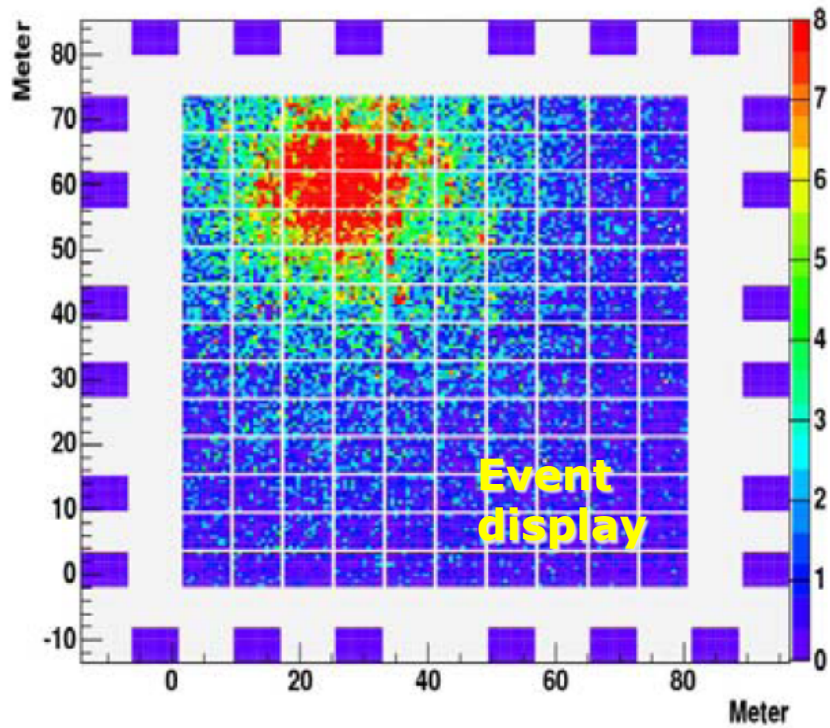
Tibet AS- γ – Air Shower Array
ARGO – Carpet array with RPC
MILAGRO – Water Cherenkov

Advantage: Wide Angle $0.5\pi \sim 1\pi$
Non-bias observation

Cons: Moderate sensitivity
 $\sim 5\sigma/\text{yr}^{1/2}$ for Crab

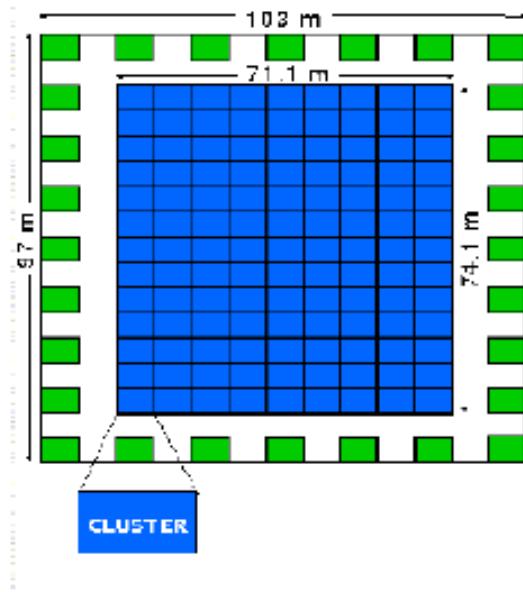


ARGO-YBJ (RPC):



ARGO

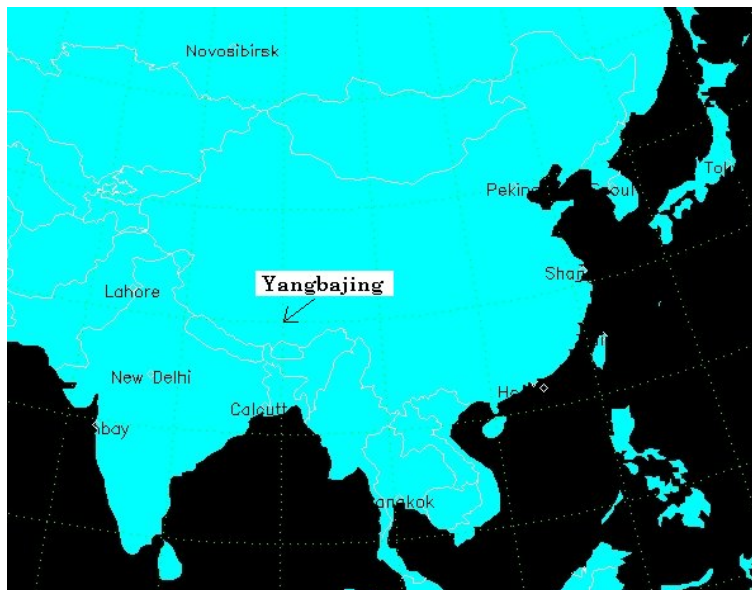
Area 5.200 m² (full coverage)
(10.000 m² with guard ring)
Field of view ~ 1 sr
E = 50 GeV - 50 TeV
Location: Tibet 4300m alt.



17400 Pads 56 by 60 cm² each of Resistive Plate Chamber (RPC).
Each pad subdivided in pick-up strips 6 cm wide for the space pattern inside the pad.
The CLUSTER is made of 12 RPCs Pads



TIBET air shower array



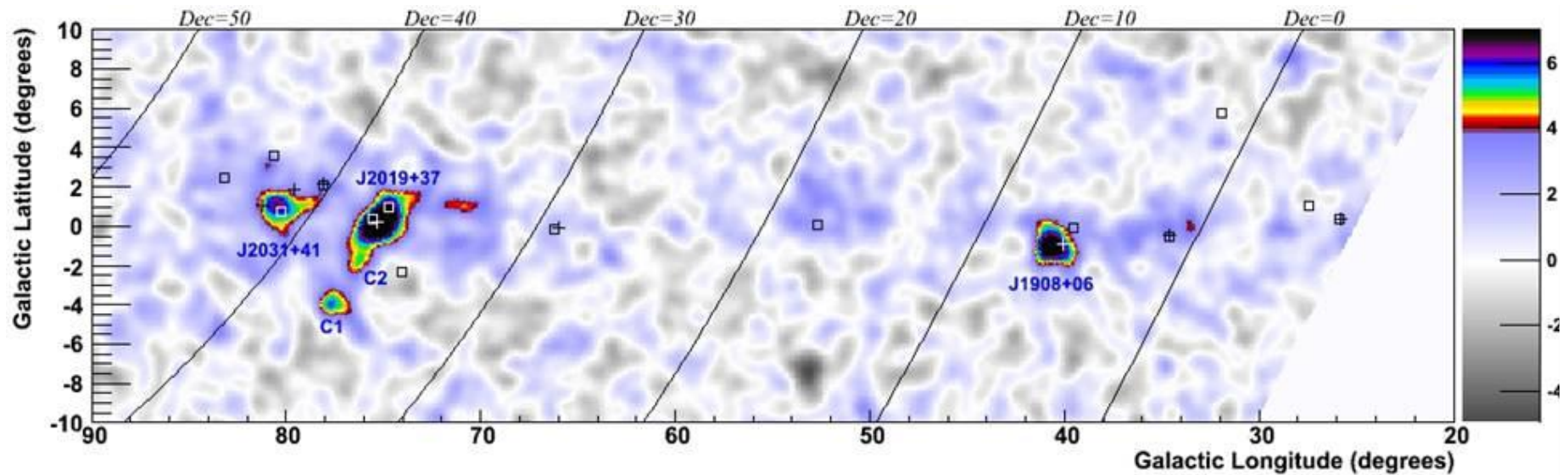
Our air shower array consists of 697 scintillation counters which are placed at a lattice with 7.5 m spacing and 36 scintillation counters which are placed at a lattice with 15 m spacing. Each counter has a plate of plastic scintillator, 0.5 m² in area and 3 cm in thickness, equipped with a 2-inch-in-diameter photomultiplier tube (PMT). The time and charge information of each PMT hit by an air shower event is recorded to determine its direction and energy. The detection threshold energy is approximately 3 TeV, which is the lowest one achieved by an air shower array in the world.

MILAGRO

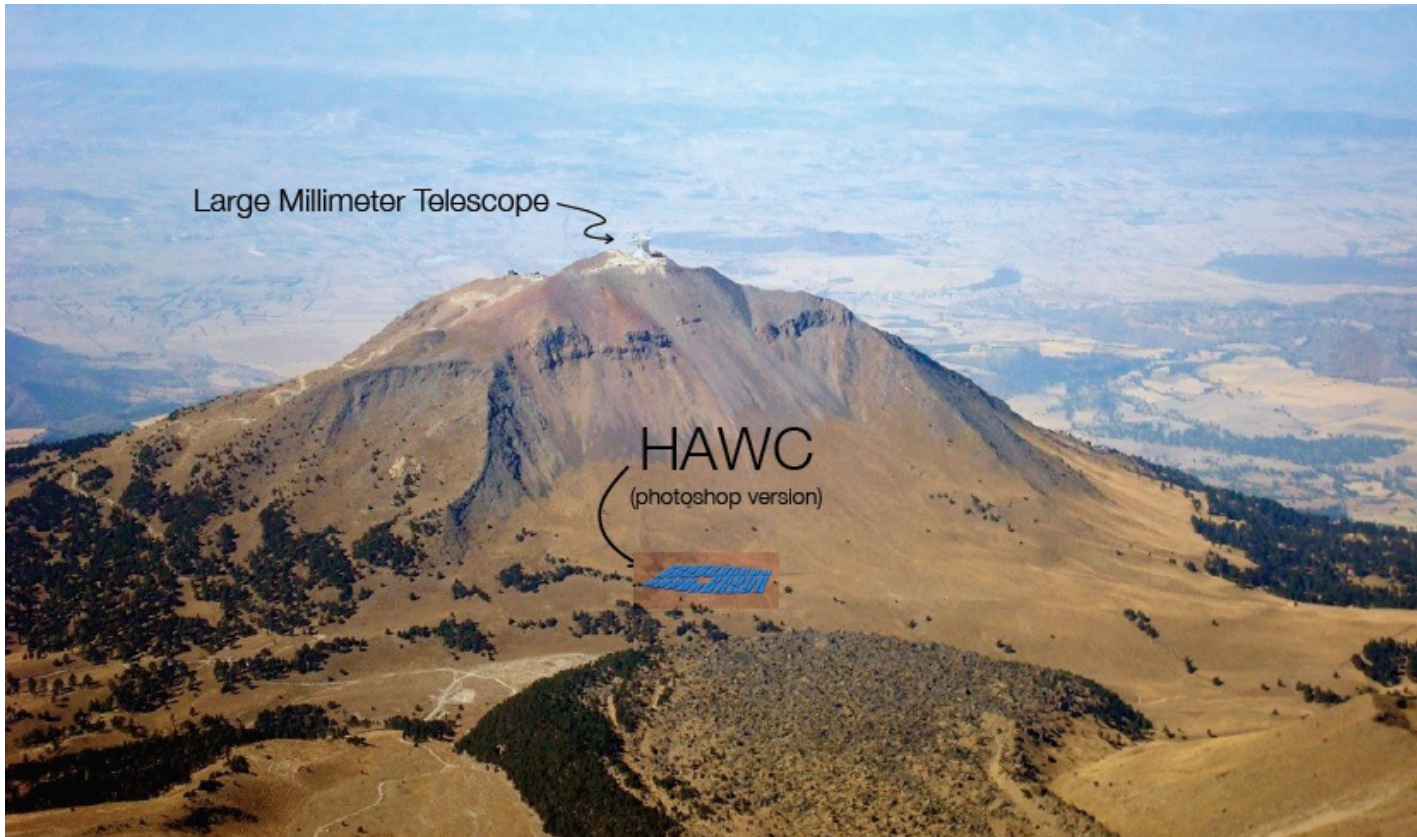
**Cherenkov in water,
Arizona**



Crab:
 $\sim 5\sigma$ in 100 days
Median energy ~ 20 TeV



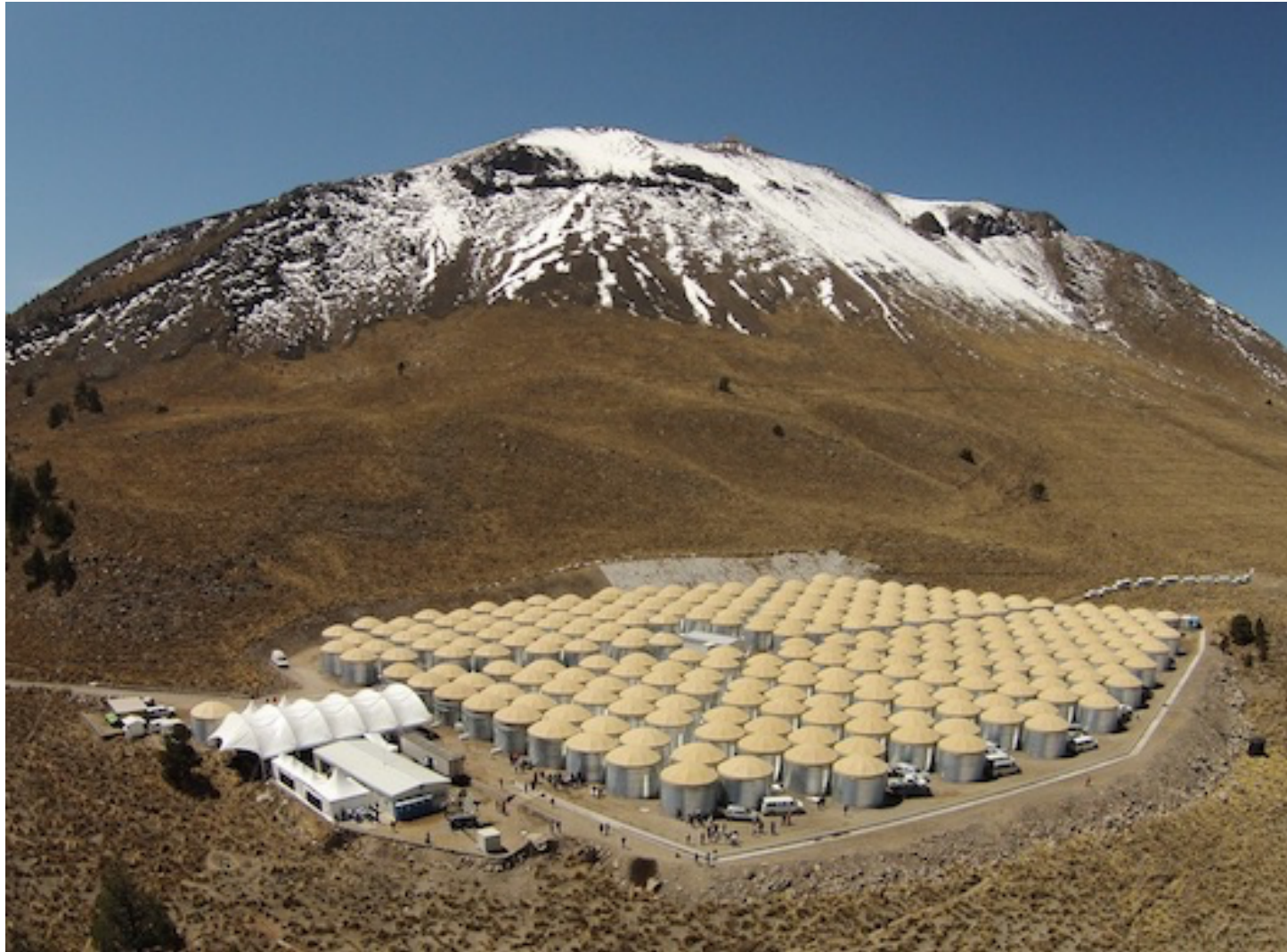
HAWC



HAWC

Pico de Orizaba, altitude 4100 m, latitude 18° 59' N
Two hours drive from Puebla, four from México City
Site of Large Millimeter Telescope (existing infrastructure)

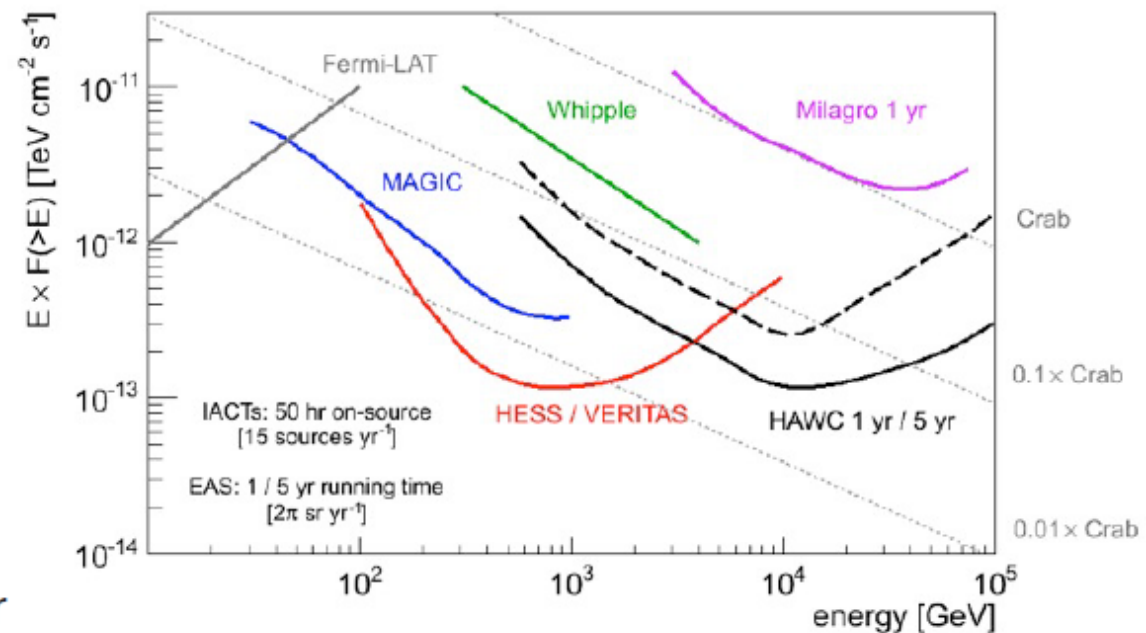
HAWC



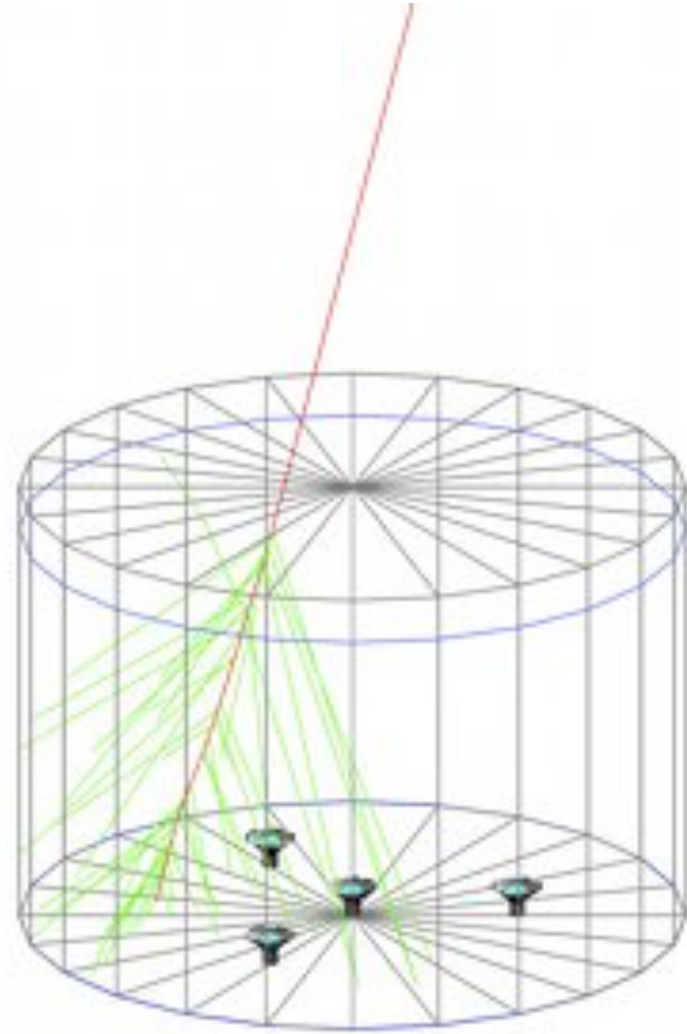
HAWC

Sensitivity to Point Sources

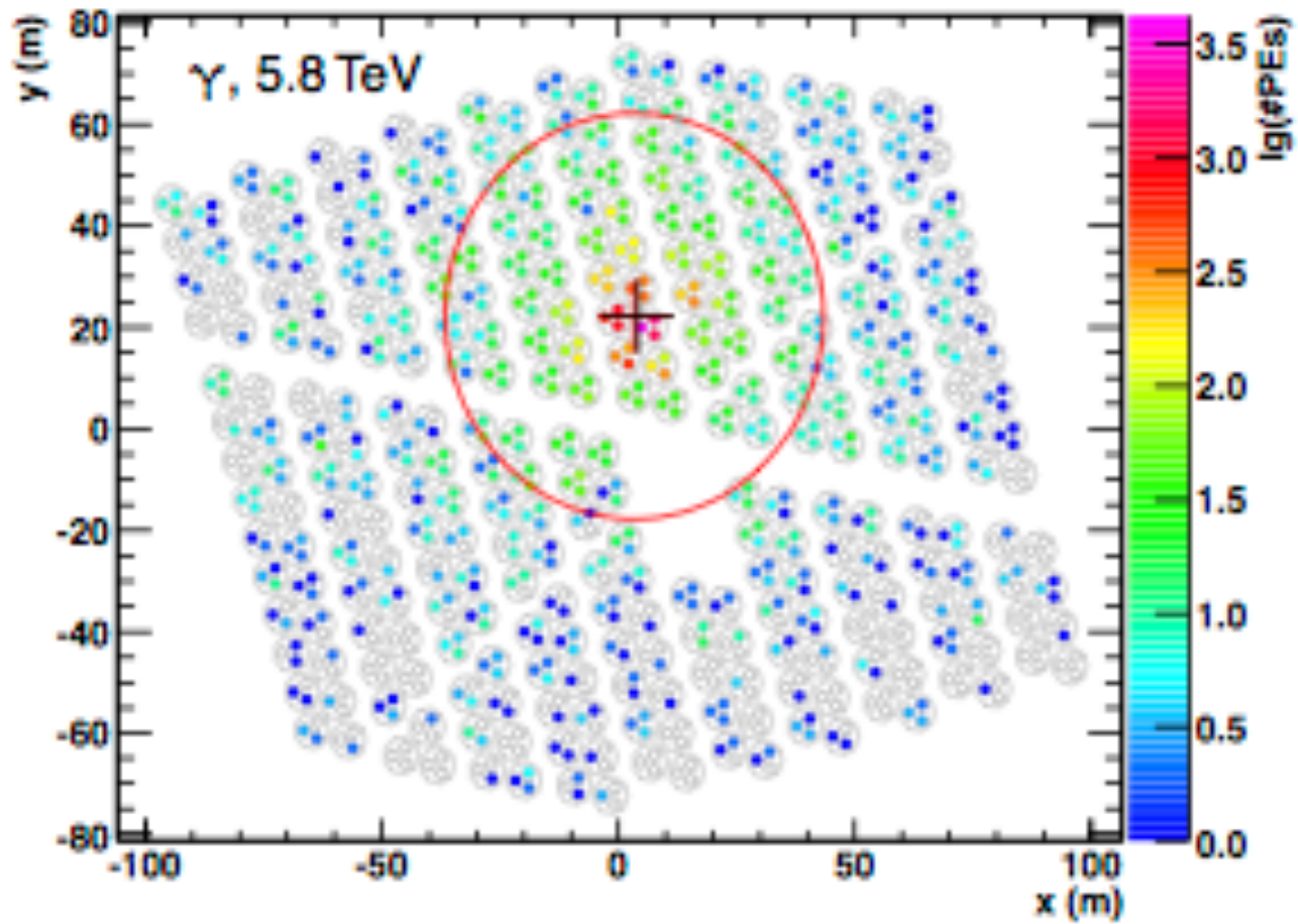
- Long integration times lead to excellent sensitivity at highest energies (> few TeV)
- 5σ sensitivity to:
 - 10 Crab in 3 min
 - 1 Crab in 5 hr
 - 0.1 Crab in $\frac{1}{3}$ year
- Around 15x the sensitivity of Milagro



HAWC



HAWC



HAWC

HAWC

The High-Altitude Water Cherenkov Gamma-Ray Observatory

Home

News

Science

Observatory

Details

Publications

Collaboration

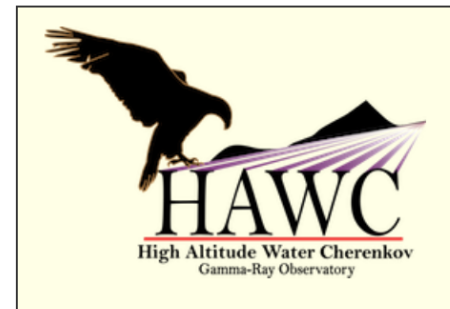
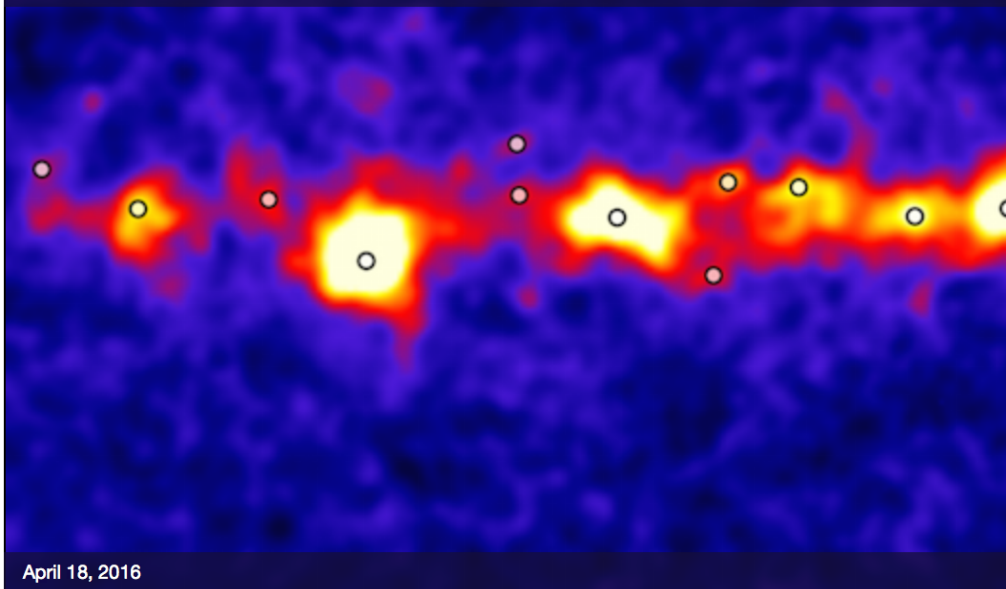
Contact

Support

Español

Latest News

HAWC reveals new look at the very high-energy sky (*read more...*)



Quick Links:

News

- [Latest news from HAWC](#)
- [f Like](#) [Share](#)
- [Follow @HAWC_Obs](#)

TeV Astronomy

- [Catalog of TeV Sources](#)
- [TeV Review Papers](#)

Milagro Links

- [Milagro \$\gamma\$ -Ray Observatory](#)

<http://www.hawc-observatory.org>

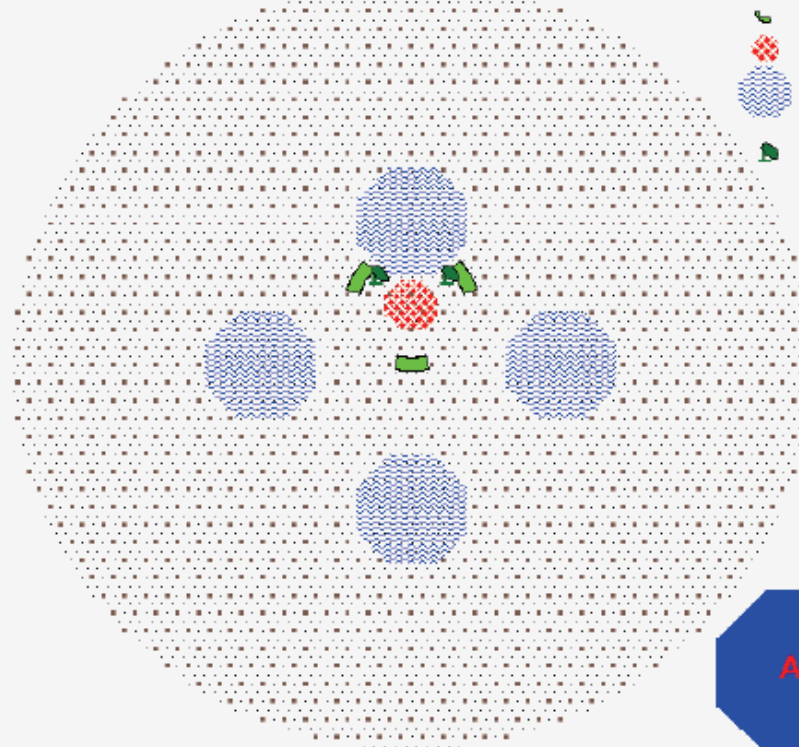
LHAASO

Project Overview

Large High Altitude Air Shower Observatory

Yangbajing, 4300m a.s.l., 606g/cm²

- ED: 5137, 1m×1m×2cm
15m spacing
- MD: 1161, 6m×6m×2cm
30m spacing
- WFCAs: 3×8, 16×16pixels
150m spacing
- SCDA: 5000m² (r=80m)
- WCDA: 4×900
Φ170m×4m
300m spacing
- IACs: 2
100m spacing



1000m

Charged
Particle
Array

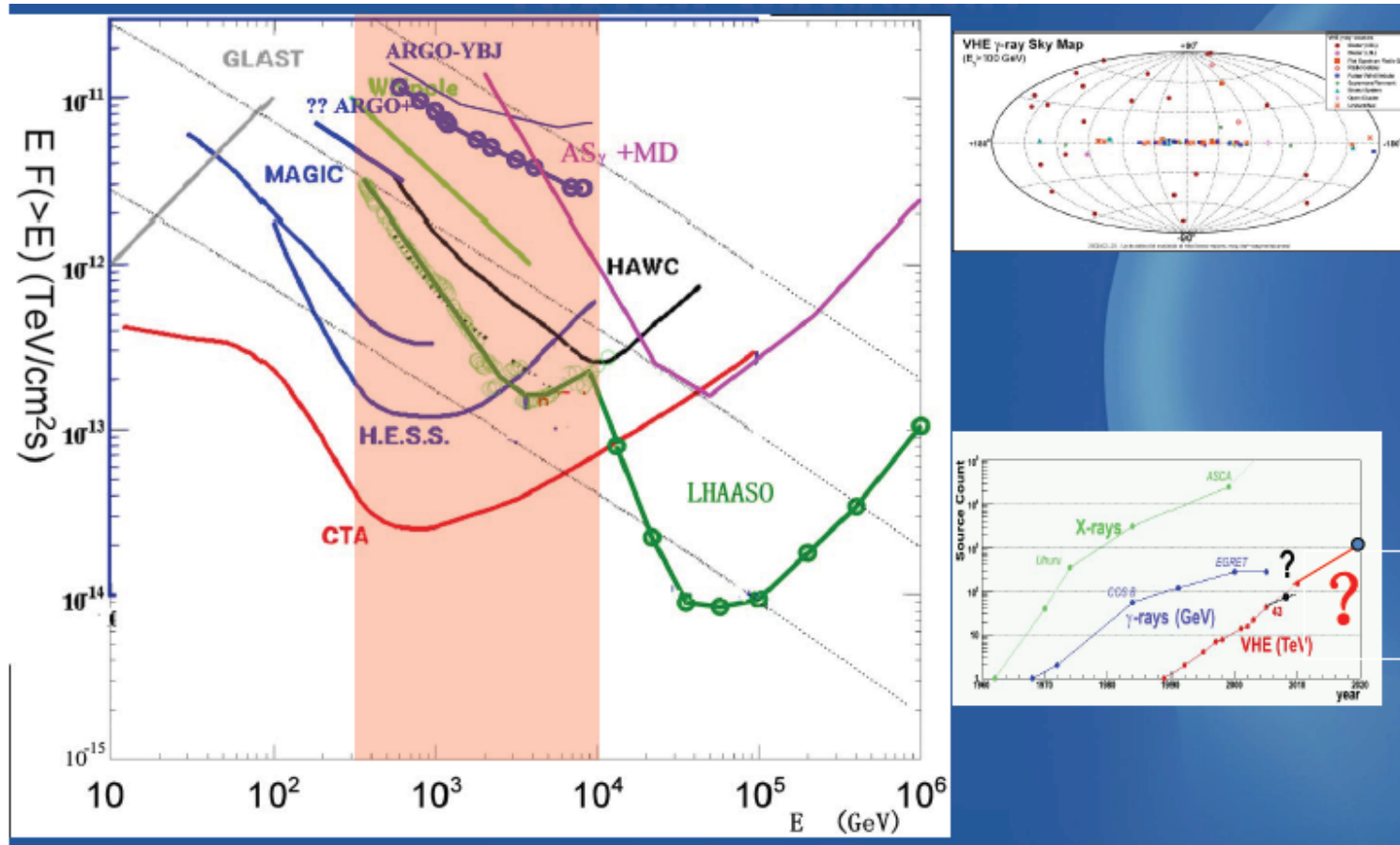
μ Detector
Array

Water C
Array

Wide FOV
C-Telescope
Array
&

Core Detector
Array

LHAASO



The LHAASO experiment

The Large High Altitude Air Shower Observatory (LHAASO) project is a new generation all-sky instrument to investigate the 'cosmic ray connection' through a combined study of cosmic rays and gamma-rays in the wide energy range 10^{11} -- 10^{17} eV.

The first phase of LHAASO will consist of the following major components:

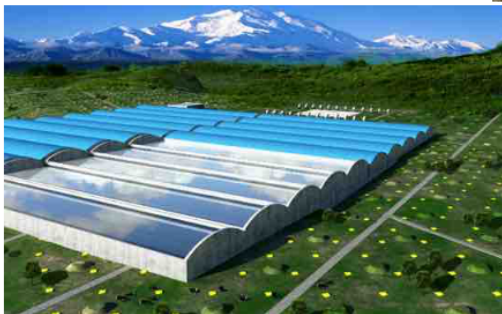
- 1 km² array (LHAASO-KM2A), including 5635 scintillator detectors, with 15 m spacing, for electromagnetic particle detection.
- An overlapping 1 km² array of 1221, 36 m² underground water Cherenkov tanks, with 30 m spacing, for muon detection (total sensitive area 40,000 m²).
- A close-packed, surface water Cherenkov detector facility with a total area of 90,000 m² (LHAASO-WCDA), four times that of HAWC.
- 24 wide field-of-view air Cherenkov (and fluorescence) telescopes (LHAASO-WFCTA).
- 452 close-packed burst detectors, located near the centre of the array, for detection of high energy secondary particles in the shower core region (LHAASO-SCDA).

LHAASO main components



1 KM2A:
5635 EDs
1221 MDs

WCDA:
3600 cells
90,000 m²



Coverage area: 1.3 km²

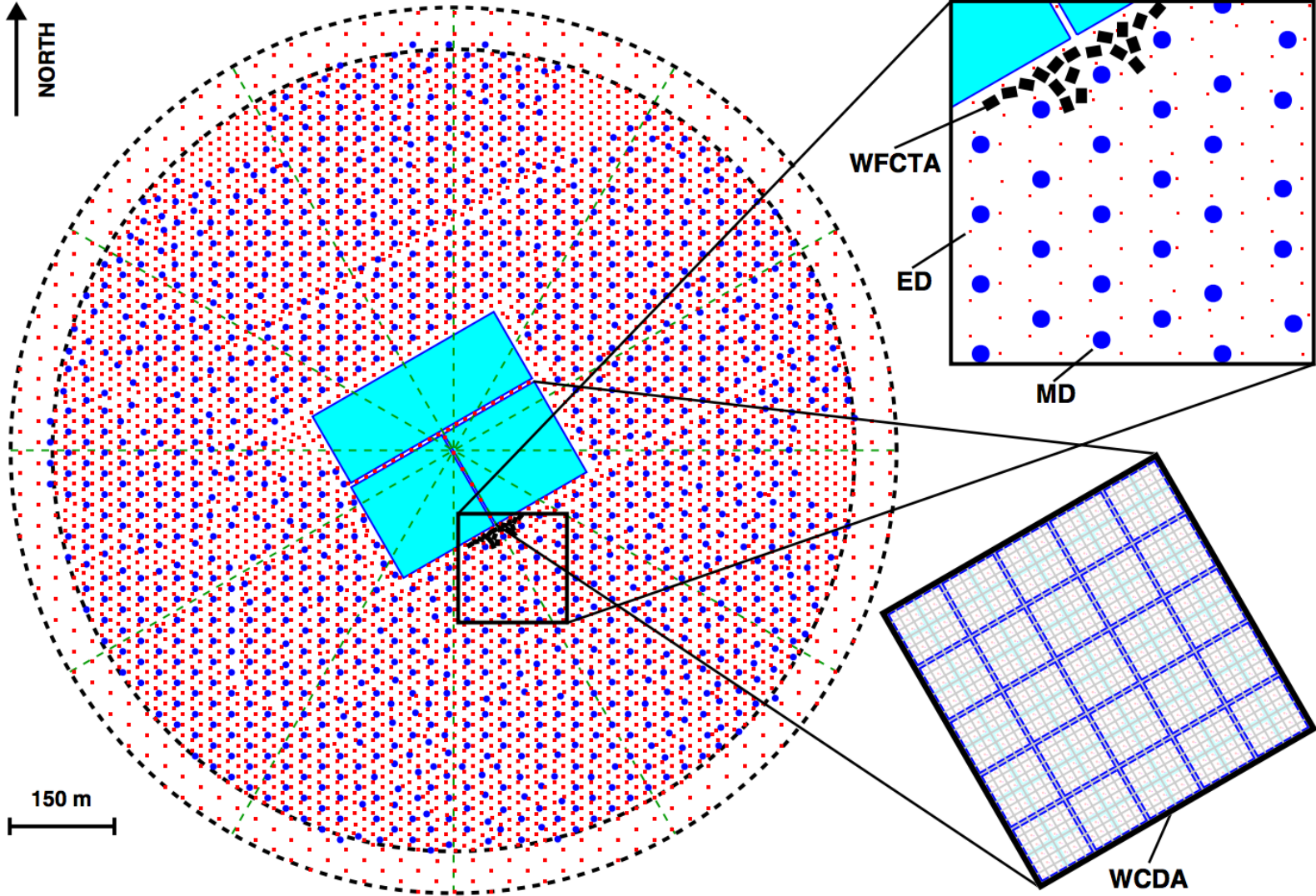


WFCTA:
24 telescopes
1024 pixels each

SCDA:
452 detectors



LHAASO



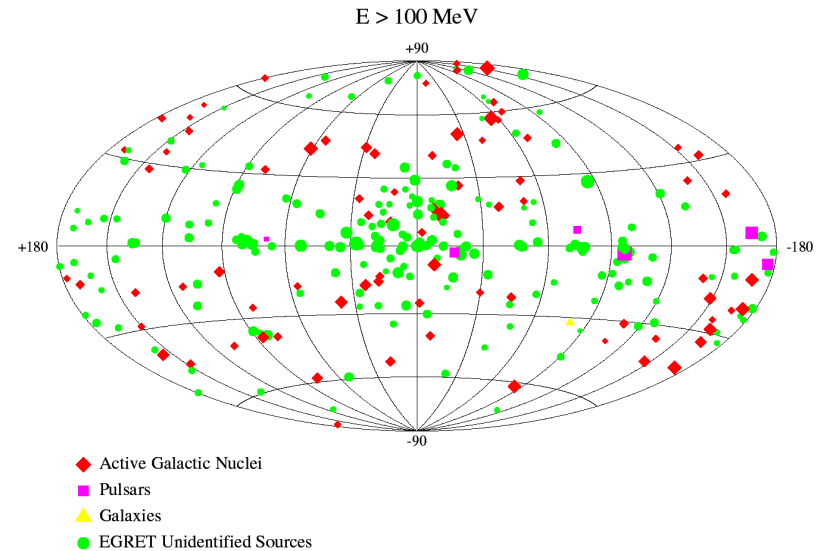
Astrofisica Nucleare e Subnucleare

VHE Gamma Astrophysics

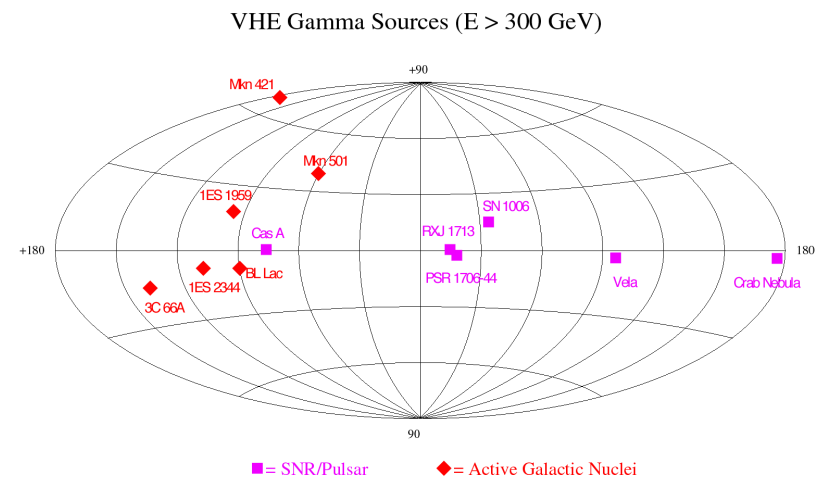
The unexplored spectrum gap

THIRD EGRET CATALOGUE OF GAMMA-RAY POINT SOURCES

- Satellites give a nice **crowded** picture of energies up to 10 GeV.

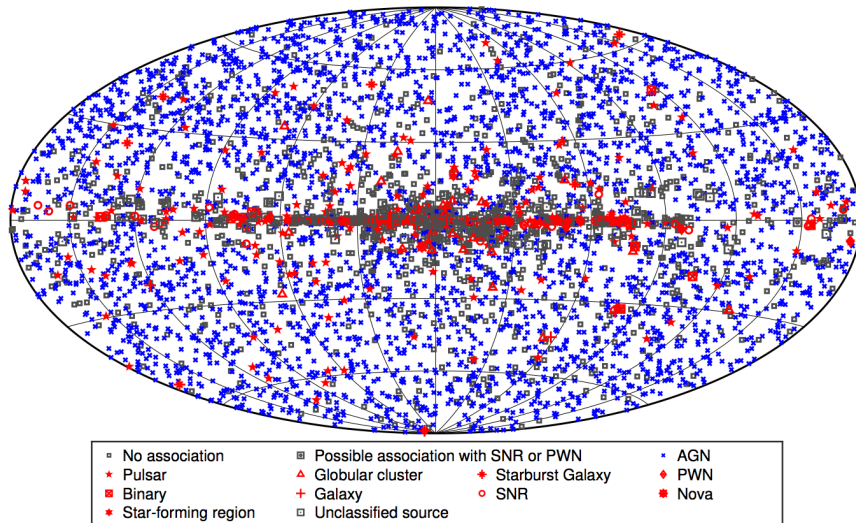


- Ground based experiments show very **few sources** with energies > ~300 GeV.

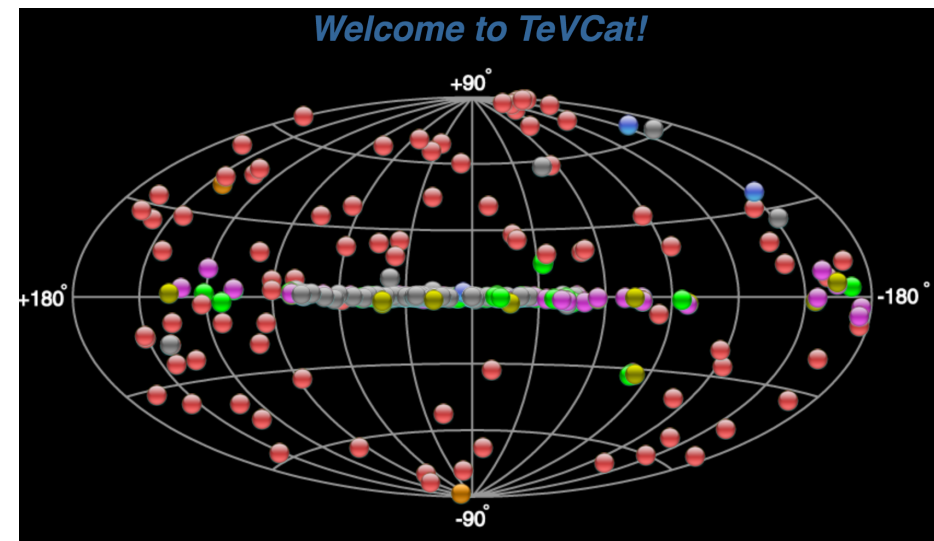


VHE sky

- The HE sky up to 100 GeV.



- The VHE sky from 50 GeV.



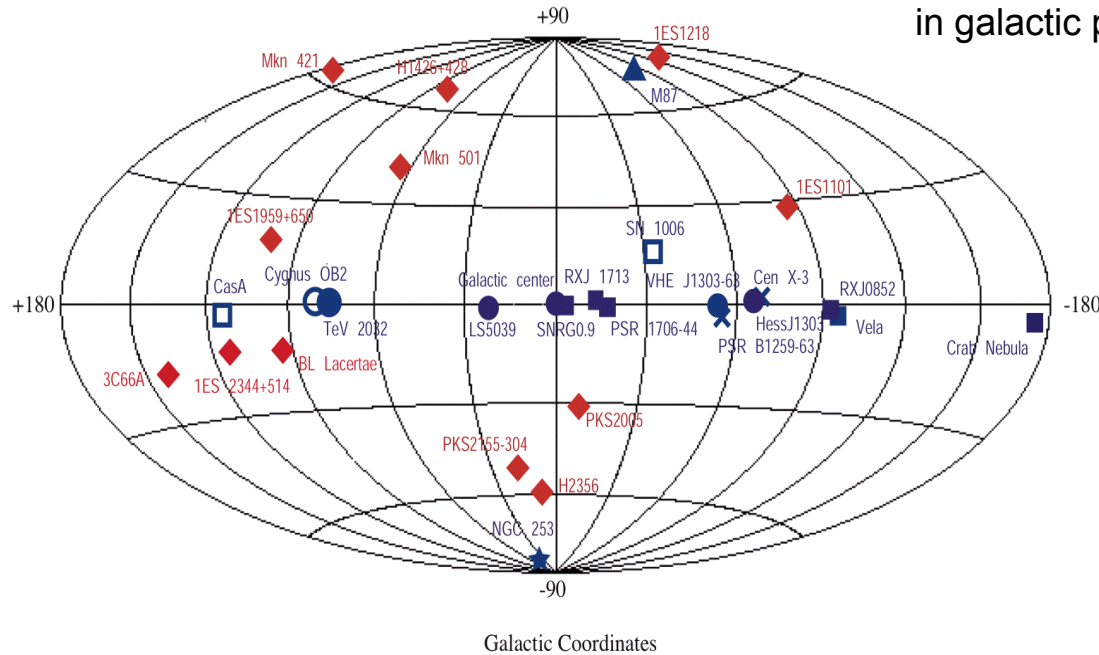
<http://tevcat.uchicago.edu/>

The VHE γ ray sky

2005

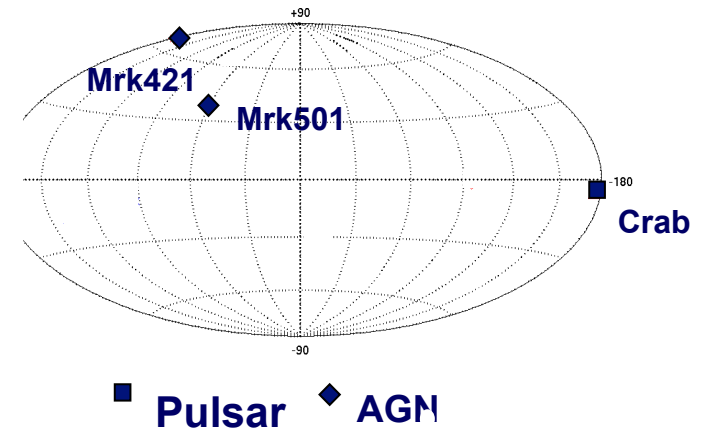
VHE Gamma Sources ($E > 100$ GeV)

(Status August 2005)



+ some additional sources in galactic plane.

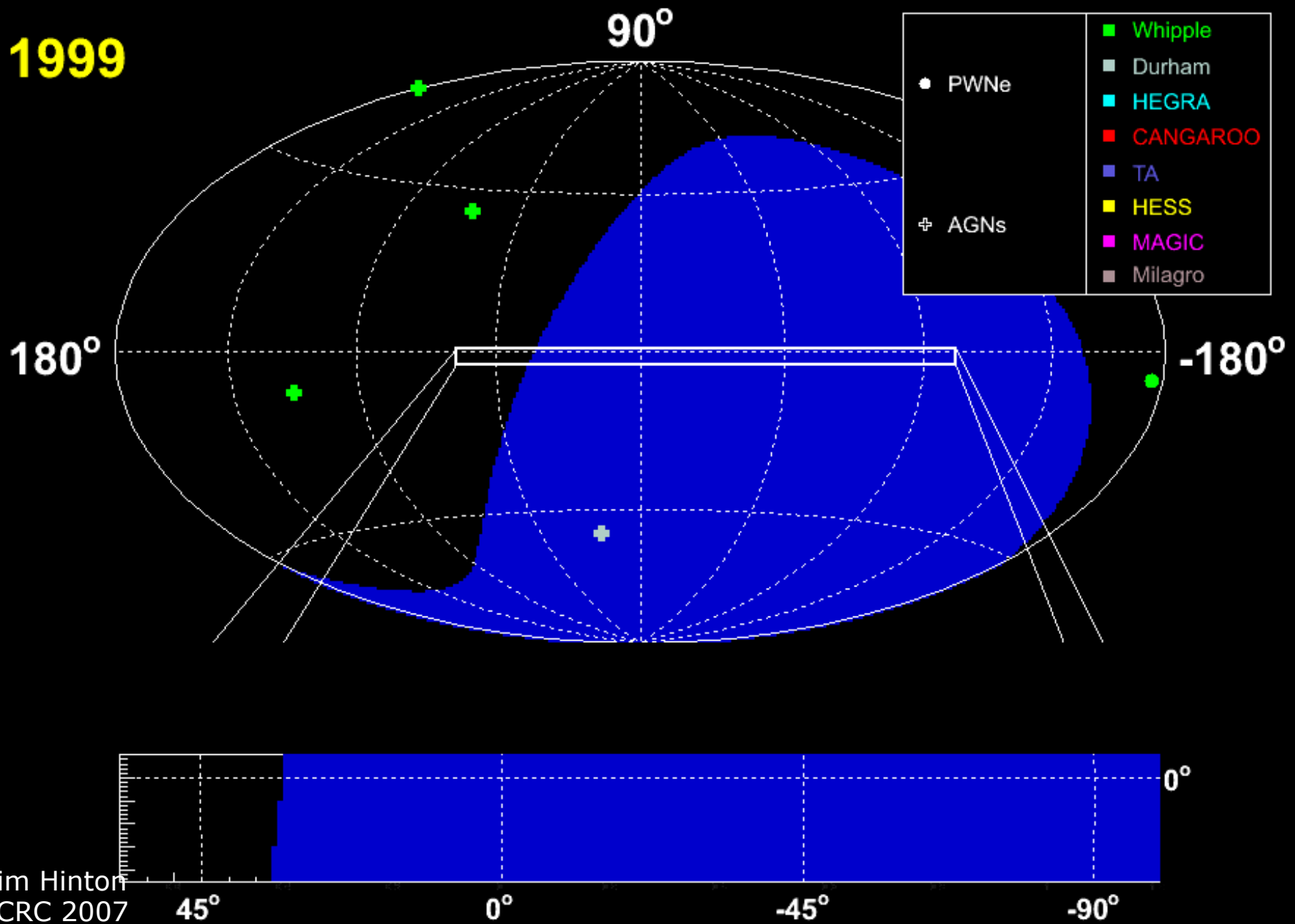
1995



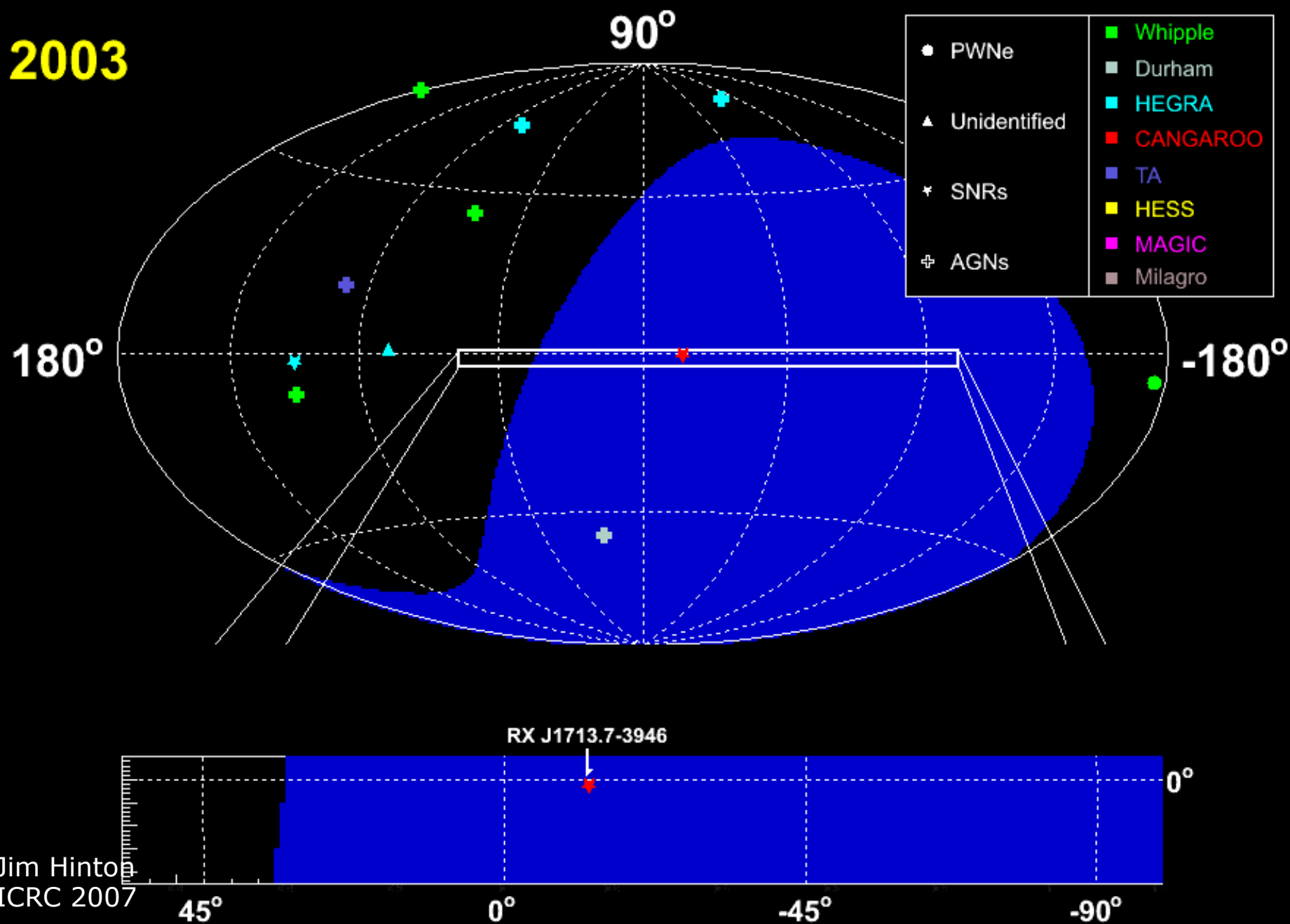
- = Pulsar/Plerion □ = SNR ★ = Starburst galaxy ○ = OB association
- ◆ = AGN (BL Lac) ▲ = Radio galaxy × = XRB ● = Undetermined

■ Pulsar ◆ AGN

1999

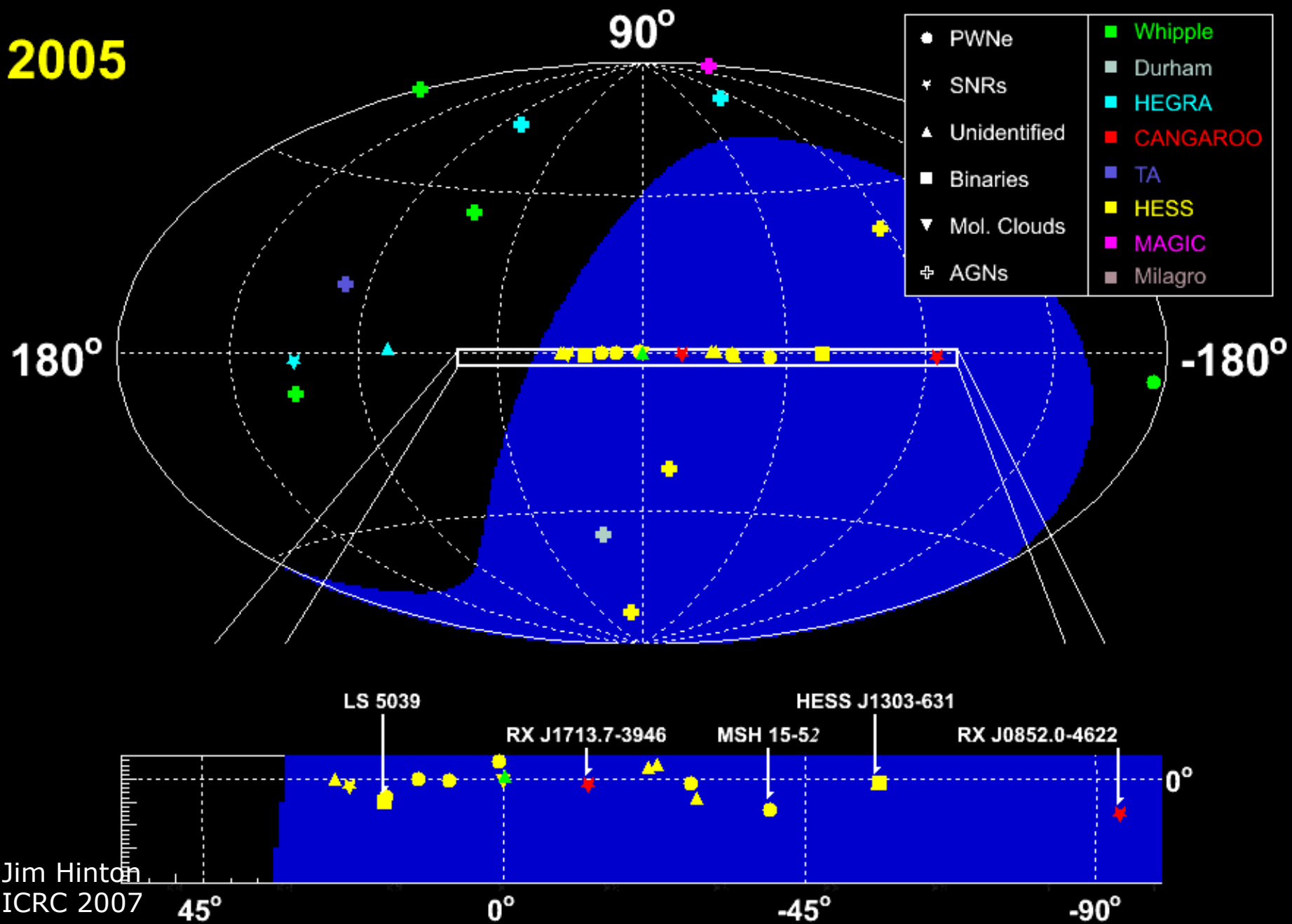


2003

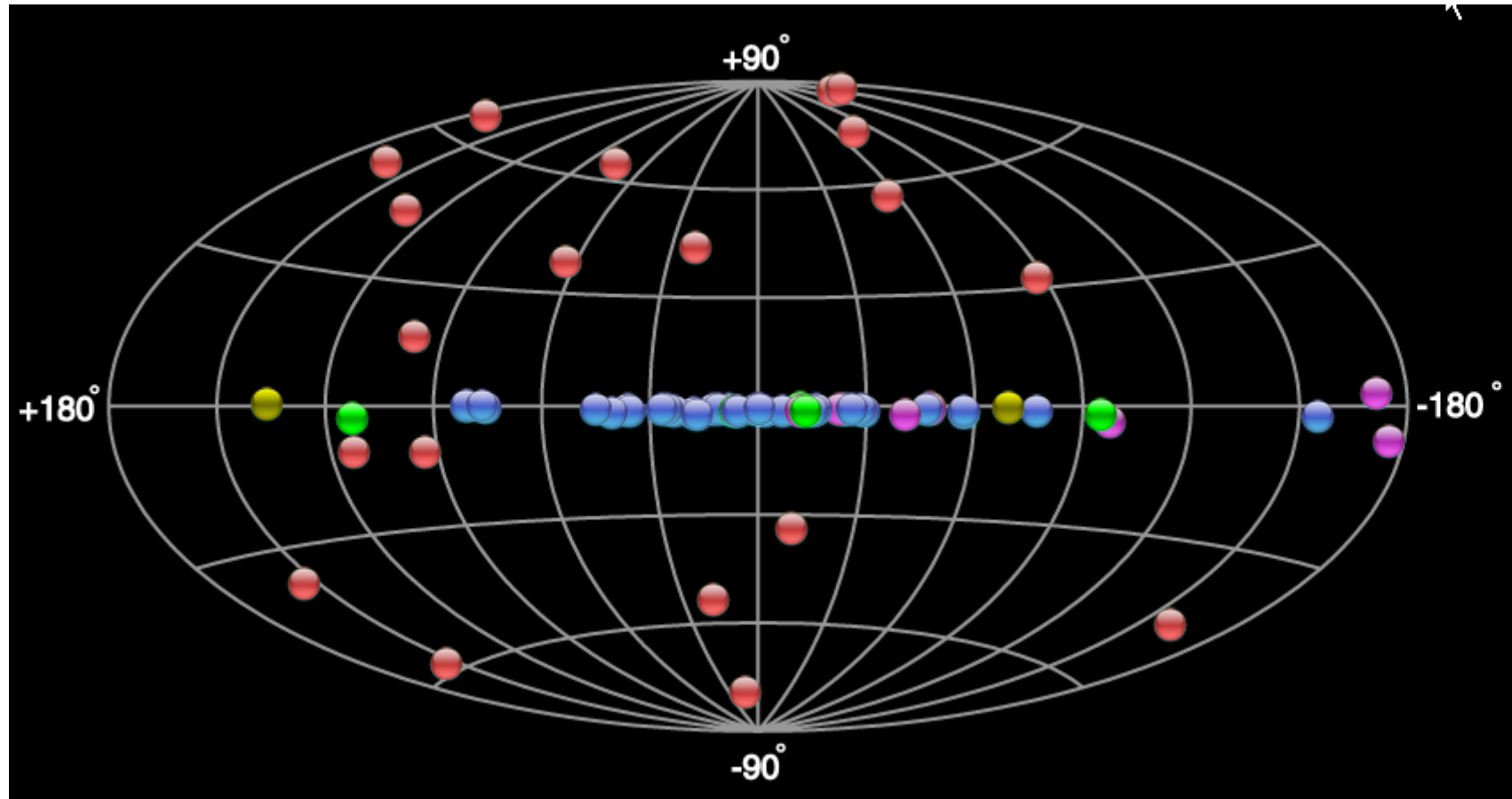


Jim Hinton
ICRC 2007

2005

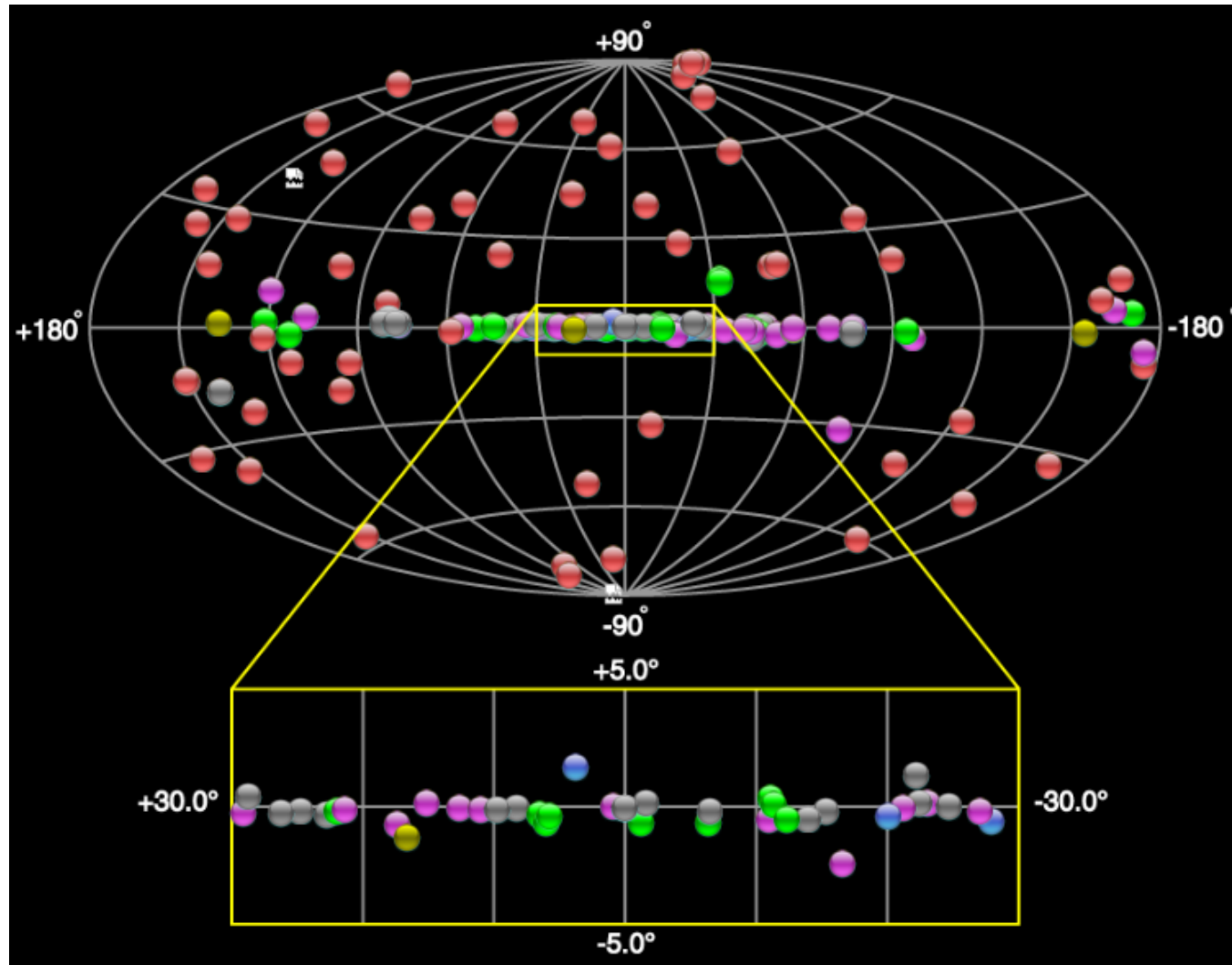


TeV Source Catalog

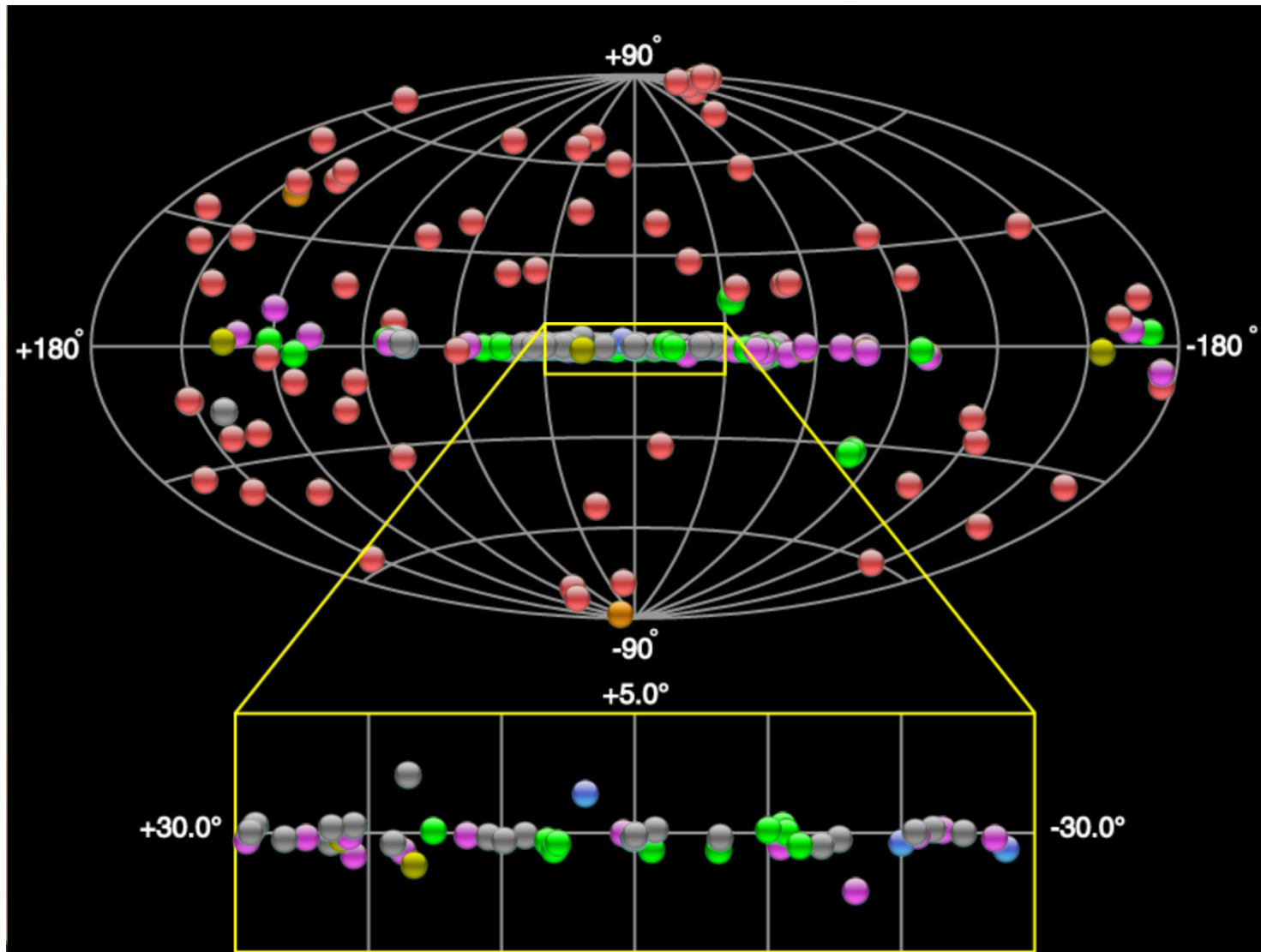


<http://tevcat.uchicago.edu/>

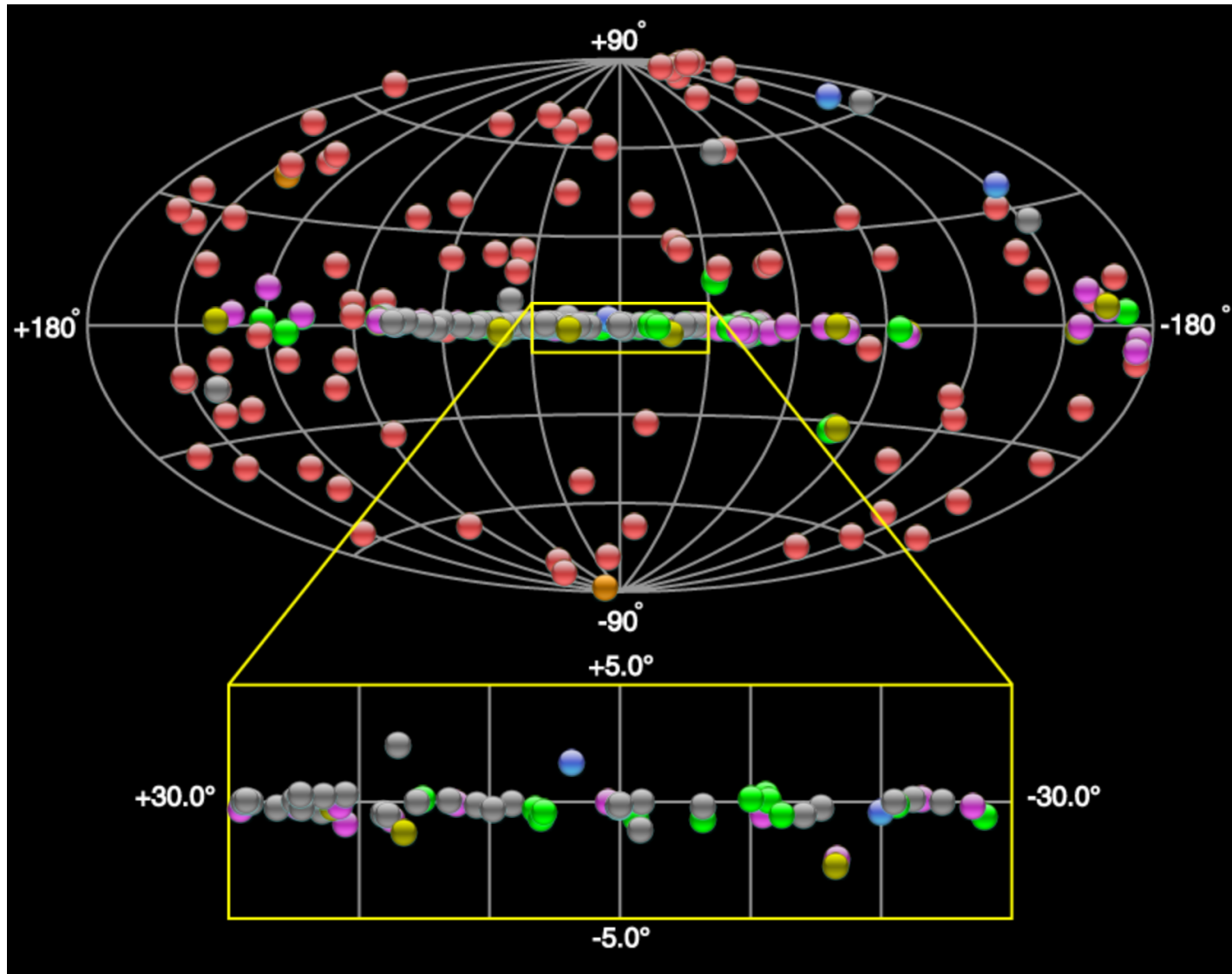
The TeV Catalog 2012



The TeV Catalog 2016

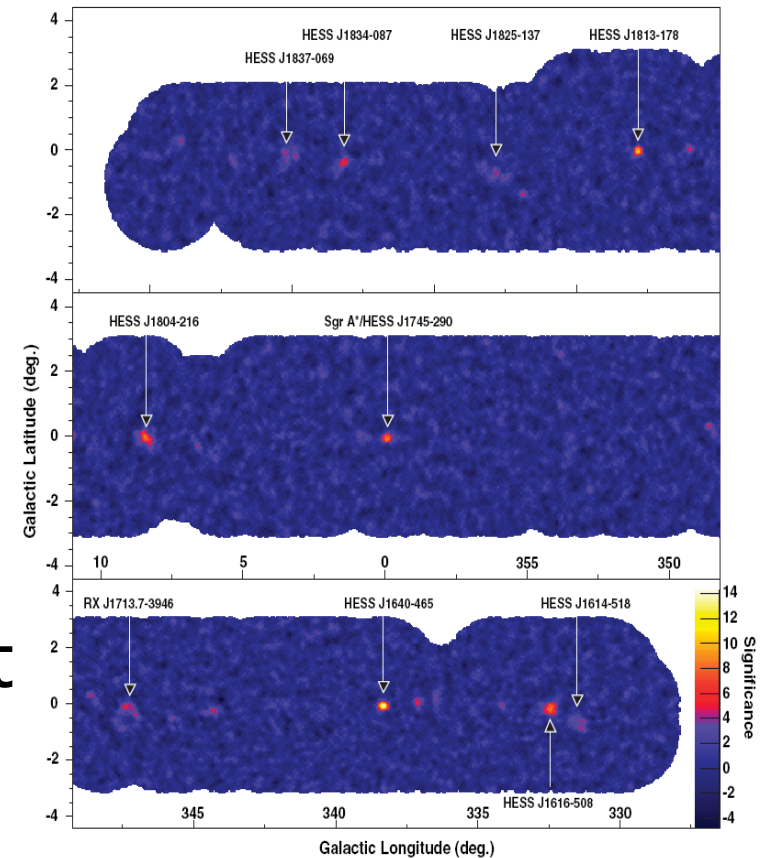


The TeV Catalog 2021

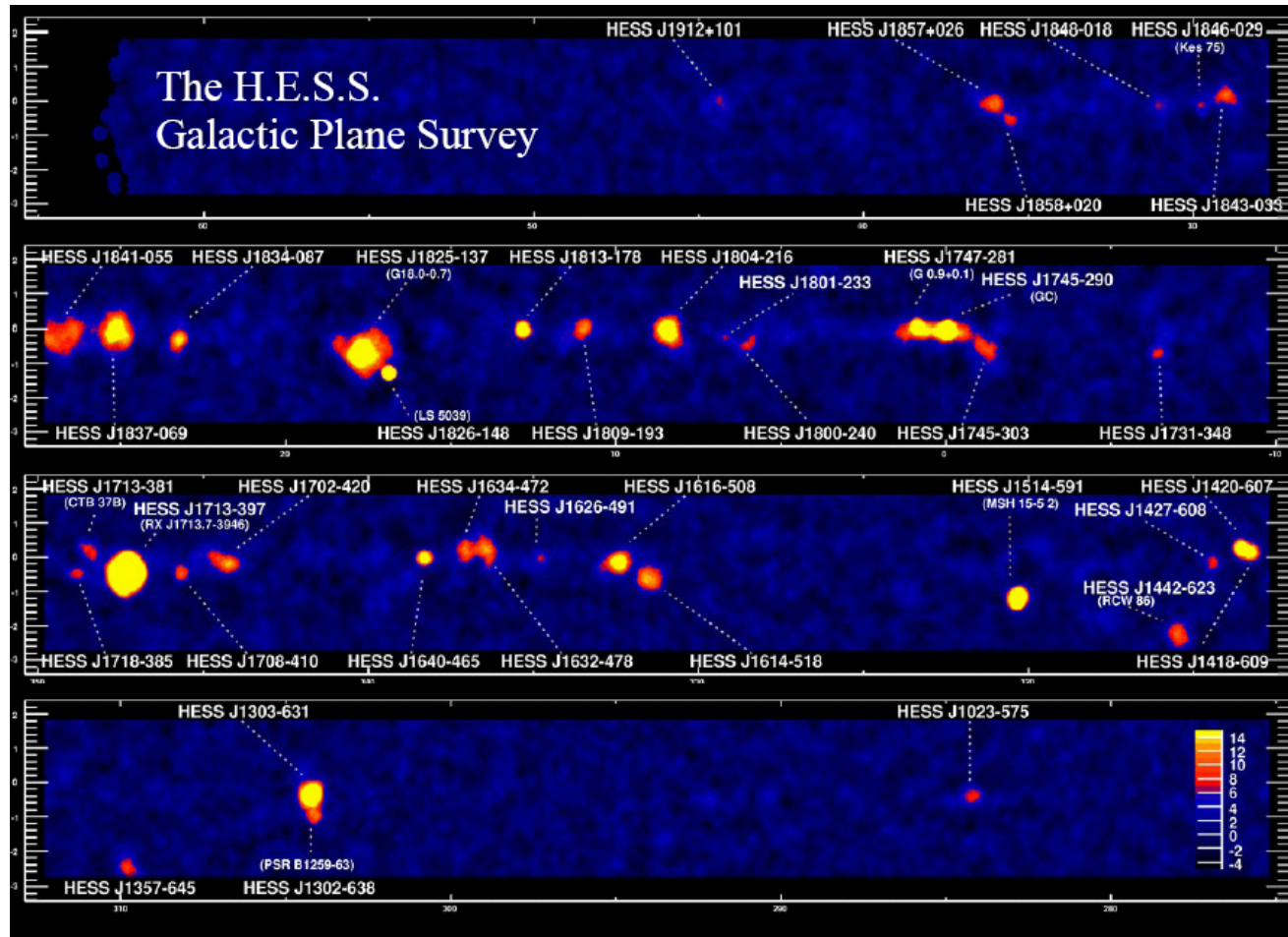


TeV Sky Survey

- HESS Galactic plane survey sees many new TeV sources (Aharonian et al. 2005)
 - This might possibly inform a detailed model of the distribution of CR sources, although the distribution is so confined to the plane that the sources (probably plerions and SNR) are at least several kpc distant

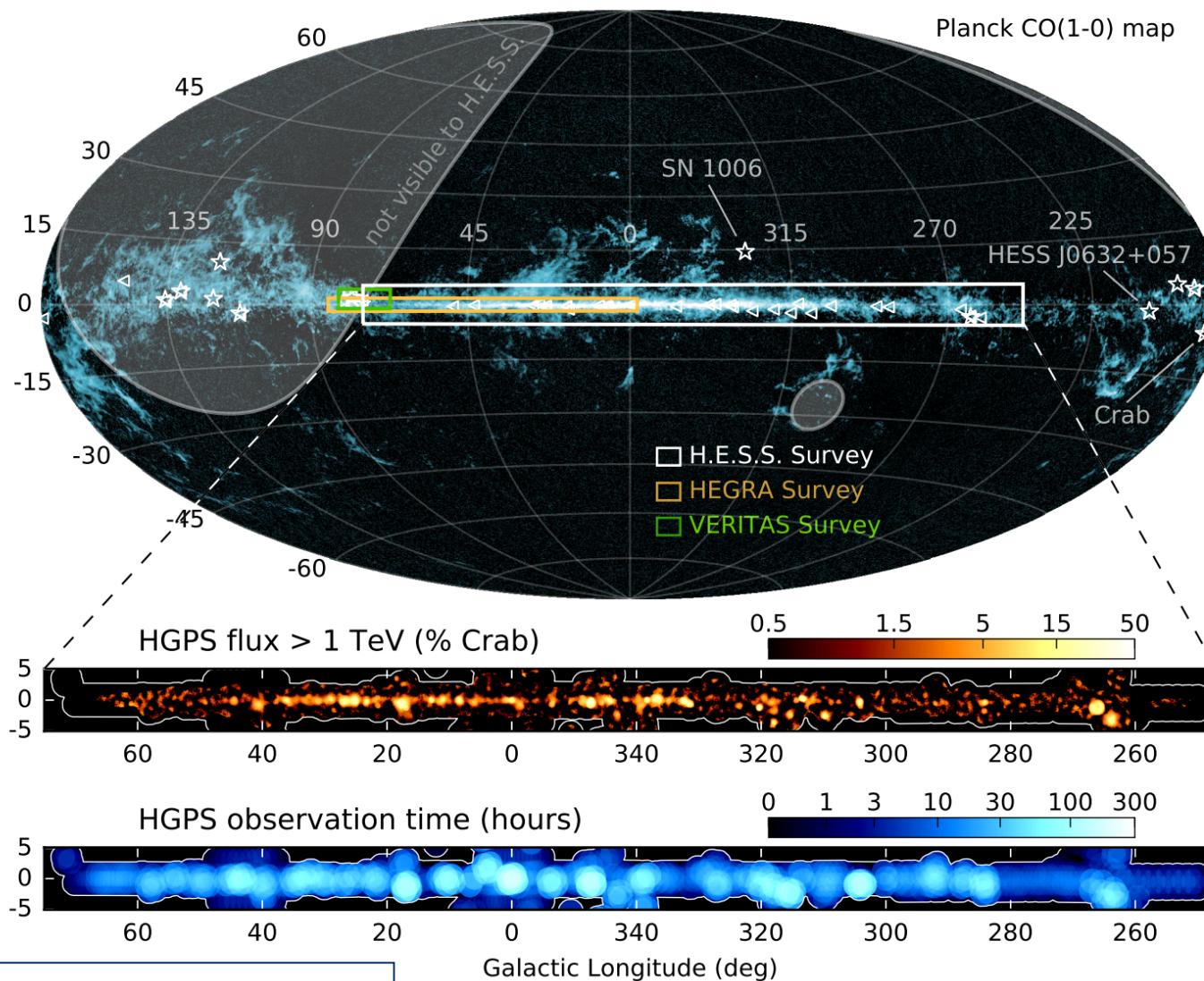


The Galactic Plane survey



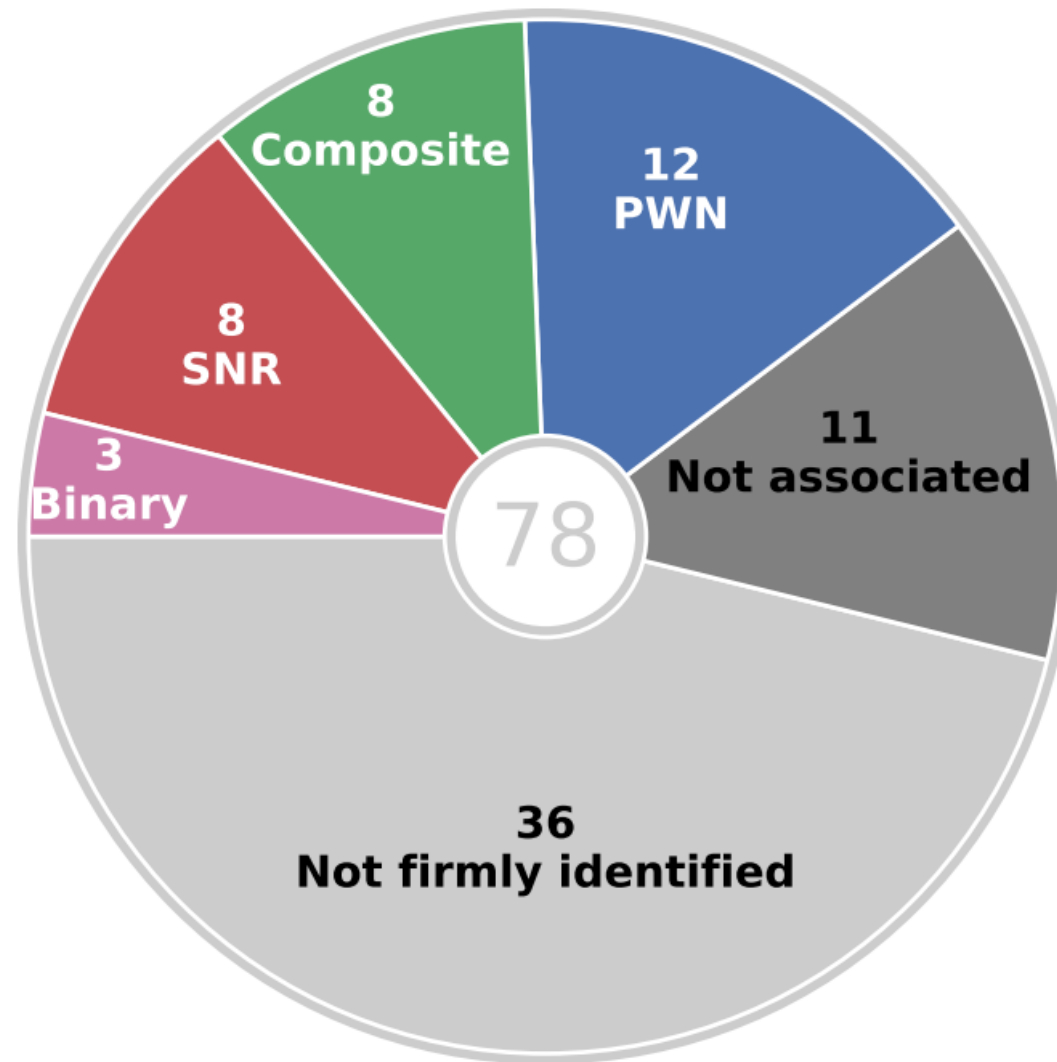
Aharonian et al. 2006

The Galactic Plane survey



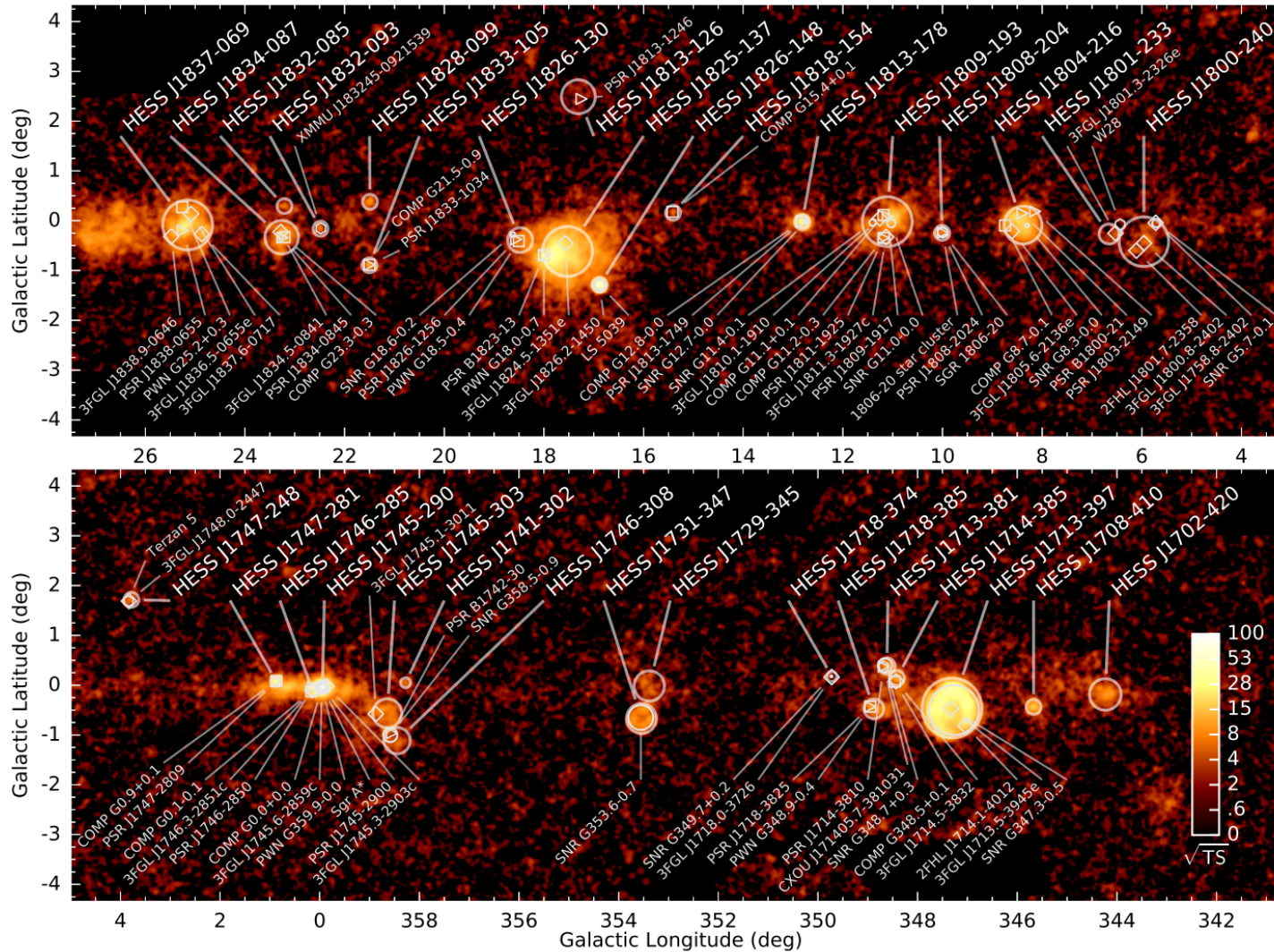
Aharonian et al. 2018

The Galactic Plane survey



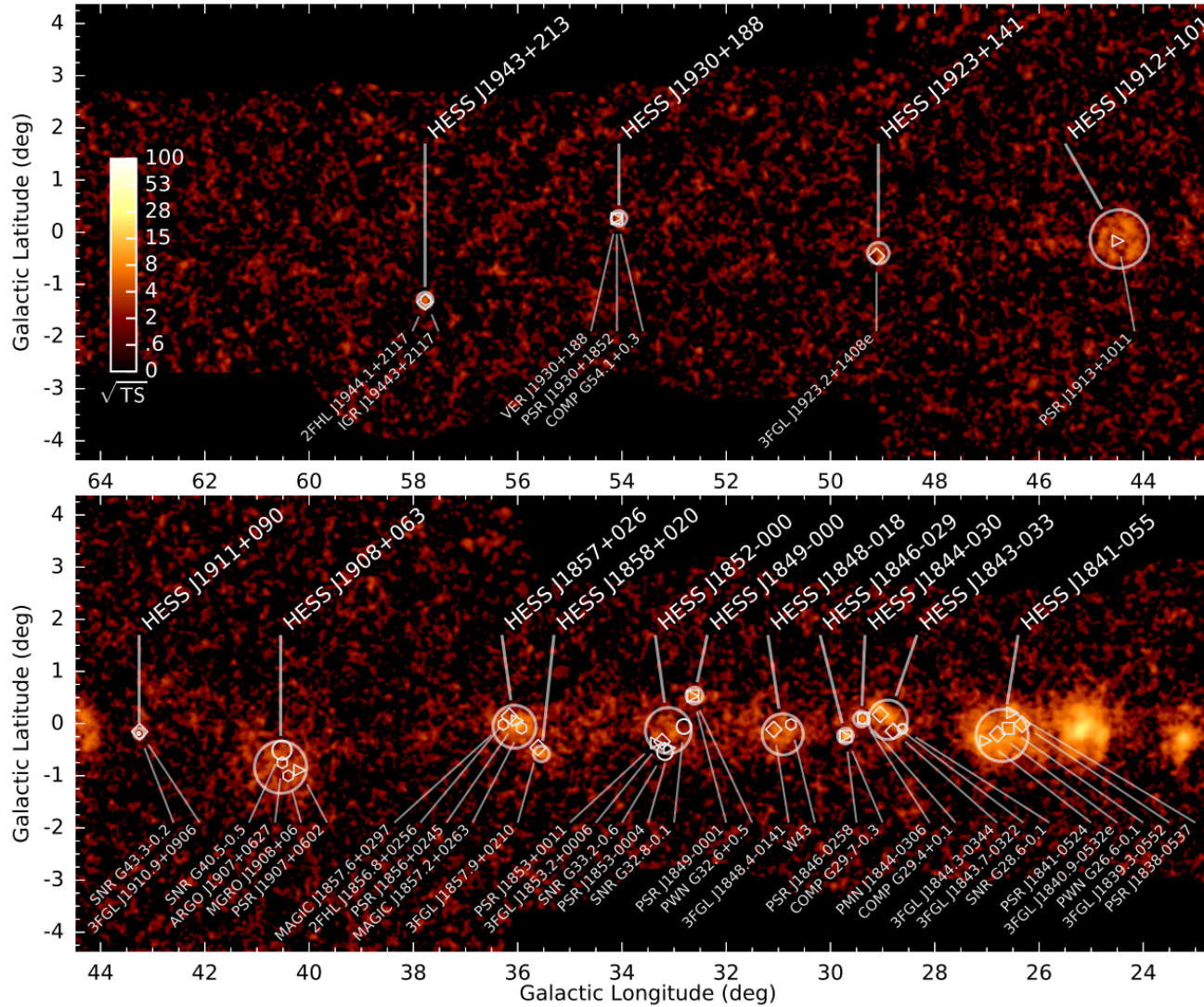
Aharonian et al. 2018

The Galactic Plane survey



Aharonian et al. 2018

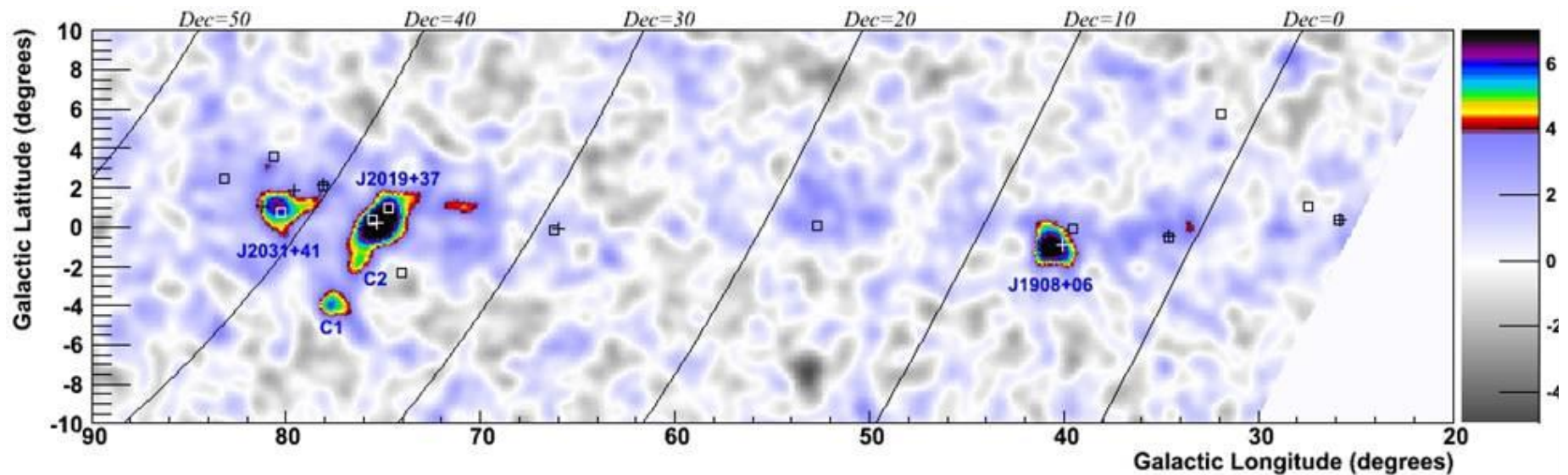
The Galactic Plane survey



Aharonian et al. 2018

MILAGRO Sky Survey

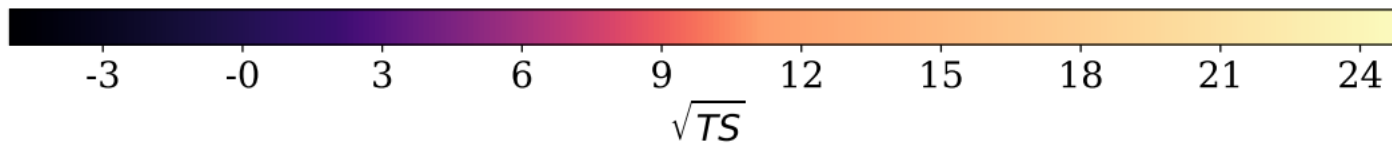
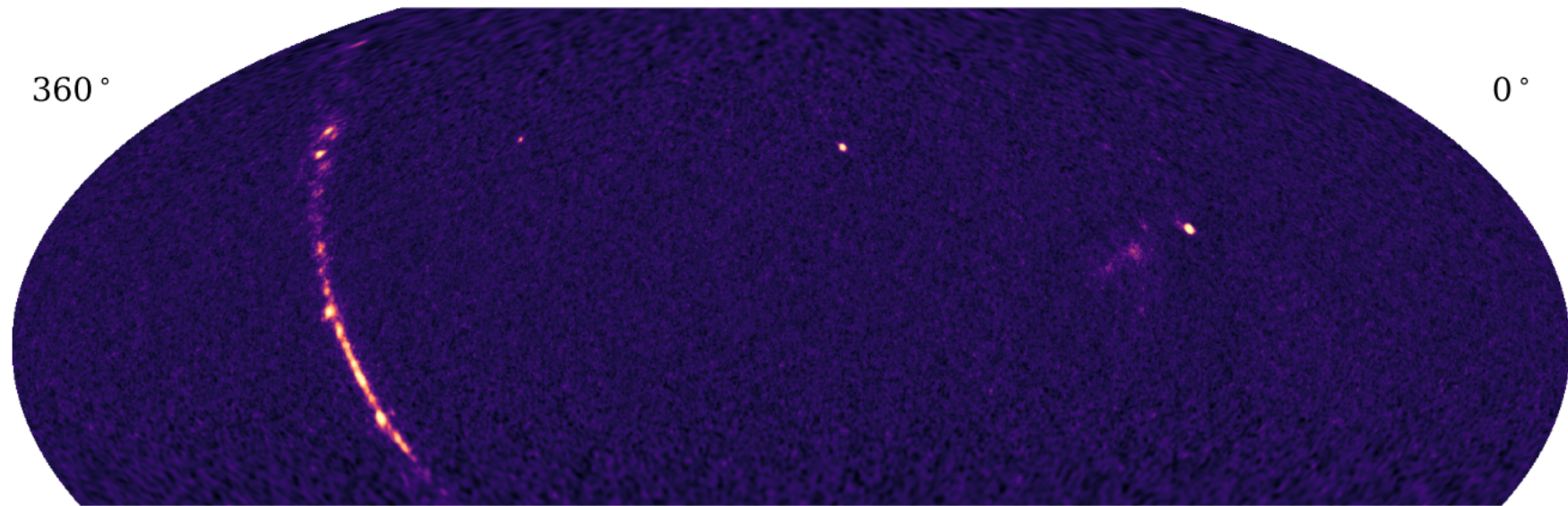
- Milagro reports detecting the diffuse emission of the Milky Way at >1 TeV energies (Abdo et al 2008)



Abdo et al. 2008

HAWC Sky Survey

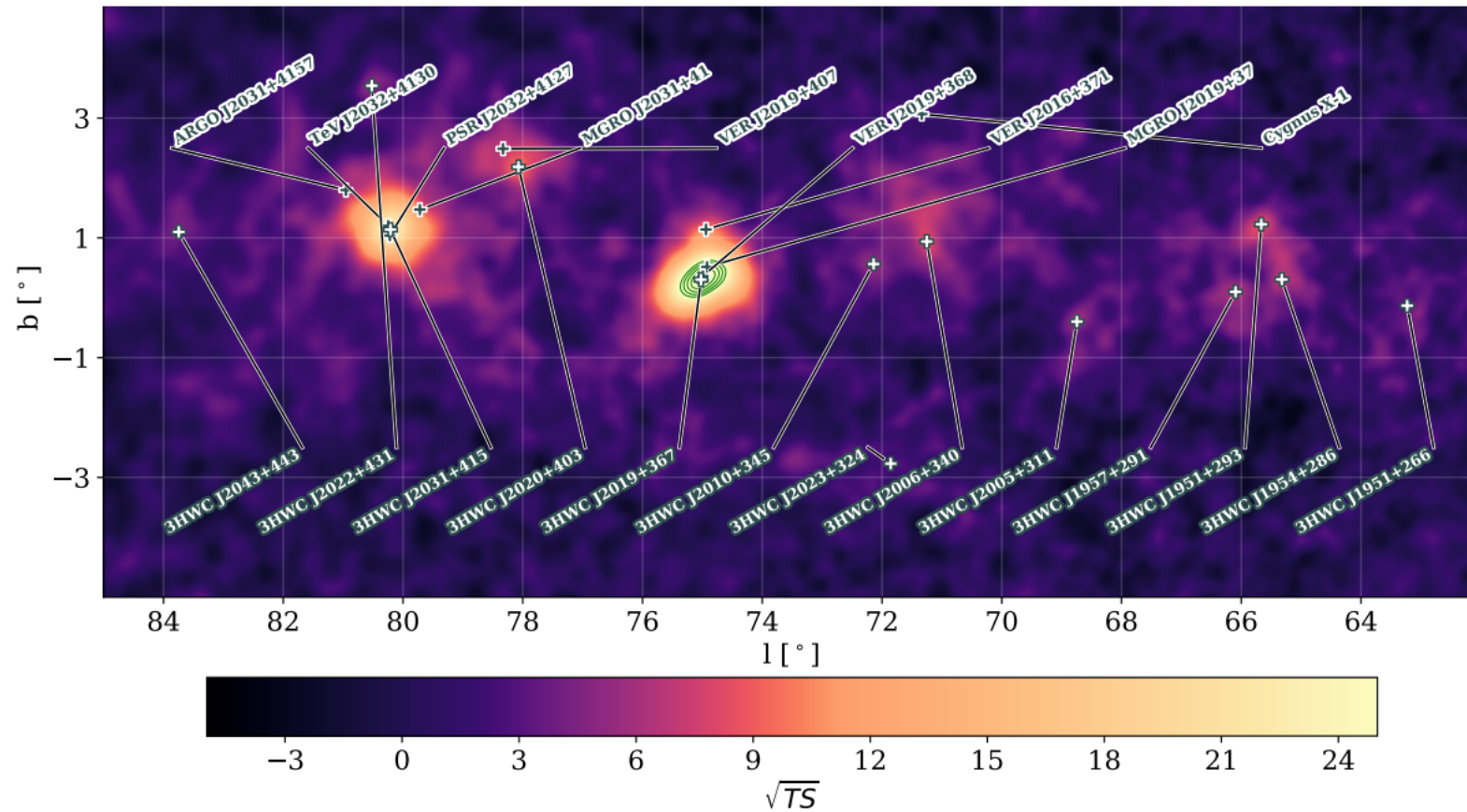
- HAWC 3rd catalog of Gamma Ray sources



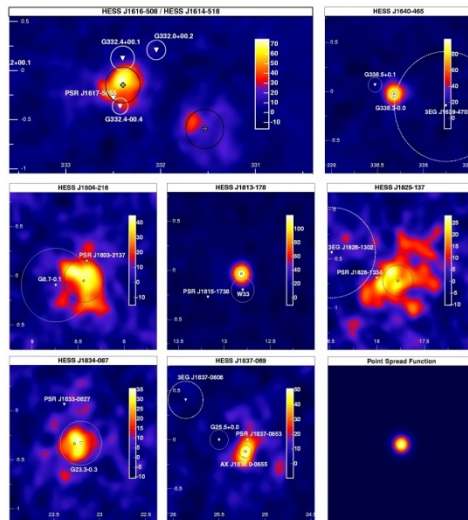
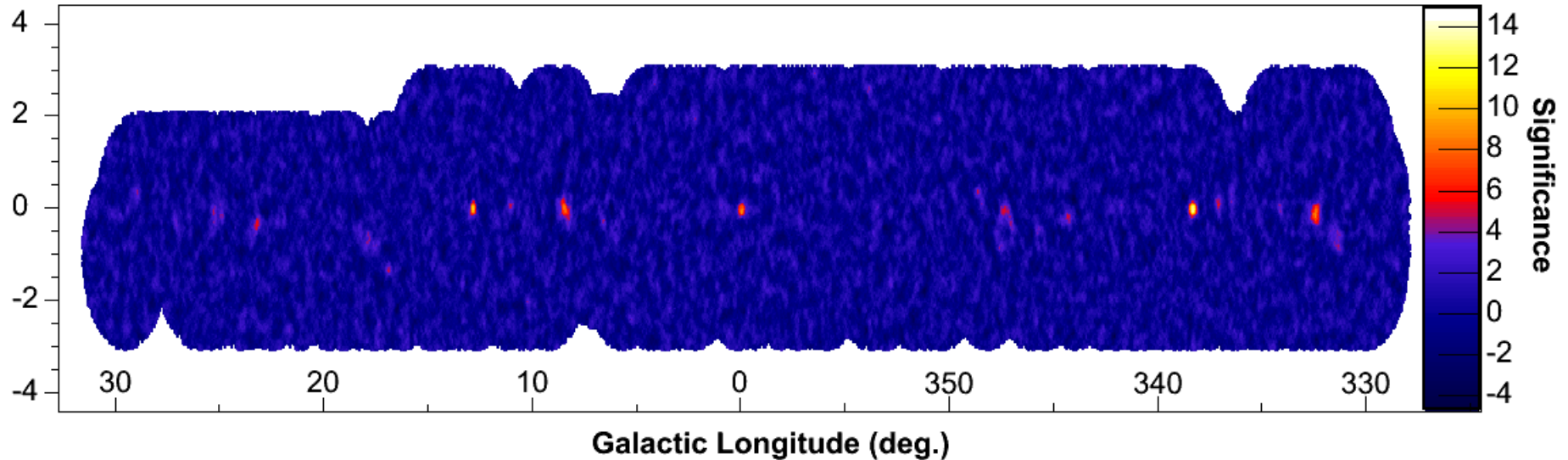
Albert et al. 2021

HAWC Sky Survey

- HAWC 3rd catalog of Gamma Ray sources

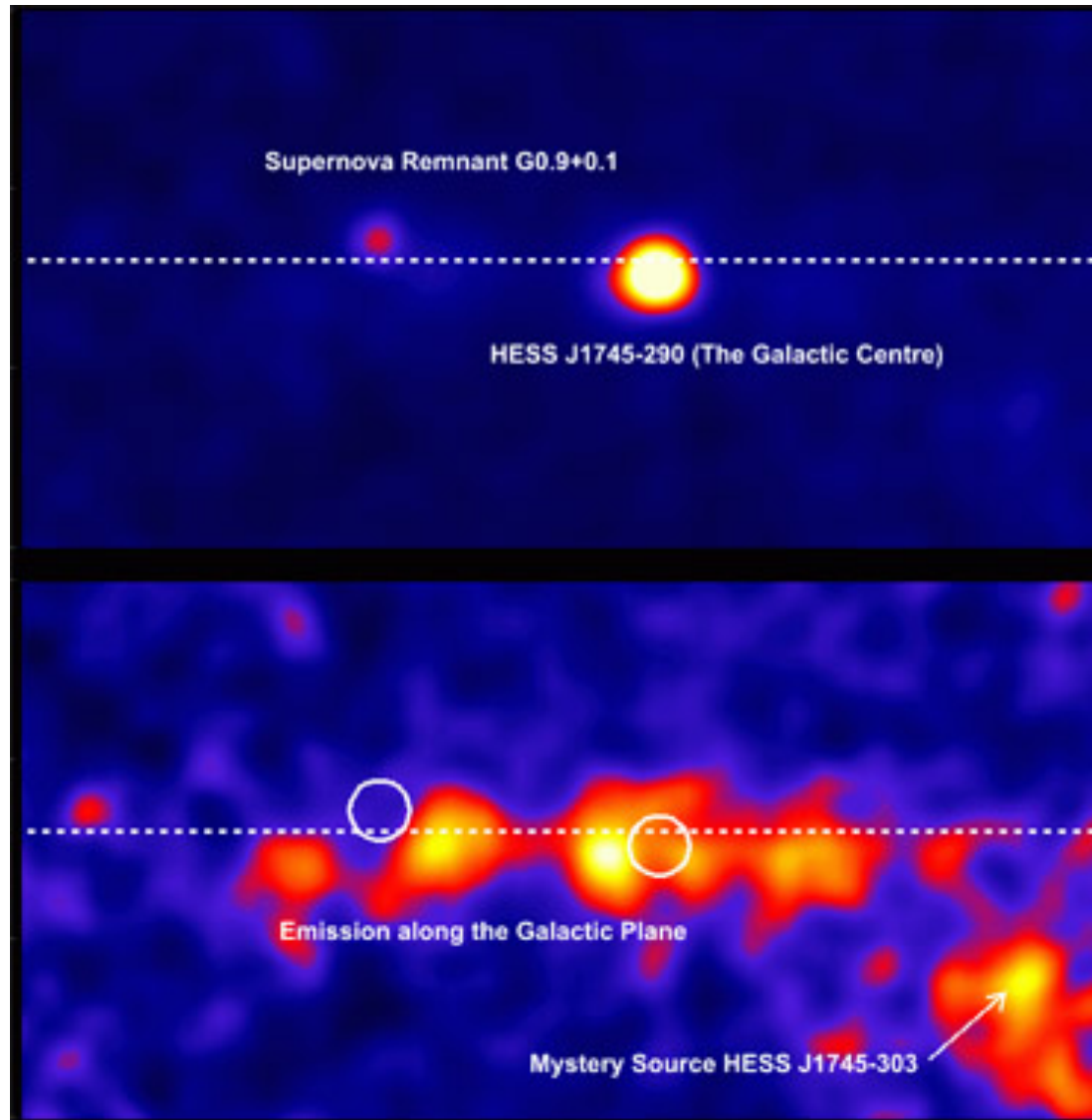


HESS "new" sources

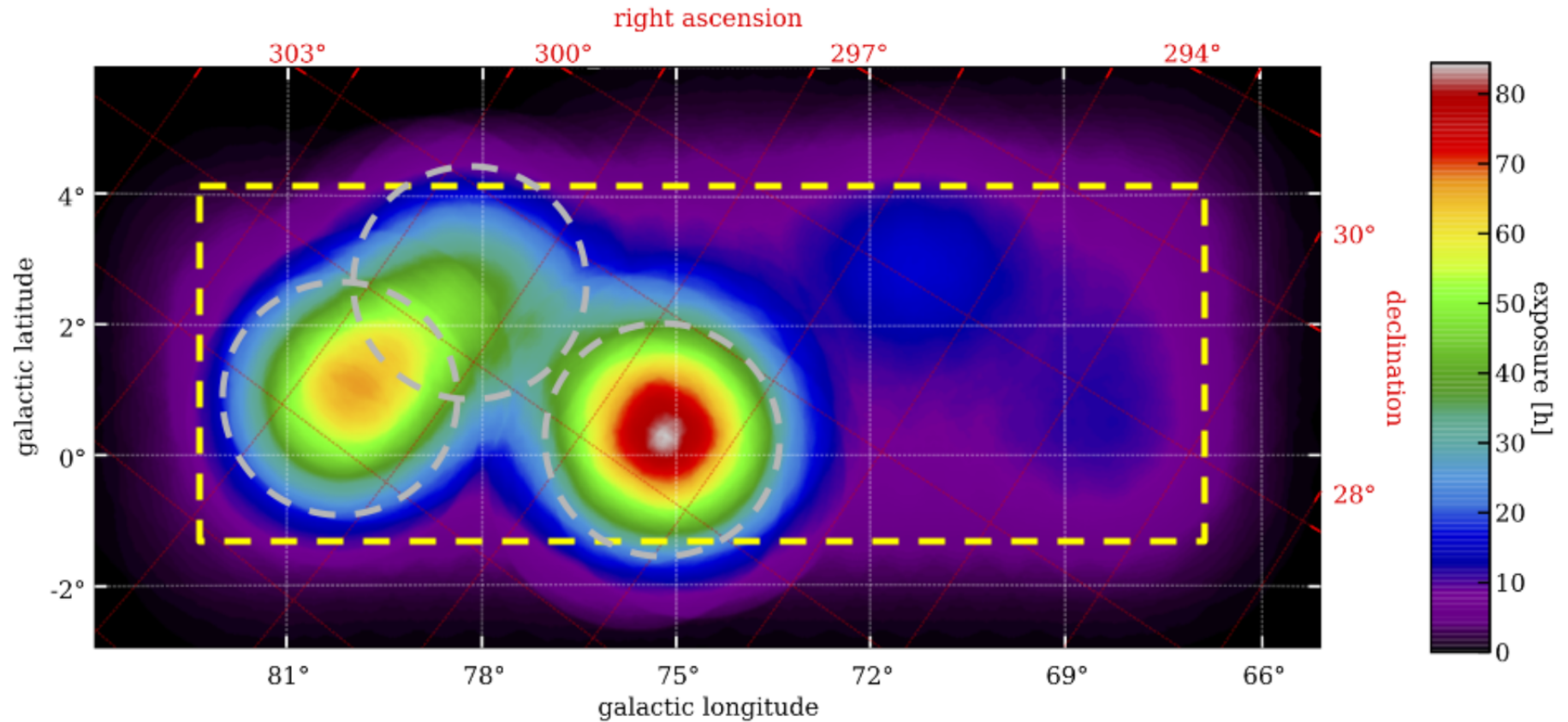


Close-up view of the new sources, discovered in the Galactic plane scan. Shown as white circles are close-by supernova remnants, that are known to be sources of very high energy gamma-rays (with the radius of the circle representing the size of the supernova remnant). Also shown in white are close-by pulsars, another class of sources of very high energy gamma-rays.

HESS Diffuse Gamma-Ray

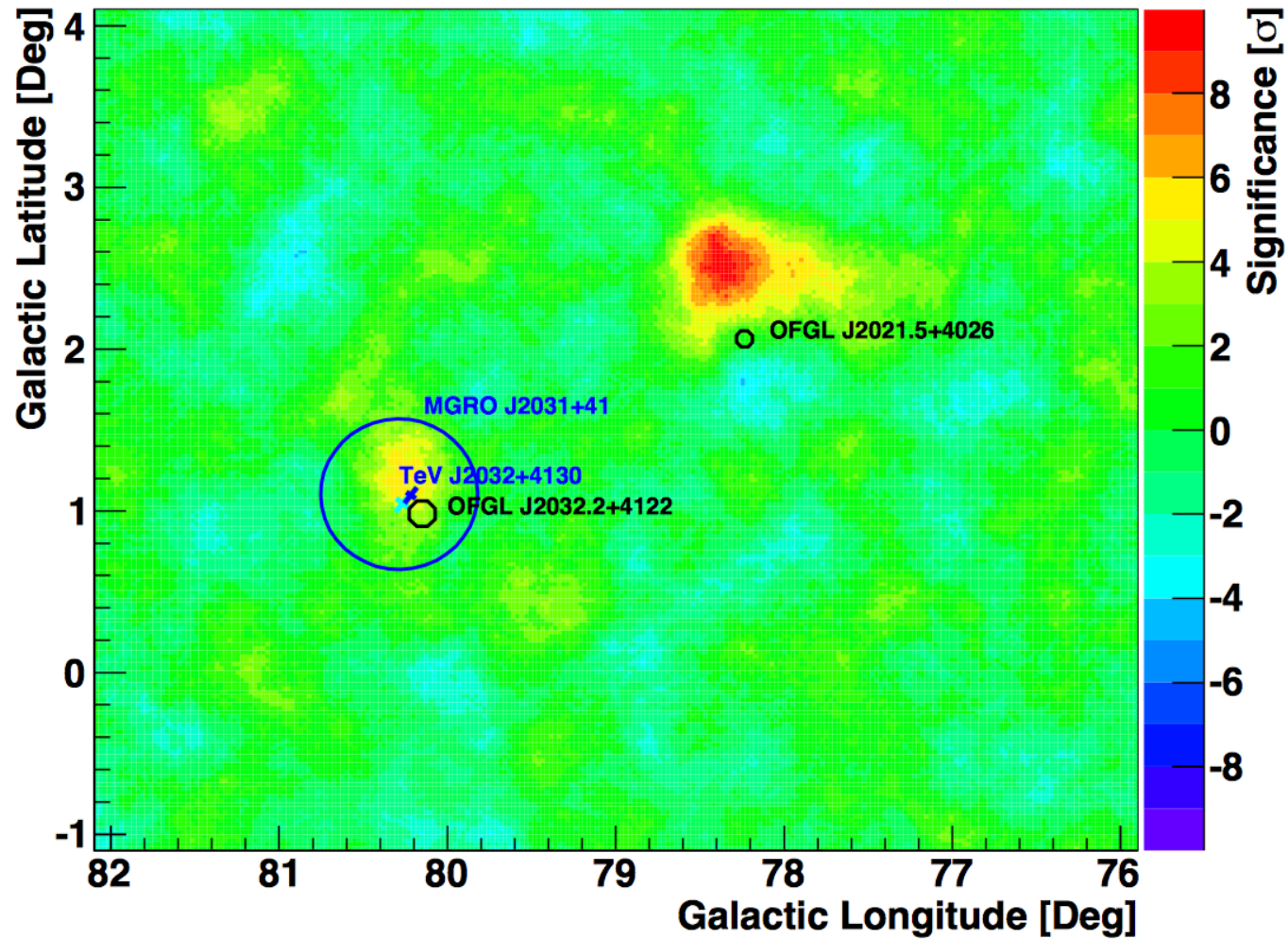


VERITAS Cygnus Survey



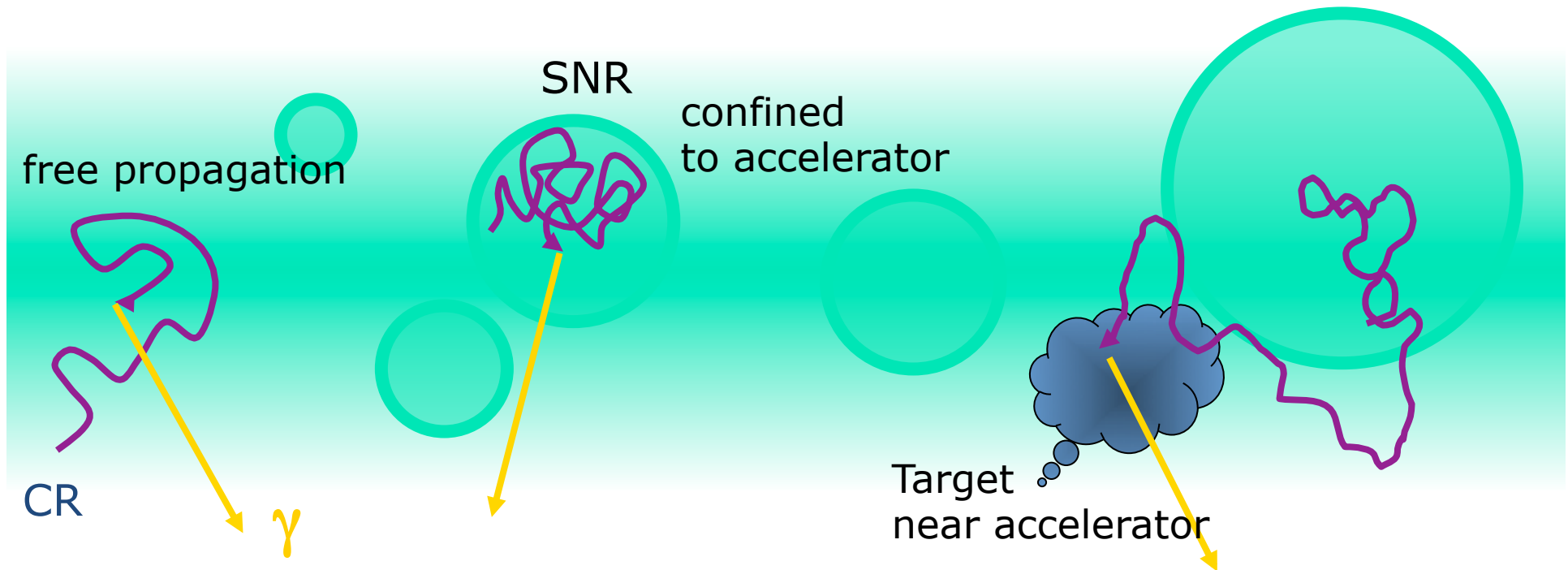
<http://arxiv.org/abs/1508.06684>

VERITAS Cygnus Survey



<http://arxiv.org/abs/0912.4492>

CR origin and propagation



VHE gamma rays from secondary interactions:

p: π^0 production and decay

e: Inverse Compton scattering and Bremsstrahlung

Trace beam density x target density

<https://arxiv.org/pdf/2111.06545.pdf>The LHAASO Collaboration^{*†}

^{*}Collaboration authors and affiliations are listed in the Supplementary Material

[†]Correspondence to: caozh@ihep.ac.cn; chensz@ihep.ac.cn; linsj6@mail.sysu.edu.cn; zhangss@ihep.ac.cn; zham@ihep.ac.cn; licong@ihep.ac.cn; wangly@ihep.ac.cn; yinlq@ihep.ac.cn; felix.aharonian@mpi-hd.mpg.de; ryliu@nju.edu.cn





The Crab pulsar and the surrounding nebula powered by the pulsar's rotational energy through the formation and termination of a relativistic electron-positron wind is a bright source of gamma-rays carrying crucial information about this complex conglomerate. We report the detection of γ -rays with a spectrum showing gradual steepening over three energy decades, from 5×10^{-4} to 1.1 petaelectronvolt (PeV). The ultra-high-energy photons exhibit the presence of a PeV electron accelerator (a pevatron) with an acceleration rate exceeding 15 % of the absolute theoretical limit. Assuming that unpulsed γ -rays are produced at the termination of the pulsar's wind, we constrain the pevatron's size, between 0.025 and 0.1 pc, and the magnetic field, $\approx 110 \mu\text{G}$. The production rate of PeV electrons, $2.5 \times 10^{36} \text{erg s}^{-1}$, constitutes 0.5% of the pulsar's spin-down luminosity, although we do not exclude a non-negligible contribution of PeV protons to the production of the highest energy γ -rays.

JC - 04

Ultrahigh-energy photons up to 1.4 petaelectronvolts from 12 γ -ray Galactic sources

Show affiliations

Show all authors

Cao, Zhen  ; Aharonian, F. A.  ; An, Q. ; Axikegu, Bai, L. X. ; Bai, Y. X. ; Bao, Y. W. ; Bastieri, D.  ; Bi, X. J.  ; Bi, Y. J. ; Cai, H. ; Cai, J. T. ; Cao, Zhe ; Chang, J. ; Chang, J. F. ; Chang, X. C. ; Chen, B. M. ; Chen, J. ; Chen, L. ; Chen, Liang ; Chen, Long ; ...

The extension of the cosmic-ray spectrum beyond 1 petaelectronvolt (PeV; 10^{15} electronvolts) indicates the existence of the so-called PeVatrons—cosmic-ray factories that accelerate particles to PeV energies. We need to locate and identify such objects to find the origin of Galactic cosmic rays¹. The principal signature of both electron and proton PeVatrons is ultrahigh-energy (exceeding 100 TeV) γ radiation. Evidence of the presence of a proton PeVatron has been found in the Galactic Centre, according to the detection of a hard-spectrum radiation extending to 0.04 PeV (ref. ²). Although γ -rays with energies slightly higher than 0.1 PeV have been reported from a few objects in the Galactic plane³⁻⁶, unbiased identification and in-depth exploration of PeVatrons requires detection of γ -rays with energies well above 0.1 PeV. Here we report the detection of more than 530 photons at energies above 100 teraelectronvolts and up to 1.4 PeV from 12 ultrahigh-energy γ -ray sources with a statistical significance greater than seven standard deviations. Despite having several potential counterparts in their proximity, including pulsar wind nebulae, supernova remnants and star-forming regions, the PeVatrons responsible for the ultrahigh-energy γ -rays have not yet been firmly localized and identified (except for the Crab Nebula), leaving open the origin of these extreme accelerators.

Publication:

Nature, Volume 594, Issue 7861, p.33-36

JC-04

Revealing X-ray and gamma ray temporal and spectral similarities in the GRB 190829A afterglow

H.E.S.S. Collaboration*†

Gamma-Ray Bursts (GRBs), bright flashes of gamma rays from extragalactic sources followed by fading afterglow emission, are associated with stellar core collapse events. We report the detection of very-high-energy (VHE) gamma rays from the afterglow of GRB 190829A, between 4 and 56 hrs after the trigger, using the High Energy Stereoscopic System. The low luminosity and redshift of GRB 190829A reduce both internal and external absorption, allowing determination of its intrinsic energy spectrum. Between energies of 0.18 and 3.3 teraelectronvolts, this spectrum is described by a power law with photon index of 2.07 ± 0.09 , similar to the X-ray spectrum. The X-ray and VHE gamma-ray light curves also show similar decay profiles. These similar characteristics in the X-ray and gamma-ray bands challenge GRB afterglow emission scenarios.

JC-04

Multi-wavelength view of the close-by GRB 190829A sheds light on gamma-ray burst physics

OM SHARAN SALAFIA,^{1,2,3} MARIA EDVIGE RAVASIO,^{3,1} JUN YANG,⁴ TAO AN,^{5,6} MONICA ORIENTI,⁷
GIANCARLO GHIRLANDA,^{1,2} LARA NAVA,^{1,8} MARCELLO GIROLETTI,⁷ PRASHANTH MOHAN,⁶ RICCARDO SPINELLI,^{9,1}
YINGKANG ZHANG,⁵ BENITO MARCOTE,¹⁰ GIUSEPPE CIMÒ,¹⁰ XUEFENG WU,¹¹ AND ZHIXUAN LI¹²

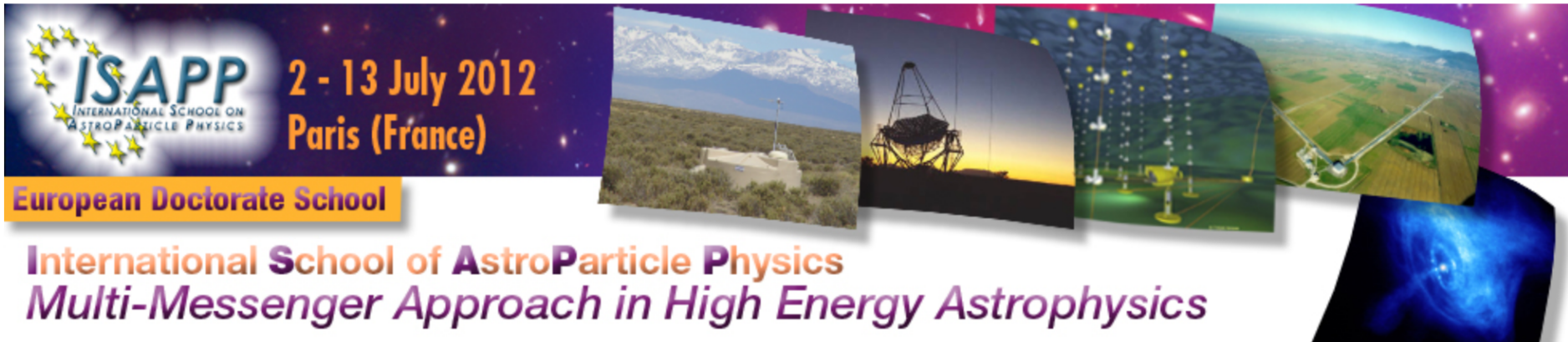
ABSTRACT

We monitored the position of the close-by (about 370 Mpc) gamma-ray burst GRB 190829A, which originated from a massive star collapse, through very long baseline interferometry (VLBI) observations with the European VLBI Network and the Very Long Baseline Array, carrying out a total of 9 observations between 9 and 117 days after the gamma-ray burst at 5 and 15 GHz, with a typical resolution of few mas. From a state-of-the-art analysis of these data, we obtained valuable limits on the source size and expansion rate. The limits are in agreement with the size evolution entailed by a detailed modelling of the multi-wavelength light curves with a forward plus reverse shock model, which agrees with the observations across almost 18 orders of magnitude in frequency (including the HESS data at TeV photon energies) and more than 4 orders of magnitude in time. Thanks to the multi-wavelength, high-cadence coverage of the afterglow, inherent degeneracies in the afterglow model are broken to a large extent, allowing us to capture some unique physical insights: we find a low prompt emission efficiency $\lesssim 10^{-3}$; a low fraction of relativistic electrons in the forward shock downstream $\chi_e < 13\%$ (90% credible level); a rapid decay of the magnetic field in the reverse shock downstream after the shock crossing. While our model assumes an on-axis jet, our VLBI astrometry is not sufficiently tight as to exclude any off-axis viewing angle, but we can exclude the line of sight to have been more than ~ 2 deg away from the border of the gamma-ray-producing region based on compactness arguments.

<https://arxiv.org/pdf/2106.07169.pdf>

Astrofisica Nucleare e Subnucleare

Radiation Processes



MAIN MENU

[Home](#)

[Circulars](#)

[Scientific programme](#)





[Schedule](#)

[Lecturers](#)

[Important dates](#)

Programme

Introductory courses

- From particle physics to astroparticle physics (3h) : Pierre Salati  (slides [1](#), [2](#))
- Radiation mechanisms (3h) : Malcolm S. Longair  (slides : [1](#), [2](#), [3](#))
- Multi-messenger astronomy (3h) : Jacques Paul  (slides : [1](#), [2](#))
- High energy showers (4h) : Ralph Engel  (slides : [1](#), [2](#), [3](#))

Basic Radiation Concepts

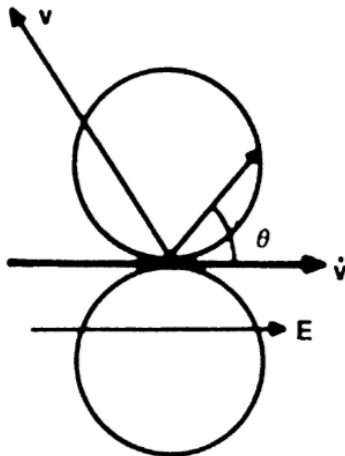
Much of what we need to understand radiation processes in X-ray and γ -ray astronomy can be derived using classical electrodynamics and central to that development is the physics of the radiation of accelerated charged particles. The central relation is the *radiation loss rate of an accelerated charged particle* in the non-relativistic limit

$$-\left(\frac{dE}{dt}\right)_{\text{rad}} = \frac{|\ddot{\mathbf{p}}|^2}{6\pi\epsilon_0 c^3} = \frac{q^2 |\ddot{\mathbf{r}}|^2}{6\pi\epsilon_0 c^3}. \quad (1)$$

$\mathbf{p} = q\mathbf{r}$ is the *dipole moment* of the accelerated electron with respect to some origin. This formula is very closely related to the radiation rate of a dipole radio antenna and so is often referred to as the radiation loss rate for *dipole radiation*. Note that I will use *SI units* in all the derivations, although it will be necessary to convert the results into the conventional units used in X-ray and γ -ray astronomy when they are confronted with observations. Thus, I will normally use metres, kilograms, teslas and so on.

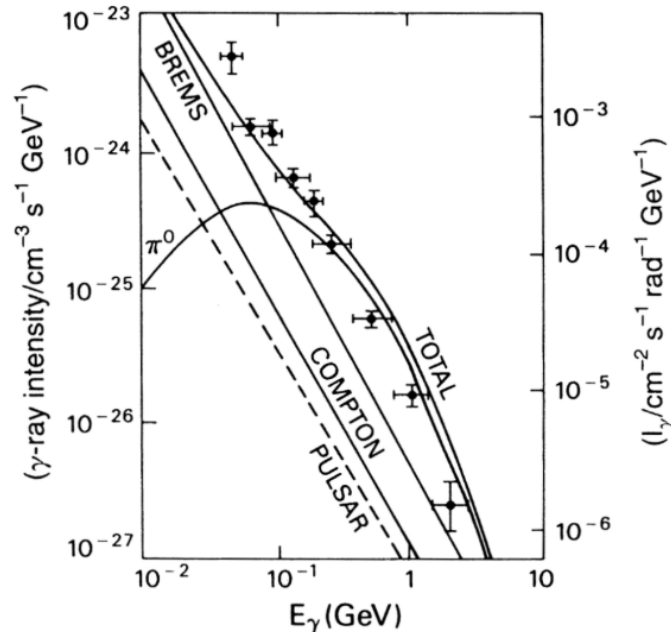
The Properties of Dipole Radiation

$$-\left(\frac{dE}{dt}\right)_{\text{rad}} = \frac{q^2 |\ddot{\mathbf{r}}|^2}{6\pi\epsilon_0 c^3}.$$



1. The total radiation rate is given by Larmor's formula. The acceleration is the *proper acceleration* of the particle and the loss rate is measured in its instantaneous rest frame.
2. The *polar diagram* of the radiation is of *dipolar* form, that is, the electric field strength varies as $\sin \theta$ and the power radiated per unit solid angle varies as $\sin^2 \theta$, where θ is the angle with respect to the acceleration vector of the particle. Notice that there is no radiation along the acceleration vector and the field strength is greatest at right angles to the acceleration vector.
3. The radiation is *polarised* with the electric field vector lying in the direction of the acceleration vector of the particle, as projected onto a sphere at distance r from the charged particle.

The Galactic Gamma-ray Emission



The diagram shows the γ -ray spectrum of our Galaxy as well as theoretical estimates of the emission by Stecker (1977). At energies $\epsilon > 70$ MeV, the dominant emission mechanism is the decay of neutral pions created in collisions between cosmic rays and the nuclei of atoms and molecules of the interstellar gas. This spectrum peaks at about 70 MeV and so there must be another mechanism which contributes at the lower energies. Relativistic bremsstrahlung may be the dominant source of emission at these energies. The spectrum labelled 'brems' is derived from an extrapolation of the relativistic electron spectrum in our Galaxy to energies $1 < E < 1000$ MeV.

Synchrotron Radiation

The synchrotron radiation, the emission of very relativistic and ultrarelativistic electrons gyrating in a magnetic field, is the process which dominates much of high energy astrophysics. It was originally observed in early betatron experiments in which electrons were first accelerated to ultrarelativistic energies. This process is responsible for the radio emission from the Galaxy, from supernova remnants and extragalactic radio sources. It is also responsible for the non-thermal optical and X-ray emission observed in the Crab Nebula and possibly for the optical and X-ray continuum emission of quasars.

The word *non-thermal* is used frequently in high energy astrophysics to describe the emission of high energy particles. This is an unfortunate terminology since all emission mechanisms are 'thermal' in some sense. The word is conventionally taken to mean 'continuum radiation from particles, the energy spectrum of which is not Maxwellian'. In practice, continuum emission is often referred to as 'non-thermal' if it cannot be described by the spectrum of thermal bremsstrahlung or black-body radiation.

Motion of an Electron in a Uniform, Static Magnetic field

We begin by writing down the equation of motion for a particle of rest mass m_0 , charge ze and Lorentz factor $\gamma = (1 - v^2/c^2)^{-1/2}$ in a uniform static magnetic field \mathbf{B} .

$$\frac{d}{dt}(\gamma m_0 \mathbf{v}) = ze(\mathbf{v} \times \mathbf{B}) \quad (1)$$

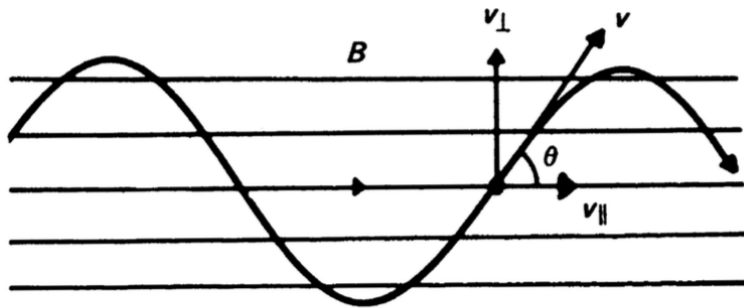
We recall that the left-hand side of this equation can be expanded as follows:

$$m_0 \frac{d}{dt}(\gamma \mathbf{v}) = m_0 \gamma \frac{d\mathbf{v}}{dt} + m_0 \gamma^3 \mathbf{v} \frac{(\mathbf{v} \cdot \mathbf{a})}{c^2} \quad (2)$$

because the Lorentz factor γ should be written $\gamma = (1 - \mathbf{v} \cdot \mathbf{v}/c^2)^{-1/2}$. In a magnetic field, the three-acceleration $\mathbf{a} = d\mathbf{v}/dt$ is always perpendicular to \mathbf{v} and consequently $\mathbf{v} \cdot \mathbf{a} = 0$. As a result,

$$\gamma m_0 d\mathbf{v}/dt = ze(\mathbf{v} \times \mathbf{B}) \quad (3)$$

Motion of an Electron in a Uniform, Static Magnetic field



We now split v into components parallel and perpendicular to the uniform magnetic field, v_{\parallel} and v_{\perp} respectively. The pitch angle θ of the particle's path is given by $\tan \theta = v_{\perp}/v_{\parallel}$, that is, θ is the angle between the vectors v and B .

Since $v_{\parallel} \times B = 0$, $v_{\parallel} = \text{constant}$. The acceleration is perpendicular to the magnetic field direction and to v_{\parallel} .

$$\gamma m_0 \frac{dv}{dt} = ze v_{\perp} B (i_{\perp} \times i_B) = ze v B (i_v \times i_B) \quad (4)$$

where i_v and i_B are unit vectors in the directions of v and B respectively.

Gyrofrequencies

Thus, the motion of the particle consists of a constant velocity along the magnetic field direction and circular motion with radius r about it. This means that the particle moves in a *spiral path* with *constant pitch angle* θ . The radius r is known as the *gyroradius* of the particle. The angular frequency of the particle in its orbit ω_g is known as the *angular cyclotron frequency* or *angular gyrofrequency* and is given by

$$\omega_g = v_{\perp}/r = zeB/\gamma m_0 \quad (5)$$

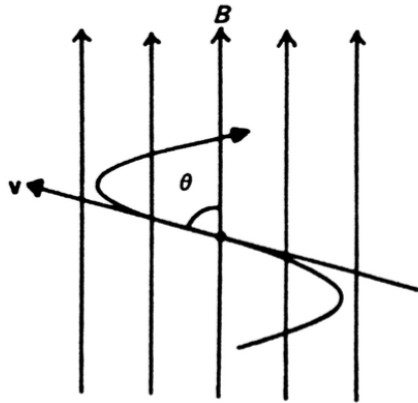
The corresponding *gyrofrequency* ν_g , that is, the number of times per second that the particle rotates about the magnetic field direction, is

$$\nu_g = \omega_g/2\pi = zeB/2\pi\gamma m_0 \quad (6)$$

In the case of a non-relativistic particle, $\gamma = 1$ and hence $\nu_g = zeB/2\pi m_0$.

A useful figure to remember is the non-relativistic gyrofrequency of an electron $\nu_g = eB/2\pi m_e = 28 \text{ GHz T}^{-1}$ where the magnetic field strength is measured in tesla; alternatively, $\nu_g = 2.8 \text{ MHz G}^{-1}$ for those not yet converted from gauss (G) to teslas (T).

The Total Energy Loss Rate



Most of the essential tools needed in this analysis have already been derived. First of all, use the expression for the acceleration of the electron in its orbit and insert this into the expression for the radiation rate of a relativistic electron. The acceleration is always perpendicular to the velocity vector of the particle and to B and hence $a_{\parallel} = 0$. Therefore, the total radiation loss rate of the electron is

$$-\left(\frac{dE}{dt}\right) = \frac{\gamma^4 e^2}{6\pi\epsilon_0 c^3} |a_{\perp}|^2 = \frac{\gamma^4 e^2}{6\pi\epsilon_0 c^3} \frac{e^2 v^2 B^2 \sin^2 \theta}{\gamma^2 m_e^2} \quad (7)$$

$$= \frac{e^4 B^2}{6\pi\epsilon_0 c m_e^2} \frac{v^2}{c^2} \gamma^2 \sin^2 \theta \quad (8)$$

The Average Energy Loss Rate

In the ultrarelativistic limit, $v \rightarrow c$, we may approximate this result by

$$-\left(\frac{dE}{dt}\right) = 2\sigma_T c U_{\text{mag}} \gamma^2 \sin^2 \theta \quad (14)$$

These results apply for electrons of a specific pitch angle θ . Particles of a particular energy E , or Lorentz factor γ , are often expected to have an isotropic distribution of pitch angles and therefore we can work out their average energy loss rate by averaging over such a distribution of pitch angles $p(\theta) d\theta = \frac{1}{2} \sin \theta d\theta$

$$\begin{aligned} -\left(\frac{dE}{dt}\right) &= 2\sigma_T c U_{\text{mag}} \gamma^2 \left(\frac{v}{c}\right)^2 \frac{1}{2} \int_0^\pi \sin^3 \theta d\theta \\ &= \frac{4}{3} \sigma_T c U_{\text{mag}} \left(\frac{v}{c}\right)^2 \gamma^2 \end{aligned} \quad (15)$$

There is a deeper sense in which (15) is the average loss rate for a particle of energy E . During its lifetime, it is likely that the high energy particle is randomly scattered in pitch angle and then (15) is the correct expression for its average energy loss rate.

The Synchrotron Radiation of a Power-law Distribution of Electron Energies

The emitted spectrum of electrons of energy E is quite sharply peaked near the critical frequency ν_c and is very much narrower than the breadth of the electron energy spectrum. Therefore, to a good approximation, it may be assumed that all the radiation of an electron of energy E is radiated at the critical frequency ν_c which we may approximate by

$$\nu \approx \nu_c \approx \gamma^2 \nu_g = \left(\frac{E}{m_e c^2} \right)^2 \nu_g; \quad \nu_g = \frac{eB}{2\pi m_e}. \quad (34)$$

Therefore, the energy radiated in the frequency range ν to $\nu + d\nu$ can be attributed to electrons with energies in the range E to $E + dE$, which we assume to have power-law form $N(E) = \kappa E^{-p}$. We may therefore write

$$J(\nu) d\nu = \left(-\frac{dE}{dt} \right) N(E) dE. \quad (35)$$

(continued)

Now

$$E = \gamma m_e c^2 = \left(\frac{\nu}{\nu_g} \right)^{1/2} m_e c^2, \quad dE = \frac{m_e c^2}{2\nu_g^{1/2}} \nu^{-1/2} d\nu, \quad (36)$$

and

$$-\left(\frac{dE}{dt} \right) = \frac{4}{3} \sigma_T c \left(\frac{E}{m_e c^2} \right)^2 \frac{B^2}{2\mu_0}. \quad (37)$$

Substituting these quantities into (35), the emissivity may be expressed in terms of κ, B, ν and fundamental constants.

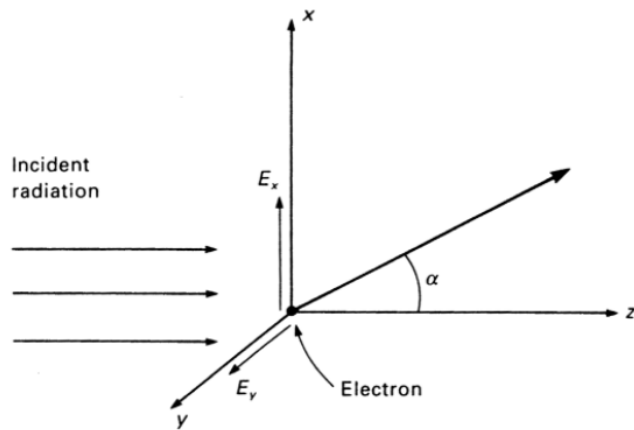
$$J(\nu) = (\text{constants}) \kappa B^{(p+1)/2} \nu^{-(p-1)/2}. \quad (38)$$

If the electron energy spectrum has power law index p , the spectral index of the synchrotron emission of these electrons, defined by $J(\nu) \propto \nu^{-\alpha}$, is $\alpha = (p - 1)/2$. The spectral shape is determined by the shape of the electron energy spectrum rather than by the shape of the emission spectrum of a single particle. The quadratic nature of the relation between emitted frequency and the energy of the electron accounts for the difference in slopes of the emission spectrum and the electron energy spectrum.

Thomson Scattering

Thomson scattering is the scattering of electromagnetic waves by free electrons in the classical limit. Thomson first published the formula for the *Thomson cross-section* in 1906 in connection with the scattering of X-rays.

We seek the formula describing the scattering of a beam of radiation incident upon a stationary electron. We assume that the beam of incident radiation propagates in the positive z -direction. Without loss of generality, we arrange the geometry of the scattering so that the scattering angle α lies in the $x - z$ plane. In the case of unpolarised radiation, we resolve the electric field strength into components of equal intensity in the i_x and i_y directions.



Thomson Scattering

The electric fields experienced by the electron in the x and y directions, $E_x = E_{x0} \exp(i\omega t)$ and $E_y = E_{y0} \exp(i\omega t)$ respectively, cause the electron to oscillate and the accelerations in these directions are:

$$\ddot{r}_x = eE_x/m_e \quad \ddot{r}_y = eE_y/m_e. \quad (10)$$

We can therefore enter these accelerations into the radiation formula (9) which shows the angular dependence of the emitted radiation upon the polar angle θ . Let us treat the x -acceleration first. In this case, we can use the formula (9) directly with the substitution $\alpha = \pi/2 - \theta$. Therefore, the intensity of radiation scattered through angle θ into the solid angle $d\Omega$ is

$$-\left(\frac{dE}{dt}\right)_x d\Omega = \frac{e^2 |\ddot{r}_x|^2 \sin^2 \theta}{16\pi^2 \epsilon_0 c^3} d\Omega = \frac{e^4 |E_x|^2}{16\pi^2 m_e^2 \epsilon_0 c^3} \cos^2 \alpha d\Omega. \quad (11)$$

Thomson Scattering

We have to take time averages of E_x^2 and we find that $E_x^2 = E_{x0}^2/2$, where E_{x0} is the maximum field strength of the wave. We sum over all waves contributing to the E_x -component of radiation and express the result in terms of the incident energy per unit area upon the electron. The latter is given by Poynting's theorem, $S_x = (\mathbf{E} \times \mathbf{H}) = c\epsilon_0 E_x^2 \mathbf{i}_z$. Again, we take time averages and find that the contribution to the intensity in the direction α from the x -component of the acceleration is $S_x = \sum_i c\epsilon_0 E_{x0}^2/2$. Therefore

$$-\left(\frac{dE}{dt}\right)_x d\Omega = \frac{e^4 \cos^2 \alpha}{16\pi^2 m_e^2 \epsilon_0 c^3} \sum_i \overline{E_x^2} d\Omega = \frac{e^4 \cos^2 \alpha}{16\pi^2 m_e^2 \epsilon_0^2 c^4} S_x d\Omega. \quad (12)$$

Thomson Scattering

Now let us look at the scattering of the E_y -component of the incident field. From the geometry of the previous diagram, it can be seen that the radiation in the $x - z$ plane from the acceleration of the electron in the y -direction corresponds to scattering at $\theta = 90^\circ$ and so the scattered intensity in the α -direction is

$$-\left(\frac{dE}{dt}\right)_y d\Omega = \frac{e^4}{16\pi^2 m_e^2 \epsilon_0^2 c^4} S_y d\Omega. \quad (13)$$

The total scattered radiation into $d\Omega$ is the sum of these components (notice that we add the intensities of the two independent field components).

$$-\left(\frac{dE}{dt}\right) d\Omega = \frac{e^4}{16\pi^2 m_e^2 \epsilon_0^2 c^4} (1 + \cos^2 \alpha) \frac{S}{2} d\Omega \quad (14)$$

where $S = S_x + S_y$ and $S_x = S_y$ for unpolarised radiation. We now express the scattered intensity in terms of a differential scattering cross-section $d\sigma_T$ in the following way. We define the scattered intensity in direction α by the following relation

$$\frac{d\sigma_T(\alpha)}{d\Omega} = \frac{\text{energy radiated per unit time per unit solid angle}}{\text{incident energy per unit time per unit area}}. \quad (15)$$

Thomson Scattering

Since the total incident energy is S , the differential cross-section for Thomson scattering is

$$d\sigma_T(\alpha) = \frac{e^4}{16\pi^2\epsilon_0^2 m_e^2 c^4} \frac{(1 + \cos^2 \alpha)}{2} d\Omega. \quad (16)$$

In terms of the *classical electron radius* $r_e = e^2/4\pi\epsilon_0 m_e c^2$, this can be expressed

$$d\sigma_T = \frac{r_e^2}{2} (1 + \cos^2 \alpha) d\Omega. \quad (17)$$

To find the total cross-section, we integrate over all angles α ,

$$\sigma_T = \int_0^\pi \frac{r_e^2}{2} (1 + \cos^2 \alpha) 2\pi \sin \alpha d\alpha = \frac{8\pi}{3} r_e^2 = \frac{e^4}{6\pi\epsilon_0^2 m_e^2 c^4}. \quad (18)$$

$$\boxed{\sigma_T = 6.653 \times 10^{-29} \text{ m}^2.} \quad (19)$$

This is Thomson's famous result for the total cross-section for scattering by stationary free electrons and is justly referred to as the *Thomson cross-section*.

Thomson Scattering

- The scattering is symmetric with respect to the scattering of angle α . Thus as much radiation is scattered backwards as forwards.
- Another useful calculation is the scattering cross-section for 100% polarised emission. We can work this out by integrating the scattered intensity (11) over all angles.

$$-\left(\frac{dE}{dt}\right)_x = \frac{e^2 |\ddot{\mathbf{r}}_x|^2}{16\pi^2 \epsilon_0 c^3} \int \sin^2 \theta \, 2\pi \sin \theta \, d\theta = \left(\frac{e^4}{6\pi \epsilon_0^2 m_e^2 c^4}\right) S_x. \quad (20)$$

We find the same total cross-section for scattering as before because it does not matter how the electron is forced to oscillate. The only important quantity is the total intensity incident upon it and it does not matter how anisotropic the radiation is. This result can be written in terms to the energy density of radiation u_{rad} in which the electron is located,

$$u_{\text{rad}} = \sum_i u_i = \sum_i S_i/c, \quad (21)$$

and hence

$$-(dE/dt) = \sigma_T c u_{\text{rad}}. \quad (22)$$

- Thomson scattering is one of the most important processes which impedes the escape of photons from any region. We write down the expression for the energy scattered by the electron in terms of the number density N of photons of frequency ν so that

$$-\frac{d(Nh\nu)}{dt} = \sigma_T c N h \nu. \quad (23)$$

There is no change of energy of the photons in the scattering process and so, if there are N_e electrons per unit volume, the number density of photons decreases exponentially with distance

$$\begin{aligned} -\frac{dN}{dt} &= \sigma_T c N_e N & -\frac{dN}{dx} &= \sigma_T N_e N \\ N &= N_0 \exp\left(-\int \sigma_T N_e dx\right). \end{aligned} \quad (24)$$

Thus, the *optical depth* of the medium to Thomson scattering is

$$\tau = \int \sigma_T N_e dx. \quad (25)$$

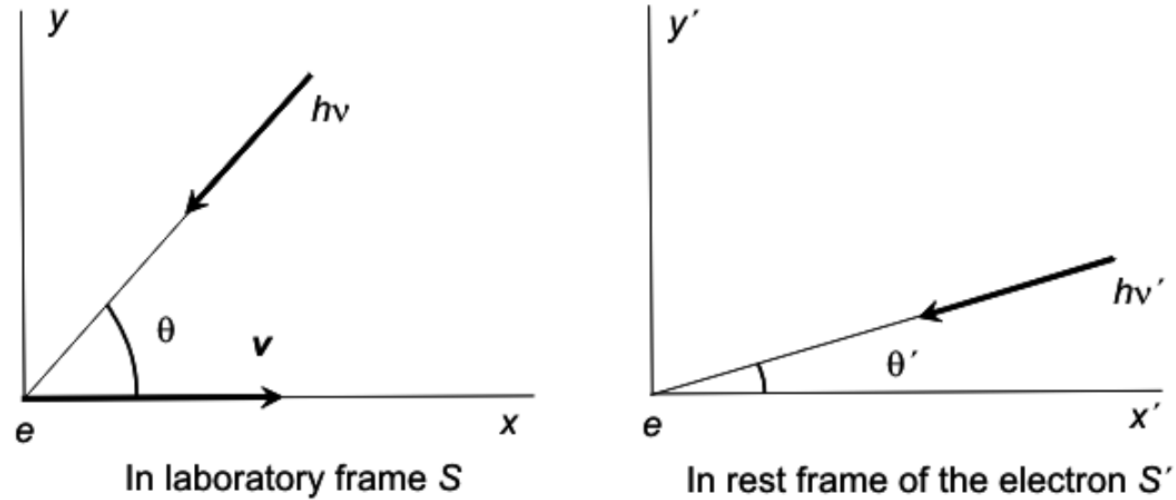
- In this process, the photons are scattered in random directions and so they perform a random walk, each step corresponding to the *mean free path* λ_T of the photon through the electron gas where $\lambda_T = (\sigma_T N_e)^{-1}$.

Inverse Compton Scattering

Comptonisation is a vast subject. *Inverse Compton scattering* involves the scattering of low energy photons to high energies by ultrarelativistic electrons so that the photons gain and the electrons lose energy. The process is called *inverse* because the electrons lose energy rather than the photons, the opposite of the standard Compton effect. We will treat the case in which the energy of the photon in the centre of momentum frame of the interaction is much less than $m_e c^2$, and consequently the Thomson scattering cross-section can be used to describe the probability of scattering.

Many of the most important results can be worked out using simple physical arguments, as for example in Blumenthal and Gould (1970) and Rybicki and Lightman (1979).

Inverse Compton Scattering



Consider a collision between a photon and a relativistic electron as seen in the laboratory frame of reference S and in the rest frame of the electron S' . Since $\hbar\omega' \ll m_e c^2$ in S' , the centre of momentum frame is very closely that of the relativistic electron. If the energy of the photon is $\hbar\omega$ and the angle of incidence θ in S , its energy in the frame S' is

$$\hbar\omega' = \gamma\hbar\omega[1 + (v/c) \cos \theta] \quad (1)$$

according to the standard relativistic Doppler shift formula.

Inverse Compton Scattering

Similarly, the angle of incidence θ' in the frame S' is related to θ by the formulae

$$\sin \theta' = \frac{\sin \theta}{\gamma[1 + (v/c) \cos \theta]} \quad ; \quad \cos \theta' = \frac{\cos \theta + v/c}{1 + (v/c) \cos \theta}. \quad (2)$$

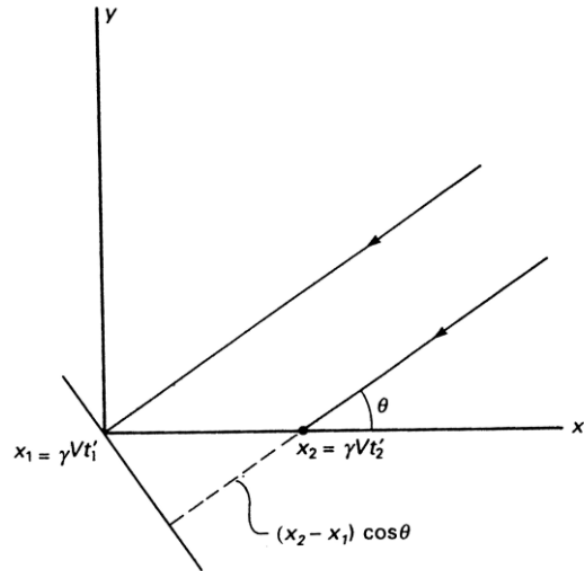
Now, provided $\hbar\omega' \ll m_e c^2$, the Compton interaction in the rest frame of the electron is simply Thomson scattering and hence the energy loss rate of the electron in S' is just the rate at which energy is reradiated by the electron.

According to the analysis of Thomson scattering, the loss rate is

$$-(dE/dt)' = \sigma_T c U'_{\text{rad}}, \quad (3)$$

where U_{rad} is the energy density of radiation in the rest frame of the electron. As discussed in that section, it is of no importance whether or not the radiation is isotropic. The free electron oscillates in response to any incident radiation field. Our strategy is therefore to work out U'_{rad} in the frame of the electron S' and then to use (3) to work out $(dE/dt)'$. Because dE/dt is an invariant between inertial frames, this is also the loss rate (dE/dt) in the observer's frame S .

Working out U'_{rad} in S'



In S , the electron moves from x_1 to x_2 in the time interval t_1 to t_2 . These are transformed into S' by the standard Lorentz transformation

Suppose the number density of photons in a beam of radiation incident at angle θ to the x -axis is N . Then, the energy density of these photons in S is $N\hbar\omega$. The flux density of photons incident upon an electron stationary in S is $U_{\text{rad}}c = N\hbar\omega c$.

Now let us work out the flux density of this beam in the frame of reference of the electron S' . We need two things, the energy of each photon in S' and the rate of arrival of these photons at the electron in S' . The first of these is given by (3). The second factor requires a little bit of care, although the answer is obvious in the end. The beam of photons incident at angle θ in S arrives at an angle θ' in S' according to the aberration formulae (2).

Working out U'_{rad} in S'

We are interested in the rate of arrival of photons at the origin of S' and so let us consider two photons which arrive there at times t'_1 and t'_2 . The coordinates of these events in S are

$$[x_1, 0, 0, t_1] = [\gamma V t'_1, 0, 0, \gamma t'_1] \quad \text{and} \quad [x_2, 0, 0, t_2] = [\gamma V t'_2, 0, 0, \gamma t'_2] \quad (4)$$

respectively. This calculation makes the important point that the photons in the beam are propagated along parallel but separate trajectories in S as illustrated by Fig. 30. From the geometry of the figure, it is apparent that the time difference when the photons arrive at a plane perpendicular to their direction of propagation in S is

$$\Delta t = t_2 + \frac{(x_2 - x_1)}{c} \cos \theta - t_1 = (t'_2 - t'_1) \gamma [1 + (v/c) \cos \theta], \quad (5)$$

that is, the time interval between the arrival of photons from the direction θ is shorter by a factor $\gamma [1 + (v/c) \cos \theta]$ in S' than it is in S .

Working out U'_{rad} in S'

Thus, the rate of arrival of photons, and correspondingly their number density, is greater by this factor $\gamma[1 + (v/c) \cos \theta]$ in S' as compared with S . This is exactly the same factor by which the energy of the photon has increased (3). On reflection, we should not be surprised by this result because these are two different aspects of the same relativistic transformation between the frames S and S' , in one case the frequency interval and, in the other, the time interval.

Thus, as observed in S' , the energy density of the beam is therefore

$$U'_{\text{rad}} = [\gamma(1 + (v/c) \cos \theta)]^2 U_{\text{rad}}. \quad (6)$$

Now, this energy density is associated with the photons incident at angle θ in the frame S and consequently arrives within solid angle $2\pi \sin \theta d\theta$ in S . We assume that the radiation field in S is isotropic and therefore we can now work out the total energy density seen by the electron in S' by integrating over solid angle in S , that is,

$$U'_{\text{rad}} = U_{\text{rad}} \int_0^\pi \gamma^2 [1 + (v/c) \cos \theta]^2 \frac{1}{2} \sin \theta d\theta. \quad (7)$$

The Inverse Compton Energy Loss Rate

Integrating, we find

$$U'_{\text{rad}} = \frac{4}{3}U_{\text{rad}}(\gamma^2 - \frac{1}{4}). \quad (8)$$

Therefore, substituting into (3), we find

$$(dE/dt)' = (dE/dt) = \frac{4}{3}\sigma_{\text{T}}cU_{\text{rad}}(\gamma^2 - \frac{1}{4}). \quad (9)$$

Now, this is the energy gained by the photon field due to the scattering of the low energy photons. We have therefore to subtract the energy of these photons to find the total energy gain to the photon field in S. The rate at which energy is removed from the low energy photon field is $\sigma_{\text{T}}cU_{\text{rad}}$ and therefore, subtracting, we find

$$dE/dt = \frac{4}{3}\sigma_{\text{T}}cU_{\text{rad}}(\gamma^2 - \frac{1}{4}) - \sigma_{\text{T}}cU_{\text{rad}} = \frac{4}{3}\sigma_{\text{T}}cU_{\text{rad}}(\gamma^2 - 1). \quad (10)$$

We now use the identity $(\gamma^2 - 1) = (v^2/c^2)\gamma^2$ to write the loss rate in its final form

$$\boxed{dE/dt = \frac{4}{3}\sigma_{\text{T}}cU_{\text{rad}} \left(\frac{v^2}{c^2} \right) \gamma^2.} \quad (11)$$

Synchrotron Radiation and Inverse Compton Losses

This is the remarkably elegant result we have been seeking. It is exact so long as $\gamma \hbar \omega \ll m_e c^2$.

Notice the remarkable similarity between the expressions for the loss rates by synchrotron radiation and by inverse Compton scattering, even down to the factor of $\frac{4}{3}$ in front of the two expressions.

$$-\left(\frac{dE}{dt}\right)_{\text{IC}} = \frac{4}{3}\sigma_{\text{T}}cU_{\text{rad}}\left(\frac{v^2}{c^2}\right)\gamma^2 \quad -\left(\frac{dE}{dt}\right)_{\text{sync}} = \frac{4}{3}\sigma_{\text{T}}cU_{\text{mag}}\left(\frac{v}{c}\right)^2\gamma^2 \quad (12)$$

This is not an accident. The reason for the similarity is that, in both cases, the electron is accelerated by the electric field which it observes in its instantaneous rest-frame. The electron does not really care about the origin of the electric field. In the case of synchrotron radiation, the constant accelerating electric field is associated with the motion of the electron through the magnetic field \mathbf{B} , $\mathbf{E}' = \mathbf{v} \times \mathbf{B}$, and, in the case of inverse Compton scattering, it is the sum of all the electric fields of the incident waves. Notice that, in the latter case, the fields of the waves add incoherently and it is the sum of the squares of the electric field strengths of the waves which appears in the formulae.

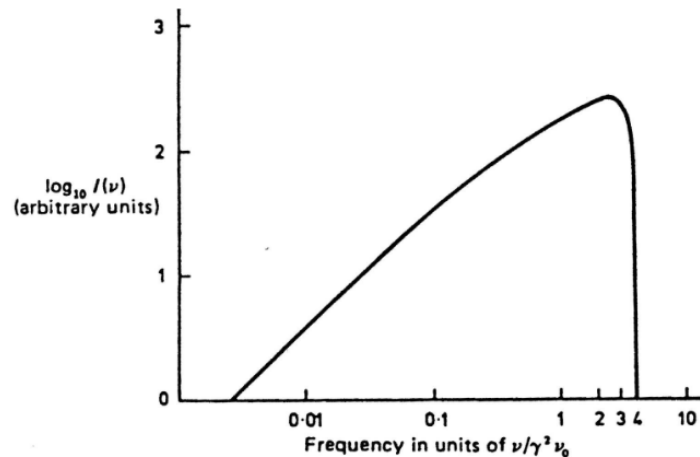
The Spectrum of Inverse Compton Radiation

The next calculation is the determination of the spectrum of the scattered radiation. This can be found by performing two successive Lorentz transformations, first transforming the photon distribution into the frame S' and then transforming the scattered radiation back into the laboratory frame of reference S . This is not a trivial calculation, but the exact result is given by Blumenthal and Gould (1970) for an incident isotropic photon field at a single frequency ν_0 . They show that the spectral emissivity $I(\nu)$ may be written

$$I(\nu) d\nu = \frac{3\sigma_T c N(\nu_0)}{16\gamma^4 \nu_0^2} \nu \left[2\nu \ln \left(\frac{\nu}{4\gamma^2 \nu_0} \right) + \nu + 4\gamma^2 \nu_0 - \frac{\nu^2}{2\gamma^2 \nu_0} \right] d\nu, \quad (13)$$

where the radiation field is assumed to be monochromatic with frequency ν_0 ; $N(\nu_0)$ is the number density of photons. At low frequencies, the term in square brackets in (13) is a constant and hence the scattered radiation has the form $I(\nu) \propto \nu$.

The Spectrum of Inverse Compton Radiation



It is an easy calculation to show that the maximum energy which the photon can acquire corresponds to a head-on collision in which the photon is sent back along its original path. The maximum energy of the photon is

$$(\hbar\omega)_{\max} = \hbar\omega\gamma^2(1 + v/c)^2 \approx 4\gamma^2\hbar\omega_0. \quad (14)$$

Another interesting result comes out of the formula for the total energy loss rate of the electron (11). The number of photons scattered per unit time is $\sigma_T c U_{\text{rad}} / \hbar\omega_0$ and hence the average energy of the scattered photons is

$$\hbar\omega = \frac{4}{3}\gamma^2(v/c)^2\hbar\omega_0 \approx \frac{4}{3}\gamma^2\hbar\omega_0. \quad (15)$$

This result gives substance to the hand-waving argument that the photon gains one factor of γ in transforming into S' and then gains another on transforming back to S .

Inverse Compton Radiation

The general result that the frequency of the scattered photons is $\nu \approx \gamma^2 \nu_0$ is of profound importance in high energy astrophysics. We know that there are electrons with Lorentz factors $\gamma \sim 100 - 1000$ in various types of astronomical source and consequently they scatter any low energy photons to very much higher energies. Consider the scattering of radio, infrared and optical photons scattered by electrons with $\gamma = 1000$.

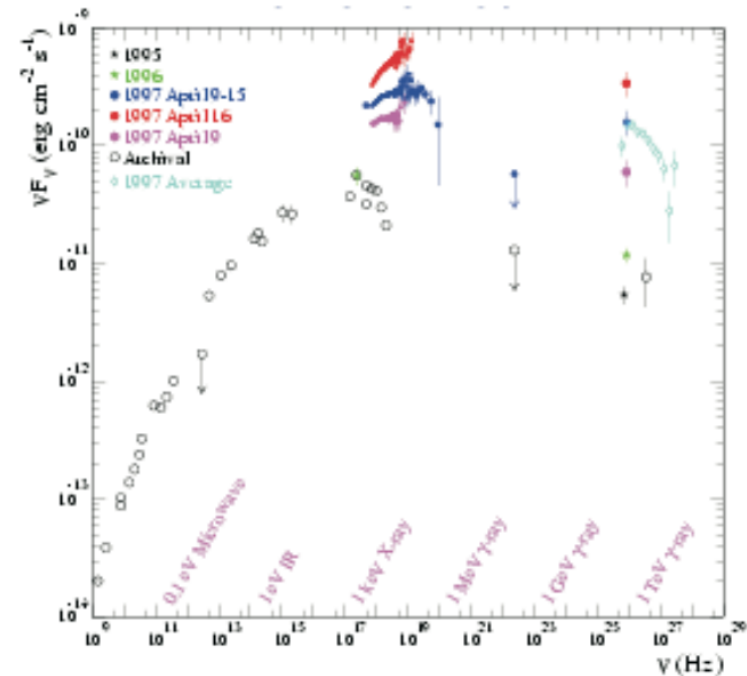
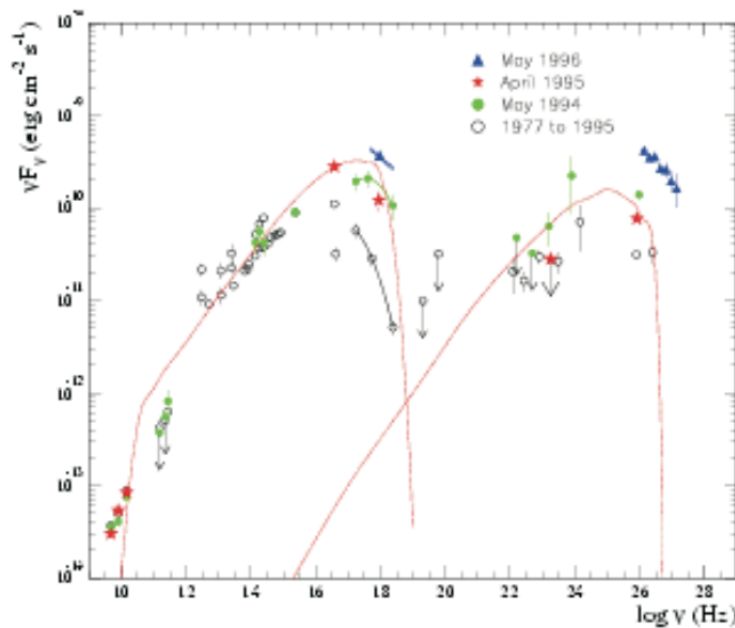
<i>Waveband</i>	<i>Frequency (Hz)</i> ν_0	<i>Scattered Frequency (Hz)</i> <i>and Waveband</i>
Radio	10^9	$10^{15} = \text{UV}$
Far-infrared	3×10^{12}	$3 \times 10^{18} = \text{X-rays}$
Optical	4×10^{14}	$4 \times 10^{21} \equiv 1.6\text{MeV} = \gamma\text{-rays}$

Thus, inverse Compton scattering is a means of creating very high energy photons indeed. It also becomes an inevitable drain of energy for high energy electrons whenever they pass through a region in which there is a large energy density of photons.

Synchro-Compton Radiation and the Inverse Compton Catastrophe

Inverse Compton scattering is likely to be an important source of X-rays and γ -rays, for example, in the intense extragalactic γ -ray sources. Wherever there are large number densities of soft photons, the presence of ultrarelativistic electrons must result in the production of high energy photons, X-rays and γ -rays. The case of special interest in this chapter is that in which the same relativistic electrons which are the source of the soft photons are also responsible for scattering these photons to X-ray and γ -ray energies – this is the process known as *synchro-Compton Radiation*. One case of special importance is that in which the number density of low energy photons is so great that most of the energy of the electrons is lost by synchro-Compton radiation rather than by synchrotron radiation. This line of reasoning leads to what is known as the *inverse Compton catastrophe*.

Ultra-High Energy γ -ray Sources



In the extreme γ -ray sources Markarian 421 and 501, it is very likely that some form of inverse Compton radiation is occurring, quite possible via the Synchro-Compton mechanism. These γ -ray sources are quite enormously luminous and variable. It is therefore likely that relativistic motions have to be involved to explain their luminosities and variability.

Radiation processes

Lecture Notes



Selected Radiation Mechanisms in High Energy Astrophysics

Roberto Aloisio

Gran Sasso Science Institute – L'Aquila (Italy)

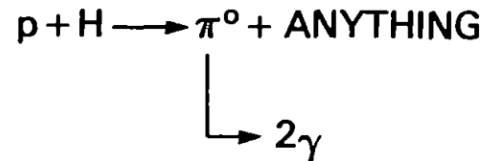
INFN – Laboratori Nazionali Gran Sasso – L'Aquila (Italy)

<https://indico.ijclab.in2p3.fr/event/7633/>



Neutral pion production

We discuss now the process of proton-proton interaction that gives rise to the production of neutral pions that in turn decay feeding the galactic gamma ray background. The process at hand is the interaction of cosmic rays protons with the protons of the interstellar medium that can be considered at rest and indicated with H



To fix the energetic scale of the problem let us start from the threshold for this reaction, that can be computed (using the definition) as the energy in the LAB frame of the incident proton needed to produce the final particles at rest in the CoM frame, i.e.

$$(E + m_p)^2 - p^2 = (M_{any} + m_\pi)^2 \quad \Rightarrow \quad E_{th}^{pp} = \frac{(M_{any} + m_\pi)^2 - 2m_\pi^2}{2m_p}$$

Being M_{any} the total rest mass of the final products apart from π^0 . The typical reaction of this kind implies the production of two protons in the final state in this case the threshold is:

$$p + H \rightarrow \pi^0 pp \quad E_{th}^{pp} \simeq m_p + 2m_\pi$$

NOTE: Comparing the time scales for pp and diffusion it follows that the pp mechanism is irrelevant as energy losses mechanism for CR. Let us assume: constant pH cross-section $\sigma_{pH} \approx 30 \text{ mb}$ ($3 \times 10^{-26} \text{ cm}^2$), number density for protons in the ISM $n_H = 1 \text{ cm}^{-3}$, constant diffusion coefficient $D = 3 \times 10^{28} \text{ cm}^2/\text{s}$, galactic halo and disk heights respectively $H = 3 \text{ Kpc}$ and $h = 0.15 \text{ kpc}$.

Taking into account that the time spent in the disk is roughly h/H of the total diffusion time, one has

$$\tau_{pp} = \frac{H}{n_H h c \sigma_{pH}} \simeq 2 \times 10^{16} \text{s} \quad \tau_{diff} = \frac{H^2}{D} \simeq 2 \times 10^{15} \text{s}$$

NOTE: pH interactions are important for the production of secondary gamma rays. Apart from the disk, pp is important in those regions with increased target density (and/or protons density) such as in molecular clouds or SNR.

The number of π^0 produced per unit volume, energy and steradian (emission function or emissivity) can be computed as

$$J_\pi(E_\pi) = 4\pi n_H \int_{E_\pi}^{\infty} dE_p I_p(E_p) \frac{d\sigma(E_\pi, E_p)}{dE_\pi}$$

where I_p is the flux of CR protons and $d\sigma/dE_\pi$ is the differential cross section for the production of a π^0 with energy E_π in the LAB frame.

NOTE: Eq. above holds in the case of an isotropic distribution of both bullets and targets.

The emissivity J of secondary photons produced by the decay of pions is

$$J_\gamma(\epsilon_\gamma) = 2 \int_{\epsilon_\gamma + m_\pi^2/4\epsilon_\gamma}^{\infty} dE_\pi \frac{J_\pi(E_\pi)}{\sqrt{E_\pi^2 - m_\pi^2}}$$

and the minimum pion energy

$$E_\pi^{min} = \epsilon_\gamma + \frac{m_\pi^2}{4\epsilon_\gamma}$$

Using the spectrum of the final gamma rays given by:

$$\frac{dN}{dE_\gamma} = \frac{2}{|\vec{p}_\pi|} = \frac{2}{\sqrt{E_\pi^2 - m_\pi^2}}$$

The cross section for π^0 production from p+p interactions can be written in terms of the total inclusive cross section associated to the reaction $pp \rightarrow \pi^0 + \text{anything}$, it is given by

$$\frac{d\sigma(E_p, E_\pi)}{dE_\pi} = \sigma_{inc}(E_p) \frac{f(E_p, E_\pi)}{E_\pi}$$

The quantity f is an auxiliary function that, fitted on the experimental data, should fulfill the condition

$$\int \frac{dE_\pi}{E_\pi} f(E_p, E_\pi) = 1$$

$$f(E_p, E_\pi) = f\left(\frac{E_\pi}{E_p}\right) = f(x) = 0.5[1.22(1-x)^{3.5} + 0.92 \exp(-18x)]$$

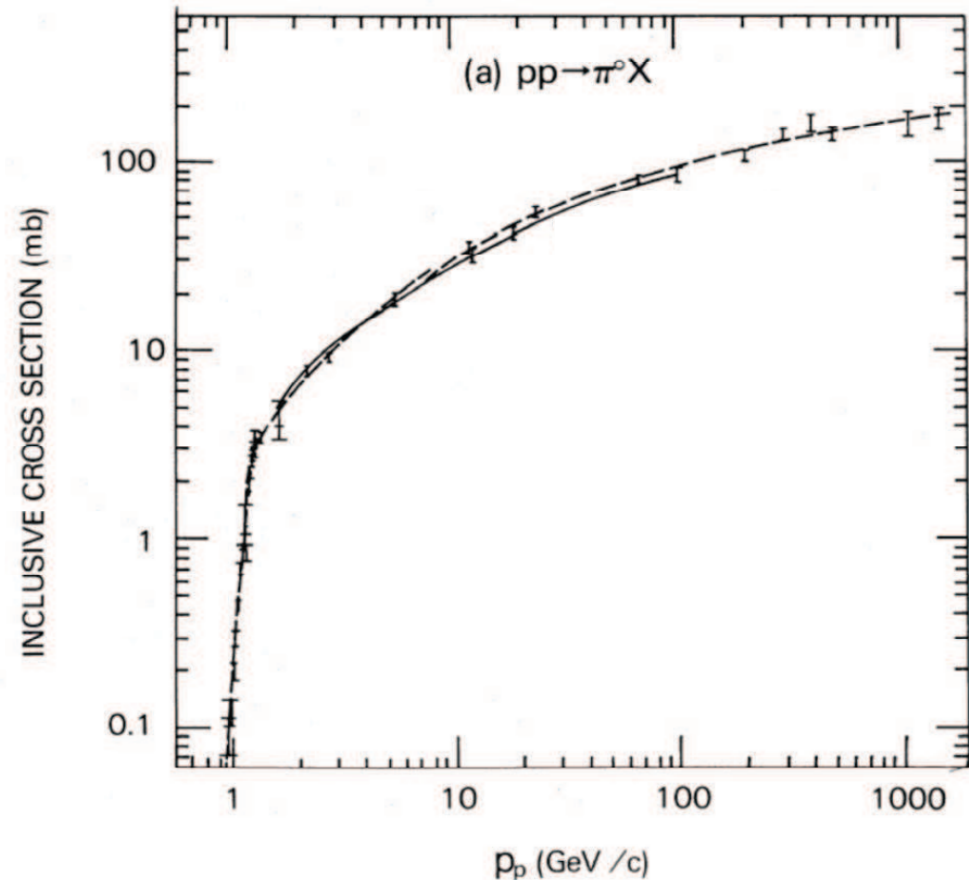
$$\sigma_{inc}(E_p) = 31 + 0.37 \ln^2\left(\frac{E_p}{50\text{GeV}}\right) \text{ mb}$$

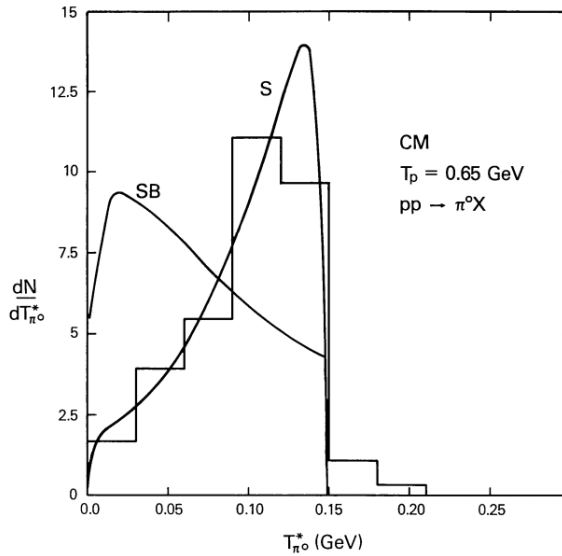
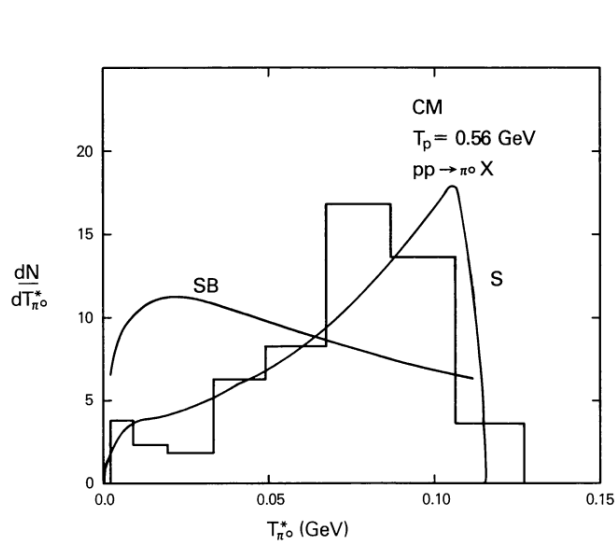
Low energies

Near the pion production threshold at energies around 1 GeV the behavior of the cross section is model dependent, it suffers large experimental uncertainties.

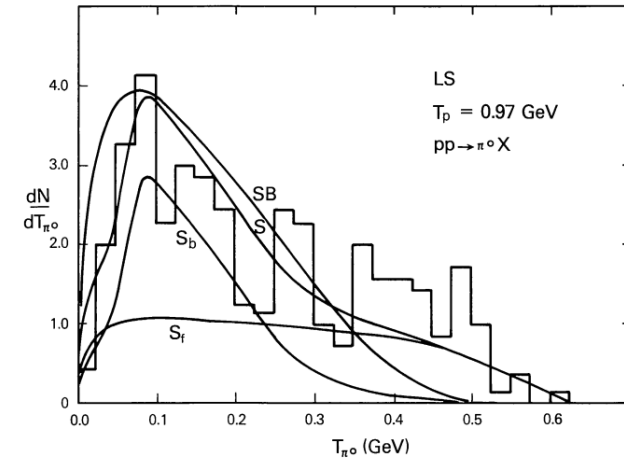
High energies

At energies larger than 10 GeV the behavior of the cross section is better understood with an almost constant (logarithmic) behavior and the function f satisfies the scaling $f=f(x)$ with $x=E_\pi/E_p$.





Dermer 1986



Comparison of the model prediction of the function $f(E_\pi, E_p)/E_\pi$ with experimental data. Photons and pions emissivity (C.D. Dermer, A&A (1986)).

NOTE: at high energies (>100 GeV) the CR spectrum as a power law behavior, which is reproduced by pions and gamma rays:

$$I_p(E) = I_0 \left(\frac{E}{E_0} \right)^{-\gamma}$$

$$J_\pi(E_\pi) = 4\pi n_H I_0 E_0^\gamma E_\pi^{-\gamma} \sigma_0 \int_0^1 x^{\gamma-2} f(x) = 4\pi n_H \sigma_0 I_p(E_\pi) \Lambda_\gamma$$

$$J_\gamma(E_\gamma) = 2 \int_{E_\gamma} \frac{dE_\pi}{E_\pi} J_\pi(E_\pi) = \frac{2}{\gamma} J_\pi(E_\gamma) = \frac{\gamma}{2} 4\pi n_H \sigma_0 I_p(E_\gamma) \Lambda_\gamma$$

with $\Lambda_\gamma = \int_0^1 dx f(x) x^{\gamma-2}$ a numerical constant.

